

3-11-2011

# A Comparison in the Accuracy of Mapping Nuclear Fallout Patterns using HPAC, HYSPLIT, DELFIC FPT and an AFIT FORTRAN95 Fallout Deposition Code

April D. Miller

Follow this and additional works at: <https://scholar.afit.edu/etd>

Part of the [Nuclear Commons](#)

## Recommended Citation

Miller, April D., "A Comparison in the Accuracy of Mapping Nuclear Fallout Patterns using HPAC, HYSPLIT, DELFIC FPT and an AFIT FORTRAN95 Fallout Deposition Code" (2011). *Theses and Dissertations*. 1465.  
<https://scholar.afit.edu/etd/1465>

This Thesis is brought to you for free and open access by the Student Graduate Works at AFIT Scholar. It has been accepted for inclusion in Theses and Dissertations by an authorized administrator of AFIT Scholar. For more information, please contact [richard.mansfield@afit.edu](mailto:richard.mansfield@afit.edu).



**A COMPARISON IN THE ACCURACY OF MAPPING NUCLEAR FALLOUT  
PATTERNS USING HPAC, HYSPLIT, DELFIC FPT AND AN AFIT  
FORTRAN95 FALLOUT DEPOSITION CODE**

THESIS

April D. Miller, Major, USA

AFIT/GNE/ENP/11-M16

**DEPARTMENT OF THE AIR FORCE  
AIR UNIVERSITY**

**AIR FORCE INSTITUTE OF TECHNOLOGY**

---

**Wright-Patterson Air Force Base, Ohio**

APPROVED FOR PUBLIC RELEASE; DISTRIBUTION UNLIMITED

The views expressed in this thesis are those of the author and do not reflect the official policy or position of the United States Air Force, Department of Defense, or the United States Government. This material is declared a work of the U.S. Government and is not subject to copyright protection in the United States.

AFIT/GNE/ENP/11-M16

A COMPARISON IN THE ACCURACY OF MAPPING NUCLEAR FALLOUT  
PATTERNS USING HPAC, HYSPLIT, DELFIC FPT AND AN AFIT FORTRAN95  
FALLOUT DEPOSITION CODE

THESIS

Presented to the Faculty

Department of Engineering Physics

Graduate School of Engineering and Management

Air Force Institute of Technology

Air University

Air Education and Training Command

In Partial Fulfillment of the Requirements for the  
Degree of Master of Science in Nuclear Engineering

April D. Miller, MS

Major, USA

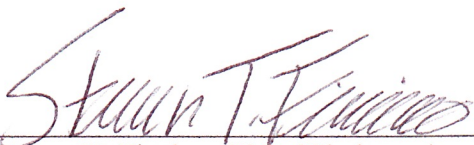
March 2011

APPROVED FOR PUBLIC RELEASE; DISTRIBUTION UNLIMITED


A COMPARISON IN THE ACCURACY OF MAPPING NUCLEAR FALLOUT  
PATTERNS USING HPAC, HYSPLIT, DELFIC FPT AND AN AFIT FORTRAN95  
FALLOUT DEPOSITION CODE

April D. Miller, MS  
Major, USA

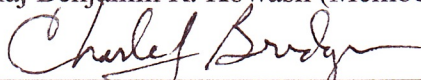
Approved:

  
\_\_\_\_\_  
Steven T. Fiorino, PhD (Chairman)

2 MAR 11  
Date

  
\_\_\_\_\_  
Maj Benjamin R. Kowash (Member)

4 Mar 11  
Date

  
\_\_\_\_\_  
Charles J. Bridgman, PhD (Member)

4 Mar 11  
Date

**Abstract**

Four nuclear fallout mapping tools are studied to determine which tool predicts the most accurate fallout dose-rate contours with low computation time and resources. The four programs consist of the FORTRAN95 based Fallout Deposition Code (FDC), the Hazard Prediction and Assessment Capability's (HPAC) Nuclear Weapon (NWP), the Defense Land Fallout Interpretative Code (DELFI) Fallout Planning Tool (FPT) and the Hybrid Single-Particle Lagrangian Integrated Trajectory (HYSPLIT) Model. The models were compared to the Defense Nuclear Agency's (DNA) DNA 1251-1-EX, *Compilation of Local Fallout Data from Test Detonations 1945-1962 Extracted from DASA 1251*, using Warner and Platt's Measure of Effectiveness (MOE) method. In order to accurately compare models the use of the FDC and low resolution weather data was validated. HYSPLIT trials were studied varying the vertical distribution, horizontal distribution, emission rate, emission time and number of equal activity particle groups. HPAC trials were run varying the use of terrain and the terrain resolution and the DELFI FPT trials were run varying the length of time the ground zero winds were incorporated. The best results of each of the four nuclear mapping tools were compared with the results culminating in the determination that the DELFI FPT is the preferred nuclear mapping tool.

## Acknowledgments

I would like to thank my advisor, Dr. Steven T. Fiorino, for his advice, continuous support and sense of humor. I would also like to thank MAJ Buckley E. O'Day for his patience, advice and willingness to answer all of my questions. A special thanks to Dr. Bridgman and Dr. Jodoin for taking the time to answer questions.

I especially thank my husband for his constant support, suggestions and love and our unborn son who did not make me to nauseous to continue my journey. I am deeply grateful to my dogs Herbie and Little Bitz for their continuous support and love. Most of all I would like to thank my father who embedded in me the can do attitude.

April Miller

## Table of Contents

	Page
Abstract.....	iv
Acknowledgments.....	v
Table of Contents.....	vi
List of Figures.....	viii
List of Tables.....	xi
List of Acronyms.....	xiii
I. Introduction.....	1
Background.....	2
Motivation.....	4
Scope.....	4
Problem Statement.....	5
Hypothesis.....	5
Document Structure.....	6
II. Theory and Literature Review.....	7
Summary of Previous Research.....	7
Nuclear Fallout.....	8
Cloud Stabilization Parameters.....	10
Particle Size Distributions.....	12
Particle Settling Velocity.....	13
Concentration to Exposure Rate Conversion Factors.....	15
DNA 1251-1-EX.....	15
Weather Reanalysis.....	17
Low and High Resolution Weather Data.....	18
HPAC.....	20
HYSPLIT.....	21
DELFIC Fallout Planning Tool.....	23
Fallout Deposition Code.....	24
Measure of Effectiveness.....	26
Normalized Absolute Difference.....	28
III. Methodology.....	30
DNA-EX Extraction.....	31



	Page
FDC Adjustment and Data Extraction .....	32
Low and High Resolution Weather Inputs.....	32
HYSPLIT Source Term .....	33
HYSPLIT .....	36
DELFIK FPT Weather Input.....	38
DELFIK FPT.....	40
HPAC .....	42
Comparison.....	42
 IV. Results and Analysis.....	 45
 FDC.....	 45
HYSPLIT .....	52
DELFIK FPT.....	70
HPAC.....	81
Overall Comparison.....	88
 V. Conclusions and Recommendations .....	 108
 Recommendations for Future Work.....	 110
 Appendix A. HYSPLIT Settings.....	 111
 Appendix B. DELFIK Input File .....	 117
 Bibliography .....	 119

## List of Figures

Figure	Page
1. HPAC's Three Step Modeling Process.....	20
2. Fallout Deposition Code Framework.....	25
3. MOE Areas of Comparison .....	26
4. Numerical Comparison of Models.....	27
5. Example of a Comparison of Four Programs .....	28
6. Isolines of Various NADs.....	29
7. Problem Solving Methodology .....	30
8. FDC – Ess Contours.....	47
9. FDC – George Contours .....	47
10. FDC – Zucchini Contours.....	48
11. FDC – Priscilla Contours.....	48
12. FDC – Smoky Contours.....	49
13. FDC – Johnie Boy Contours .....	49
14. FDC – Combined Comparison for Ess .....	50
15. FDC – Combined Comparison for Priscilla.....	51
16. HYSPLIT – Vertical Distribution Contours (George).....	53
17. HYSPLIT – 100 Particle Group (George) .....	54
18. HYSPLIT – Three Point Source (George).....	55
19. HYSPLIT – 10s Emission Rate (George).....	56
20. HYSPLIT – Hybrid Gaussian Distribution (George) .....	57
22. HYSPLIT – Ess Contours.....	61

Figure	Page
23. HYSPLIT – Zucchini Contours .....	61
24. HYSPLIT – Priscilla Contours .....	62
25. HYSPLIT – Smoky Contours .....	62
26. HYSPLIT – Johnie Boy Contours .....	63
27. DELFIC FPT – Ess Contours .....	71
28. DELFIC FPT – George Contours .....	72
29. DELFIC FPT – Zucchini Contours.....	74
30. DELFIC FPT – Priscilla Contours.....	76
31. DELFIC FPT – Smoky Contours.....	78
32. DELFIC FPT – Johnie Boy Contours.....	80
33. HPAC – Ess Contours.....	82
34. HPAC – George Contours .....	83
35. HPAC – Zucchini Contours.....	84
36. HPAC – Priscilla Contours .....	85
37. HPAC – Smoky Contours.....	86
38. HPAC – Johnie Boy Contours .....	87
39. Overall comparison of Ess.....	89
40. Overall Individual Contour Comparison for Ess .....	91
41. Overall comparison of George.....	93
42. Overall Individual Contour Comparison for George.....	94
43. Overall comparison of Zucchini .....	96
44. Overall Individual Contour Comparison for Zucchini.....	97

Figure	Page
45. Overall comparison of Priscilla .....	99
46. Overall Individual Contour Comparison for Priscilla.....	100
47. Overall comparison of Smoky .....	102
48. Overall Individual Contour Comparison for Smoky .....	103
49. Overall comparison of Johnie Boy .....	105
50. Overall Individual Contour Comparison for Johnie Boy.....	106

## List of Tables

Table	Page
1. DNA 1251-1-EX Selected Test Data.....	16
2. HYSPLIT Trials.....	37
3. DELFIC FPT Trials .....	41
4. FDC Results for Low and High Resolution Reanalysis Weather .....	46
5. NAD Difference between Low and High Resolution Data .....	46
6. HYSPLIT Results for George.....	52
7. Calculated NADs using an Emission Rate Derived from the Beta Activity.....	58
8. HYSPLIT – NADs for Remaining Five Test Cases comparing Emission Duration.....	60
9. HYSPLIT – Calculated NADs comparing 3D Particle Distribution and a Hybrid Distribution .....	65
10. DELFIC FPT – NADs for Ess .....	70
11. DELFIC FPT – NADs for George.....	72
12. DELFIC FPT – NADs for Zucchini.....	73
13. DELFIC FPT – NADs for Priscilla.....	75
14. DELFIC FPT – NADs for Smoky .....	77
15. DELFIC FPT – NADs for Johnie Boy.....	79
16. HPAC – NADs for No Terrain and 900 and 3500 Resolution .....	81
17. Overall Comparison of Ess Contours .....	88
18. NADs of Individual Contours for Ess.....	90
19. Overall Assessment of Ess.....	92
20. Overall Comparison of George Contours .....	92

Table	Page
21. NADs of Individual Contours for George .....	94
22. Overall Assessment of George.....	95
23. Overall Comparison of Zucchini Contours.....	95
24. NADs of Individual Contours for Zucchini.....	97
25. Overall Assessment of Zucchini .....	98
26. Overall Comparison of Priscilla Contours.....	98
27. Comparison of Individual Contours for Priscilla.....	100
28. Overall Assessment of Priscilla .....	101
29. Overall Comparison of Smoky Contours.....	101
30. NADs of Individual Contours for Smoky .....	103
31. Overall Assessment of Smoky .....	104
32. Overall Comparison of Johnie Boy Contours.....	104
33. NADs of the Individual Contours for Johnie Boy .....	106
34. Overall Assessment of Johnie Boy .....	107
35. Overall NADs for all Historical Test Cases.....	107

## List of Acronyms

CBRNE – Chemical, Biological, Radiological, Nuclear and High Yield Explosives

CM – Consequence Management

DTRA – Defense Threat Reduction Agency

DELFIIC – Defense Land Fallout Interpretive Code

DNA – Defense Nuclear Agency

DoD – Department of Defense

FDC – Fallout Deposition Code

FPT – Fallout Planning Tool

HPAC – Hazard Prediction and Assessment Capability

HYSPLIT – Hybrid Single-Particle Lagrangian Integrated Trajectory

MOE – Measure of Effectiveness

NAD – Normalized Absolute Difference

QDR – Quadrennial Defense Review

RAMS – Regional Atmospheric Modeling System

WMD – Weapons of Mass Destruction

A COMPARISON IN THE ACCURACY OF MAPPING NUCLEAR FALLOUT  
PATTERNS USING HPAC, HYSPLIT, DELFIC FPT AND AN AFIT FORTRAN95  
FALLOUT DEPOSITION CODE

**I. Introduction**

Accurate modeling of nuclear fallout is vital to Chemical, Biological, Radiological, Nuclear and High Yield Explosives (CBRNE) planning and execution. Knowing the nuclear fallout pattern will ensure the safety of radiological response teams by minimizing exposure time and expediting response time. With the 2010's Department of Defense's (DoD) Quadrennial Defense Review's (QDR) requirement for the establishment of Joint Task Force Elimination Headquarters in order to plan, train and execute Weapons of Mass Destruction (WMD)-elimination operations [9:ix], accurate modeling becomes a higher priority. Civilian and military CBRNE planners and response personnel require advanced modeling programs to estimate the extent of the potential fallout area in order to effectively plan for Consequence Management (CM) missions. Currently, the planners employing the current modeling programs, such as the Hazard Prediction and Assessment Capability (HPAC) modeling program, are under the impression that the results are the worst case scenarios for nuclear fallout when in reality they may underestimate the fallout patterns. This research identifies low-cost, easy to implement methods that improve the accuracy of rapid estimations of fallout patterns for emergency response and other CBRNE operations.



## **Background**

Discoveries in Europe and America in the late 1930s and the U.S.'s assumption of the Manhattan Project in 1942 propelled the world into the nuclear age. U.S.'s employment of nuclear weapons on Hiroshima and Nagasaki compelled competing world powers into the race for nuclear supremacy. In the subsequent 50 years, the U.S., Russia, France, United Kingdom and China conducted over 500 above ground nuclear tests and over a thousand underground tests.

The fallout from a nuclear detonation takes seconds to months to transport to earth. The total amount of radioactivity within the cloud formed from a detonation largely depends on the weapon's characteristics. The size of the entrained radioactive particles within the cloud depends on numerous factors, most importantly are the height of burst and interaction with the ground. As the radioactive particles translate through the atmosphere the total radioactivity in the air reduces due to decay and dispersion. Smaller particles remain aloft longer, translating thousands of miles, leading to dilution of the radioactive material and deposition over a much larger area. The larger radioactive particles fall more rapidly due to aerodynamic drag force and deposit near ground zero to hundreds of miles creating a concentrated radioactive hazard that could potentially lead to injury and possibly death to living systems.

The base knowledge of fallout deposition and residual effects are the results of the study of nuclear tests. From these studies various nuclear fallout modeling programs were developed. The modern models are able to utilize real-time weather data but vary in the atmospheric transport methods. The lack of accurate high resolution weather data

from past nuclear tests and the moratorium of testing limited the advancement of these models.

The Limited Test Ban Treaty eliminated all atmospheric nuclear tests for the U.S. and only permitted underground nuclear tests in 1963. In 1996 the limited testing was further restricted with the U.S.'s signing of the Comprehensive Test Ban Treaty that completely eliminated all nuclear testing. Since the cessation of atmospheric testing the availability of meteorology data has increased significantly with improved atmospheric modeling and extensive research in the area of weather reanalysis.

The lack of four-dimensional weather data during the time frame of the historic nuclear tests, the differences in atmospheric transport methods and the difference in the modeling of the initial cloud stabilization between nuclear fallout models lead to deviations from actual measured contours. This thesis will compare the accuracy of four models to determine which model most accurately reproduces historic dose-rate contours. To mitigate the lack of four-dimensional weather data, all models will use the same mesoscale weather reanalysis data. This thesis will consider three of the most well known models, HPAC, developed by the Defense Threat Reduction Agency (DTRA), the Defense Land Fallout Interpretive Code (DELFI) Fallout Planning Tool (FPT) and the Hybrid Single-Particle Lagrangian Integrated Trajectory (HYSPLIT) Model, developed by the National Oceanic and Atmospheric Administration's Air Resources Laboratory.

HPAC is the main program used by the military to model fallout from nuclear detonations. HPAC is the program that these planners will rely on during any CBRNE incident where WMD are used. With the military's dependency on HPAC, extensive research was devoted to the accuracy of HPAC and comparing it with known contours.

There are multiple Air Force Institute of Technology theses devoted to this comparison. From this research the Fallout Deposition Code (FDC) was developed in 2009. The FDC was developed for the use with high resolution weather data and incorporated the lessons learned from the studies utilizing HPAC while varying the resolution of terrain and weather. HPAC, FDC, DELFIC FPT and HYSPLIT are the focus of this research.

### **Motivation**

The terrorist attacks on 11 September 2001 demonstrated that terrorists will go to any extremes to cause fear in their opponents. These attacks refocused efforts of the U.S. and revamped state and federal CBRNE response capabilities.

The refocus of CBRNE response coupled with the advancement of technology began the initiative for improving nuclear fallout modeling. Throughout the years computing time and costs decreased allowing for more sophisticated computer programs that implement complex mathematical equations. These advances along with the research conducted on fallout modeling allow for faster and potentially more accurate models. The FORTRAN95 FDC takes advantage of this past research and fast computing time and more effectively models nuclear detonations in comparison with HPAC.

### **Scope**

This research focuses on providing the most effective and accurate nuclear fallout mapping tool to enable military leadership and homeland security forces to effectively make decisions and save lives. The research focuses on four main nuclear fallout mapping tools; HPAC, HYSPLIT, DELFIC FPT and FDC.

The scope of this work is two-fold. First, plot the dose-rate contours for six known tests utilizing the FDC with low and high resolution weather data. Compare the results to the Defense Nuclear Agency (DNA), *Compilation of Local Fallout Data from Test Detonations 1945 – 1962 Extracted from DASA 1251* (DNA-EX also known as DASA-EX) [11], contours and determine if high resolution weather data is required to provide the most accurate contours. Second, using the appropriate weather resolution data, compare HPAC, HYSPLIT, DELFIC FPT and FDC contours for the six known tests.

### **Problem Statement**

The intent of this research addresses two problems. The first is to determine if the FDC is efficient in nuclear fallout modeling using widely available and frequently updated low resolution weather data in order to reduce computation time and cost. Secondly, compare HPAC, HYSPLIT, DELFIC FPT and FDC with the six known nuclear tests data using either low resolution or high resolution weather data depending on the results from the accuracy of the FDC using low resolution weather data.

### **Hypothesis**

This research asserts that the FDC provides a better mapping of nuclear fallout using low resolution weather data than HPAC, allowing military officers to make effective decisions with reduced computational time and cost. Comparing HPAC, DELFIC FPT and HYSPLIT shows that a combination of the DELFIC FPT and HYSPLIT is the preferred mapping set.

## Document Structure

Chapter 2 summarizes the previous research conducted in nuclear fallout modeling and the physical processes of nuclear fallout production and dispersion. Additionally, a description of the four programs used throughout this research, including the methods the programs use to model the variables in fallout transport, is provided. Chapter 3 describes the methodology used in the execution of this research. It includes the implementation of low and high resolution weather data in order to compare the results using the FDC as well as the execution of all four programs using the test data and obtained weather data for the six historical nuclear tests. Chapter 4 provides the details of the results and analysis from the comparison of the FDC using low and high resolution weather data and the comparison of the six nuclear tests using all four programs. Chapter 5 summarizes the results and provides recommendations for future research in nuclear fallout modeling.

## II. Theory and Literature Review

This section provides the theory and background critical to understanding the importance and relevance of this research. It provides a detailed summary of previous research supporting this thesis, the basic understanding of fallout, meteorological importance and the critical comparison tools used to evaluate the data.

### Summary of Previous Research

Research to improve current nuclear fallout mapping tools has increased since the terrorist attacks on September 11, 2001. Multiple students from the Air Force Institute of Technology's (AFIT) Graduate Nuclear Engineering Program have devoted their time and research to improving nuclear fallout mapping tools. This research is a continuation of four previous AFIT students; Chancellor [6], Pace [31], Jones [23] and most recently O'Day [30].

Chancellor's research showed that HPAC has potential but deviates from the DNA-EX contours. Chancellor digitized the DNA-EX contour plots allowing ease in future comparisons. Pace continued this research by implementing weather reanalysis data with resolution of 210 km and varying the terrain resolution. He concluded that high resolution terrain data produced a poorer match to DNA-EX than low or medium resolution data when the terrain resolution is greater than the weather resolution. Pace recommended for future research to implement high resolution weather data with high resolution terrain data which was taken on by Jones in 2007. Jones concluded that HPAC fails to include advection during cloud rise through its improper integration of the DELFIC cloud rise model. This led to O'Day developing the FDC that incorporates surface and low altitude winds. O'Day proved that the FDC accurately mapped nuclear

fallout data utilizing high resolution data. This research differs from the previous research discussed above through the comparison of the newly developed nuclear fallout modeling program, FDC, with low resolution weather data. Additionally, the DELFIC FPT and HYSPLIT were never compared; this research will compare these two programs with HPAC and the FDC.

### **Nuclear Fallout**

Nuclear fallout is produced from all atmospheric nuclear detonations. The pattern and dispersion of fallout depend on the weapon yield, height of burst, meteorological conditions and location of detonation. The following paragraphs provide a brief summary of the widely-accepted knowledge of this research.

Following a nuclear detonation, the fireball formed reaches a temperature in the range of  $10^7$  Kelvin, converting the contents into a gaseous form. Convective forces cause enormous amounts of debris to be drawn up into the fireball. The difference in temperature from the surrounding ambient air causes the fireball, including fission products and debris, to rise until it reaches temperature equilibrium with the atmosphere. As the cloud rises it expands and is cooled by convective and radiative cooling. As it cools it condenses into a cloud containing solid particles of radioactive material. Radioactive material can be volumetrically distributed or surface distributed depending on the condensation temperature of the radioactive material in comparison to the solidification temperature of the soil. If some of the radioactive material's condensation temperature is greater than the soil's solidification temperature then that portion of the radioactive material will be distributed volumetrically, else it will be distributed on the surface. This is known as chemical fractionation. The amount of radioactive material

produced depends on the type and design of the weapon, meteorological conditions, location of detonation and other factors.

The radioactive debris within the cloud is divided into two main categories, local (early) and global (delayed) fallout, depending on the height of burst and explosive yield. Local fallout consists of the larger particles, generally greater than 20  $\mu\text{m}$  in diameter [4:408], that fallout within 24 hours, depositing over an area up to several hundred miles from ground zero, and is intensely radioactive. Local fallout causes the greatest threat to the local population and consequence management operations. Global fallout consists of particles that are sufficiently small and behave somewhat like aerosols. Global fallout is influenced by dispersion and rainout and descends extremely slow over large areas of the earth's surface. It can remain in the atmosphere for over eight months. Currently, the lack of global atmospheric modeling and meteorological data limit the modeling of global fallout.

As stated in Glasstone and Dolan, if the height of burst in feet is above

$$H \approx 180W^{0.4}, \quad (1)$$

known as the fallout-safe HOB, where  $W$  is the yield of the weapon in kiloton [17:71], the only vaporized material within the cloud is from the bomb debris and therefore will result in no local fallout. Detonations that fall below this fallout-safe HOB will result in the fireball reaching the ground, causing soil and other materials to be engulfed in the fireball and vaporized. All nuclear tests studied in this research fall below this height.

DELFIIC assumes a pure airburst occurs when the height in feet is greater than

$$H = 180W^{1/3.4} \quad (2)$$



where  $W$  is the yield in kilotons. DELFIC assumes that pure airbursts usually do not produce local fallout [26:11]. Using DELFIC's definition of pure airbursts, historical tests Zucchini, Priscilla and Smoky are pure airbursts and may not produce local fallout. Chancellor, Pace, Jones and O'Day showed that all three tests produced fallout and will be studied in this research.

As the radioactive particles (fallout) descend to the surface they decay according to their isotopes' half-lives giving off ionizing radiation. The rate at which this ionizing radiation is absorbed during a specified time interval is known as the dose-rate. Dose-rates are dependent on the type of radioactivity and the way that it is distributed throughout the particle.

The majority of fallout modeling programs separate the calculations into a three step process; cloud rise and particle formation, particle settling and transport, and dose-rate calculations on the ground.

### **Cloud Stabilization Parameters**

As stated above the cloud continues to rise until the temperature of the cloud is in equilibrium with the surrounding environment. Different sized particles will rise to different altitudes. The vertical center of each particle group can be modeled as a normal distribution at cloud stabilization, represented by  $Z_c^g$ . Through the study of DELFIC calculations for 30 tests of yields ranging from 1 KT to 10 MT Hopkins empirically determined that the particle stabilization height in meters is

$$Z_c^g = C_1 - C_2 r_g$$

$$\ln(C_1) = 7.889 + 0.34[\ln(Y)] + 0.001226[\ln(Y)]^2 - 0.004227[\ln(Y)]^3 + 0.000417[\ln(Y)]^4 \quad (3)$$

$$\ln(C_2) = 1.574 - 0.01197[\ln(Y)] + 0.03636[\ln(Y)]^2 - 0.0041[\ln(Y)]^3 + 0.0001965[\ln(Y)]^4$$

where  $r_g$  is the particle radius in microns and  $Y$  is the yield in kiloton [19:129].

Connors determined that the spread of each particle group depends on size and yield through the analysis of DELFIC data [7:83]. He empirically described this distribution as

$$\begin{aligned} \Delta z_c &= I_d + 2r_g s_d \\ s_d &= 7 - e^{(1.78999 - 0.048249(\ln(Y)) + 0.0230248(\ln(Y))^2 - 0.00225965(\ln(Y))^3 + 0.000161519(\ln(Y))^4)} \\ I_d &= e^{(7.03518 + 0.158914(\ln(Y)) + 0.0837539(\ln(Y))^2 - 0.0155464(\ln(Y))^3 + 0.000862103(\ln(Y))^4)}, \end{aligned} \quad (4)$$

where  $r_g$  is the particle group radius in microns,  $s_d$  is the slope in meters per micron,  $I_d$  is the line intercept in meters and  $\Delta z_c$  is the vertical thickness from top to bottom of the particle group in meters. The standard deviation,  $\sigma_z$ , is calculated using Connors'  $\Delta z_c$ , where he assumed a  $2\sigma$  distribution about a point midway between the top and bottom of  $\Delta z_c$ ,

$$\sigma_z = \frac{\Delta z_c}{4}. \quad (5)$$

Following the assumption that the vertical distribution of activity is represented by a Gaussian distribution, 68% of the group's activity will be located within one standard deviation of the group's center and 99.7% will fall within three standard deviations. In this work the particle group's top,  $Z_{top}^g$ , in meters is taken as  $3\sigma$  above the particle group's center using

$$Z_{top}^g = Z_c^g + 3\sigma_z \quad (6)$$

and the particle group's bottom,  $Z_{bottom}^g$ , in meters is taken as  $3\sigma$  below the particle group's center using

$$Z_{bottom}^g = Z_c^g - 3\sigma_z. \quad (7)$$

### Particle Size Distributions

Many researchers have modeled the particle size distributions using different methods such as power laws, lognormal distributions or a combination of both. This research will use a lognormal distribution of

$$N(r) = \frac{N_t}{\sqrt{2\pi}\beta r} e^{-\frac{1}{2}\left[\frac{\ln(r)-\alpha_0}{\beta}\right]^2}, \quad (8)$$

where  $N(r)$  is the number of particles of radius  $r$  per unit radius,  $N_t$  is the total number of particles,  $\alpha_0$  is the natural logarithm of the median radius and  $\beta$  is the logarithmic standard deviation

Baker analyzed the accumulated fallout, both airborne and ground measurements, from over 100 nuclear test explosions. From his analysis he concluded that the majority of local fallout samples and particles suspended in the cloud samples within several hours demonstrated very different particle size distributions. He further concluded that the best model for the data is the sum of two lognormal distributions, where the total population of fallout particles,  $N(r)$ , is represented as

$$N(r) = N_1(r) + N_2(r), \quad (9)$$

where  $N_1(r)$  is the population of smaller-size particles and  $N_2(r)$  is the population of larger-size particles [2]. Through further analysis Baker determined that a lognormal distribution was the best fit, described as

$$N(r) = \frac{N_1}{\sqrt{2\pi}\beta_1} e^{-\frac{1}{2}\left[\frac{\ln(r-\ln(r_{m1}))}{\beta_1}\right]^2} + \frac{N_2}{\sqrt{2\pi}\beta_2} e^{-\frac{1}{2}\left[\frac{\ln(r-\ln(r_{m2}))}{\beta_2}\right]^2} \quad (10)$$

where  $r_{m1}$  is the median radius of 0.1 microns for the small particle group,  $r_{m2}$  is the median radius of 0.2 microns for the larger particle group, and  $\beta_1$  and  $\beta_2$  are the logarithmic standard deviations for the respective particle groups ( $\ln(2)$  and  $\ln(4)$  respectively).

### Particle Settling Velocity

Bridgman developed empirical functions for the calculations of the Reynolds number and the particle velocity for a sphere falling through air [2:408-409] using Davies relationships [8:259-270].

Each particle size will fall at different rates due to different terminal velocities and is assumed to instantly fall at that terminal velocity due to their extremely small sizes. Two methods are used to calculate the particles' terminal velocities. The terminal velocity of particles less than 10 microns (global fallout) is calculated using Stokes' Law while particles greater than 10 microns (local fallout) is expressed using aerodynamic drag as

$$\frac{1}{2}\rho_a v^2 C_d \pi r^2 = \frac{4}{3}\pi r^3 \rho_p g, \quad (11)$$

where  $\rho_a$  is the air density in kilograms per meters cubed,  $v$  is the terminal velocity of the particle in meters per second,  $C_d$  is the coefficient of drag,  $r$  is the particle radius in meters,  $\rho_p$  is the particle density in kilograms per meters cubed and  $g$  is the gravitational acceleration in meters per second squared.

From Davies, the Reynolds number,  $R_y$ , for spheres moving in a viscous media is

$$R_y = \frac{2v\rho_a r}{\eta}, \quad (12)$$

where  $\eta$  is the dynamic viscosity in kilograms per meters second. Combining Equations (11) and (12) results in

$$Q = R_y^2 C_d = \frac{32\rho_a \rho_p g r^3}{3\eta^2}. \quad (13)$$

Davies discovered that the Reynolds number is related to  $Q$  by the following two empirical relationships.

For  $Q < 140$

$$R_y = \frac{Q}{24} - 2.3363E(-4)Q^2 + 2.0154E(-6)Q^3 - 6.9105E(-9)Q^4 \quad (14)$$

and for  $100 < Q < 4.5E7$

$$\log_{10} R_y = -1.29536 + 0.986[\log_{10} Q] - 0.046677[\log_{10} Q]^2 + 0.0011235[\log_{10} Q]^3. \quad (15)$$

These equations are used to find the velocity by first calculating  $Q$  from Equation (13), then  $R_y$  from Equation (14) or (15) and finally the velocity from Equation (12) [4:409].

## **Concentration to Exposure Rate Conversion Factors**

Hicks studied offsite fallout from 13 devices detonated on steel towers 300-700 ft above the ground and three balloon shots during the time period of 1951-1957. He related the ground surface contamination of every radionuclide to the external gamma-ray exposure levels. In his calculations he included 152 fission products and 25 neutron-induced nuclides. He calculated the proper distribution of its fission products and defined the appropriate refractory and volatile mass chains. An averaged fractionation was allowed through the removal of a fraction of the refractory phase. The amount of radioactivity in curies was calculated for each of the fission products and neutron-induced nuclides as mentioned above as a function of time and the total for each decay time. Using the calculated activity in curies the exposure rate in milli-roentgen per hour was calculated for each of the fission products as a function of time and the total for each decay time. The total activity and exposure rate for all fission products and neutron-induced nuclides were combined and normalized to an external gamma-ray exposure rate of 1 milli-roentgen per hour at 12 hour post-shot. This was followed by fitting the total normalized micro-curies per meter squared and milli-roentgen per hour using the method of least squares. This led to the calculation of the ratio of micro-curies per meter squared to milli-roentgen per hour [18].

### **DNA 1251-1-EX**

DNA 1251-1-EX is the compilation of data from nuclear tests conducted in the Continental United States prior to 1963. DNA 1251-1-EX was extracted from DASA 1251: *Local Fallout from Nuclear Test Detonations, Volume 2: Compilation of Fallout Patterns and Related Test Data, Parts 1 through 3*. It provides unclassified reference of

test data, fallout patterns and wind data at ground zero in order to assist in the analysis of fallout effects. Table 1, outlines the data of the six tests used in this research.

**Table 1. DNA 1251-1-EX Selected Test Data**

Operation: Test	Date Time Group (Zulu)	Location (DD.MM.SS)		Yield (kT)	HOB (ft)
		Lat	Lon		
<b>Tumble Snapper: George</b>	011155Jun1952	37.02.53	116.01.16	15	300
<b>Teapot: Ess</b>	232030Mar1955	37.10.06	116.02.38	1	-67
<b>Teapot: Zucchini</b>	151200May1955	37.05.41	116.01.26	28	500
<b>Plumbbob: Priscilla</b>	241330Jun1957	36.47.53	115.55.44	37	700
<b>Plumbbob: Smoky</b>	311240Aug1957	37.11.14	116.04.04	44	700
<b>Sunbeam: Johnie Boy</b>	111645Jul1962	37.07.21	116.19.59	0.5	-2

The fallout patterns of George, Ess and Zucchini shown in DNA-EX were drawn from the readings taken by ground mobile monitors of the Radiological Safety Organization on the day of detonation. The fallout patterns of Priscilla and Smoky were obtained using actual decay data obtained by the University of California, Los Angeles School of Medicine's Atomic Energy Project. The fallout patterns of Johnie Boy were obtained by Reynolds Electrical and Engineering Company's (REECo) Rad-Safe Group's data taken on the day of detonation and by the Public Health Service on the day following detonation [11]. All fallout patterns given for each shot show the dose-rate contours in terms of one hour after the burst reference time three feet above the ground in units of roentgens per hour. Way-Wigner's  $t^{-1.2}$  approximation [35] was used to adjust the

measurements to the one hour reference time. The wind data gives surface and upper air winds for heights up to the nuclear cloud top. The meteorological data was taken in close proximity to ground zero but may not represent the wind data downwind from ground zero [11:2-3].

### **Weather Reanalysis**

One of the key elements required to accurately model nuclear fallout with any modeling program is accurate weather data. The weather collection equipment that was available during the period of 1952 to 1962, the focus of this research, was sparse when compared to today's equipment. With climatology studies becoming of increased importance due to the apparent climate changes occurring in the past two decades, the National Centers for Environmental Prediction (NCEP) and the National Center for Atmospheric Research (NCAR) began a 40-year weather reanalysis project in 1991 for the period of 1957 to 1996 [24:437]. This was later extended back to 1 January 1948.

The reanalysis project used the raw data collected over the specified time frame combined with today's weather forecast programs to create accurate gridded weather reanalysis data. The project used three major modules consisting of data decoder and quality control preprocessor, data assimilation module with an automatic monitoring system, and an archive module. The raw data was recovered from land surface, ship, rawinsonde, pilot-balloon observation (pibal), aircraft, satellite, and other data. During the period of 1952 to 1962 raw data was primarily obtained from rawinsonde, the most available source.

The first module, the data preprocessor, reformats the data coming from all available sources. The module preprocesses one or more years at a time prior to



executing the reanalysis module. This allows for quality control and detection of major data problems with enough lead time to take corrective action [24:443-444].

The second module, the data assimilation, is the central module consisting of multiple subroutines, including an analysis module and a six-hour prediction module. The analysis module is a spectral statistical interpolation routine which is a three-dimensional variational scheme. This system's implementation in 1991 led to major improvements in analysis and forecasts. The prediction subroutine implements the T62 model which is equivalent to a horizontal resolution of 210 km with 28 vertical levels. The model includes parameterizations of all physical processes, including convection, large-scale precipitation, shallow convection, gravity wave drag and boundary layer physics. Incorporated into the data assimilation module is a quality control subroutine to eliminate errors [24:444-448].

The final module, the archive module, outputs the data in multiple formats in order to satisfy the needs of all different types of users. This research uses a temporal resolution of six hours and an evenly spaced latitudinal and longitudinal spatial resolution. The weather reanalysis data used is a global grid of 73 x 144 points with each point detailing 17 pressure levels ranging from 1000 to 10 millibars. Additional data included are temperature, height, relative humidity, wind direction and speed [24:448-451]. Readers are referred to "The NCEP/NCAR 40-Year Reanalysis Project" for more detailed information.

### **Low and High Resolution Weather Data**

Low resolution weather data has a lower spatial and temporal resolution than high resolution weather data. The results of the reanalysis program are considered low

resolution weather data with a spatial resolution of 210 km and a temporal resolution of six-hours. Weather data easily accessible on the internet is considered low resolution. This research uses low resolution weather data consisting of 73 data points spread over 180 degrees in the latitudinal direction and 144 data points spread over 360 degrees in the longitudinal direction and a temporal resolution of six-hours. This is approximately 2.5 degrees between points equating to approximately 210 km.

The low resolution weather data used in this research is obtained from previous research conducted by Kevin Pace [31]. Pace obtained the weather reanalysis data from the National Oceanic and Atmospheric Administration's Operational Model Archive Distribution System's (NOMADS) website [28]. The appropriate weather data was downloaded as a GRiB file, a World Meteorological Organization format for Gridded Binary data. The GRiB format is one-half to one-third the size of normal binary files but non-meteorological sciences cannot read or use the contents without using GRiB-reading software. Pace used the WGRIB software from the National Weather Service Climate Prediction Center's website in order to decode the GRiB file for use as inputs to the modeling programs.

Christopher Jones converted the low resolution reanalysis weather to high resolution weather data using a FORTRAN based code from the Colorado State University Regional Atmospheric Modeling System (RAMS) software during his thesis research of *High Resolution Mesoscale Weather Data Improvement to Spatial Effects for Dose-Rate Contour Plot Predictions* [23].

The choice of the RAMS was due to the program's ability to capture mesoscale events such as mountain waves and Venturi effect, updrafts, convection and

microphysical processes in order to produce high resolution weather data. The program nests smaller models within boundaries of larger models in order to capture this effect. A detailed explanation of the RAMS is outlined in Jones' thesis [23].

The high resolution weather data produced consists of a spatial domain of 74 x 60 points covering 4.6 degrees latitude and 7.1 degrees longitude (approximately 7 km x 10 km spatial resolution) with a temporal domain of one-hour and 11 pressure levels.

## HPAC

HPAC, developed by DTRA, is a modeling tool developed for the military in order to model atmospheric dispersion. HPAC allows the military to model the release of radiological, chemical and biological agents, enabling quick responses to threats of weapons of mass destruction. This research uses HPAC version 5.0 Service Pack 1 and the Nuclear Weapon Special Edition (NWPNSE) Model.

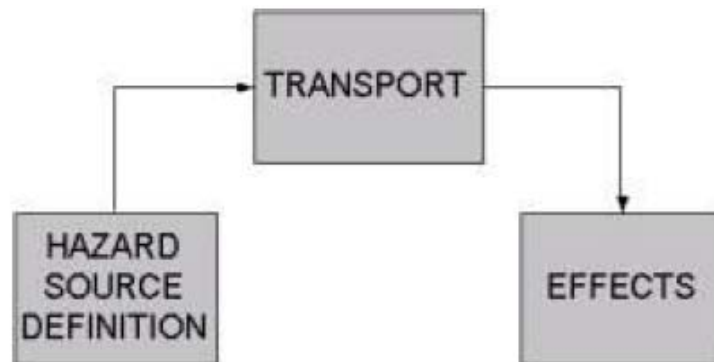


Figure 1. HPAC's Three Step Modeling Process

HPAC uses the three step process in modeling nuclear fallout shown in Figure 1 [12:23]. The first step is the hazard source definition which begins with user inputs of weapon yield, HOB and the fission fraction. These inputs are internally translated into

the technical data required to complete the calculations. The technical data defines one or more puffs of hazardous material used in internal algorithms in order to model the stabilized nuclear cloud which includes height, activity and particle size distribution. For surface bursts HPAC has the option of implementing the DELFIC cloud rise model with observed atmospheric data and a one-dimensional integration scheme in order to model the cloud height. The other option of modeling cloud height is based on a parameter fit to nuclear test data [12:507].

The second step in HPAC's modeling process is the atmospheric transport step. HPAC's transport model is the Second-order Closure Integrated Puff (SCIPUFF) model which is an advanced Lagrangian, Gaussian puff model that uses second-order turbulence techniques. The transport step implements environmental data including weather, terrain and land cover in order to calculate the downwind transport and surface deposition [12:31-32].

The final step is the effects model. The transport model calculates the deposition of the hazardous material on the ground and then HPAC will display the results on a map. Depending on user-defined inputs HPAC will compute dose-rates or integrated doses.

## **HYSPLIT**

HYSPLIT was designed for response to atmospheric emergencies. It is a complete modeling system for computing simple air parcel trajectories to complex dispersion and deposition of particles originating from single or multiple source locations. It is ideal for single point sources but is not as efficient for multiple source locations. HYSPLIT was not developed to model fallout deposition and does not simulate the dynamics leading up to the stabilization of the cloud or the radioactivity of a

particular particle size. In terms of the other studied programs, HYSPLIT is a two step modeling process implementing particle settling and transport followed by ground deposition. HYSPLIT does not include the cloud rise and particle formation. To accurately model fallout deposition, HYSPLIT can be used by assuming a reasonable distribution of particles and particle sizes throughout the stabilized cloud. In order to effectively implement this method, multiple simulations are run to transport a range of particle sizes over various altitudes and combining the particle depositions to approximate the total fallout deposited. Utilizing this method, HYSPLIT was proven to be effective in simulating the dispersion and deposition of radioactive fallout when satisfactory meteorological input data is used according to *Predictions of Dispersion and Deposition of Fallout from Nuclear Testing using the NOAA-HYSPLIT Meteorological Model* [25:252-253].

HYSPLIT uses three methods to calculate air concentrations; three-dimensional puff, three-dimensional particle modeling or a combination of both approaches. The puff model simulates the release of pollutant (radioactive) puffs at regular intervals. It is a three-dimensional cylinder with a growing concentration distribution in the vertical and horizontal (puffs may split if they become too large). The puff can be defined as a Gaussian or Top-Hat horizontal distribution and is represented by a three-dimensional cylinder with a growing concentration distribution in the vertical and horizontal. The Top-Hat uses a  $1.54\sigma$  standard deviation and the Gaussian uses a  $3\sigma$  standard deviation. Each puff contains an appropriate fraction of the pollutant and is advected according to the trajectory of its center position. The model simulates the puff expanding in time to account for dispersion. The air concentration is computed by a point from the puff. The

particle mode simulates the release of multiple particles. This approach allows a cluster of particles released at the same time to expand in space and time. This method calculates the air concentrations from the dispersal of an initial fixed number of particles [14:296]. A combination of the puff and particle approach is a circular two-dimensional object (having zero depth). The horizontal contamination is characterized by a puff distribution and the vertical is characterized using the particle mode. This research will initially utilize a three-dimensional particle mode. This method calculates the position as a function of the wind direction and speed combined with turbulence.

HYSPLIT incorporates gridded meteorological data at regular time intervals. This data is inputted through the output of meteorological models. The data is then interpolated to an internal terrain-following sigma coordinate system. HYSPLIT does allow limited user-defined wind data.

### **DELFIIC Fallout Planning Tool**

DELFIIC predicts local fallout from nuclear explosions in the range of 0.001 to 100,000 KT, with HOB ranging from shallow sub-surface to fallout-safe airbursts. DELFIIC is highly flexible, allowing multiple user-input options. It models cloud rise, growth and stabilization with a dynamic model treating the cloud as an entraining bubble of hot air with water and contaminated ground material. The fallout particle cloud and stem are formed during the cloud rise [26:7]. At cloud stabilization, the cloud is defined as functions of particle size and space above and downwind of ground zero. Each particle group is represented by cylindrical disks which represent uniformly loaded layers [22:41].

The user may define the particle size distribution from three options; lognormal distribution of the number of particles with respect to diameter, a power law distribution of particle mass fraction with respect to diameter or an arbitrary distribution of mass fraction with respect to diameter.

The user defines the type of atmospheric profile as a single vertical wind profile or a varying wind profile. DELFIC tracks the fallout parcels dispersing in the horizontal due to ambient turbulence. Two methods of transport are available, layer by layer and a quick method. The layer by layer method computes transport through each vertical wind field in a stepwise manner. The quick method computes transport in single steps from initial points to impact. Activity is calculated by summing exposure or exposure rate from all nuclides in a decay chain. Twelve different types of fission reactions may be specified [26].

The Fallout Planning Tool is the interface, developed by Oak Ridge National Laboratory (ORNL), allowing the user to define the nuclear test data, meteorological conditions, fission reaction, soil type etc. The FPT interface has 18 different output maps that can be displayed using Goggle Maps. An additional feature of the FPT allows the user to interactively define travel routes for planning damage assessments or forensics' collection missions. The FPT will calculate the estimated accumulated dose of the team executing the routes.

### **Fallout Deposition Code**

The FDC was developed following intense research of nuclear fallout modeling programs, especially HPAC. Buck O'Day developed the FDC in 2009 during his thesis research. Overall the FDC follows the three step modeling process consisting of multiple

modules per step. Figure 2 shows the modules that make up the FDC [30:47]. The FDC implements a Particle Radius Module that creates 100 equal activity particle size groups using internal algorithms and assuming 100 percent volumetrically distributed activity. The calculated particle radii are imported into the Initialize Cloud Module which models the initial stabilized cloud and particle distribution for transport. The Transport Module uses the calculations from the Winds and the Initialize Cloud Modules and executes a wafer tossing routine. These modules combined with other minor modules, including the Time Step and Fall Modules, enable the Main Program to calculate the dose-rate contours.

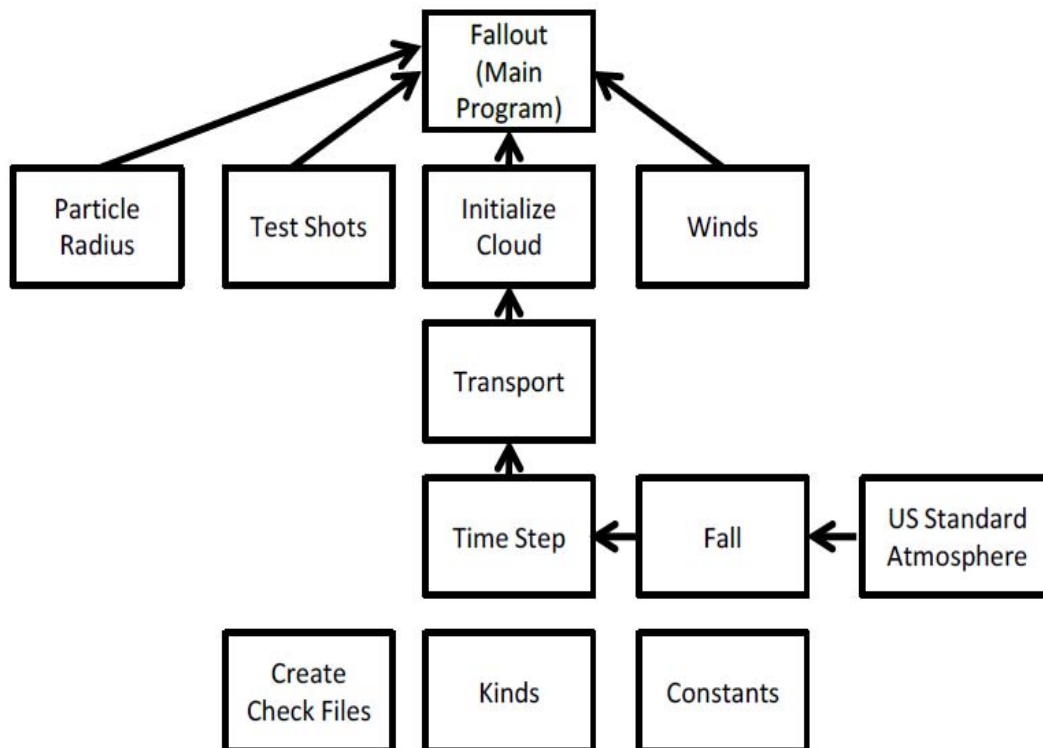
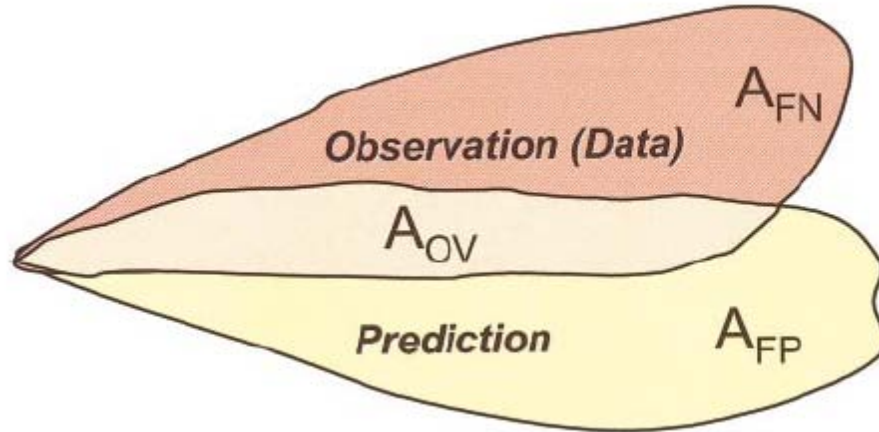


Figure 2. Fallout Deposition Code Framework



## Measure of Effectiveness



**Figure 3. MOE Areas of Comparison**

The comparison of the observed data (AOB) and the predicted data (APR) is conducted using the Warner and Platt's Measure of Effectiveness (MOE) method. In order to provide the most effective means of comparison, the area of overlap (AOV), the area of false negative (AFN) and the area of false positive (AFP) were identified and compared between models, an example is shown in Figure 3 [34:59]. In order for an area to be considered an AOV, the observed and predicted data must have at least one point of commonality. When two models are identical, their AOV is

$$AOV = APR = AOB. \quad (16)$$

An AFP occurs when the predicted data indicates an effect (dose-rate) and the observed indicates no effect. An AFN occurs when the predicted data indicates no effect and the observed indicates an effect. For this research all models will have at least one point of commonality which is the release point. When two models are correctly aligned, they are numerically compared using

$$MOE = (x, y) = \left( \frac{AOV}{AOB}, \frac{AOV}{APR} \right) = \left( \frac{AOB - AFN}{AOB}, \frac{APR - AFP}{APR} \right) \quad (17)$$

The  $x$  and  $y$  coordinate are plotted on a graph with axes ranging from zero to one, where  $(0,0)$  indicates no overlap and  $(1,1)$  indicates identical models as shown in Figure 4 [34:60].

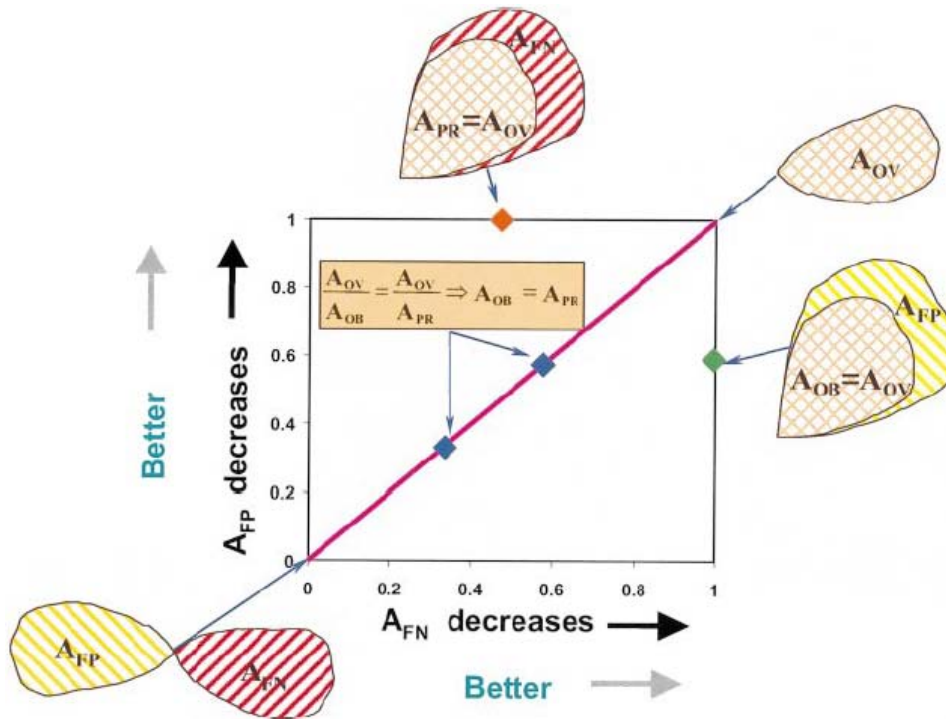


Figure 4. Numerical Comparison of Models

The MOE allows the simultaneous comparison of two or more models against a known benchmark or standard as shown in Figure 5 [34:60]. However, difficulty arises when comparing more than two models. If one model's AFP is equal to another's AFN the researcher must determine which is more important. A way to reduce this issue is the use of the Normalized Absolute Difference (NAD); it gives numerical merit to compare two similar models.

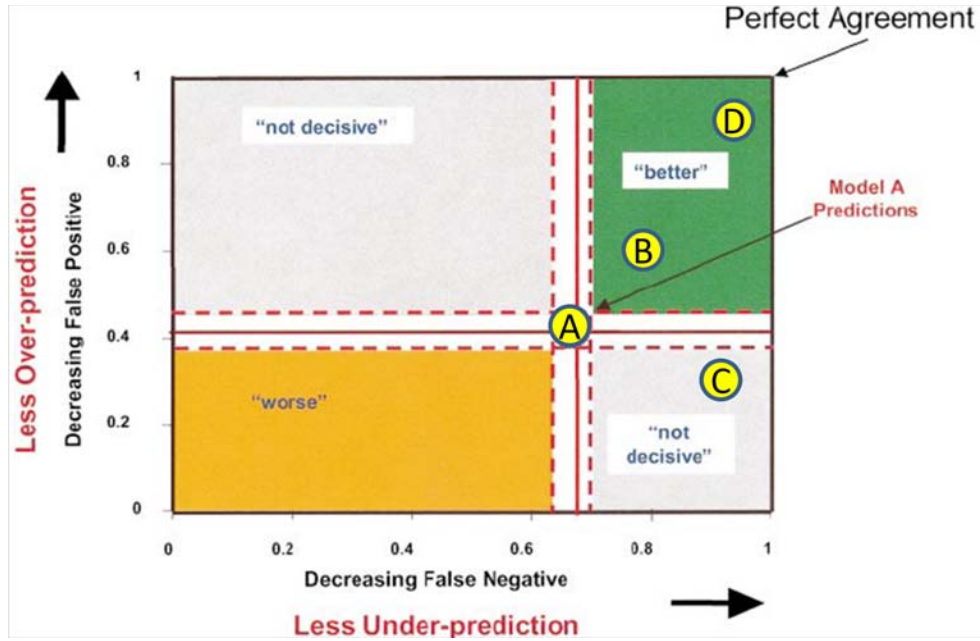


Figure 5. Example of a Comparison of Four Programs

### Normalized Absolute Difference

The NAD is implemented in this research in order to characterize the differences between observed and predicted quantities. The closer the model is to the predicted quantities the smaller the distance is between the MOE and the predicted. This distance, normalized is the NAD and can be used as a standard metric. A plot of isolines of various NADs is shown in Figure 6 [34:63]. The NAD allows the more important values (AFP or AFN) to be weighted, currently both are weighted equally. The equation for the NAD is

$$NAD = \frac{AFN + AFP}{2AOV + AFN + AFP} = \frac{x + y - 2xy}{x + y}. \quad (18)$$

The smaller the NAD the more accurately the predicted represents the observed.

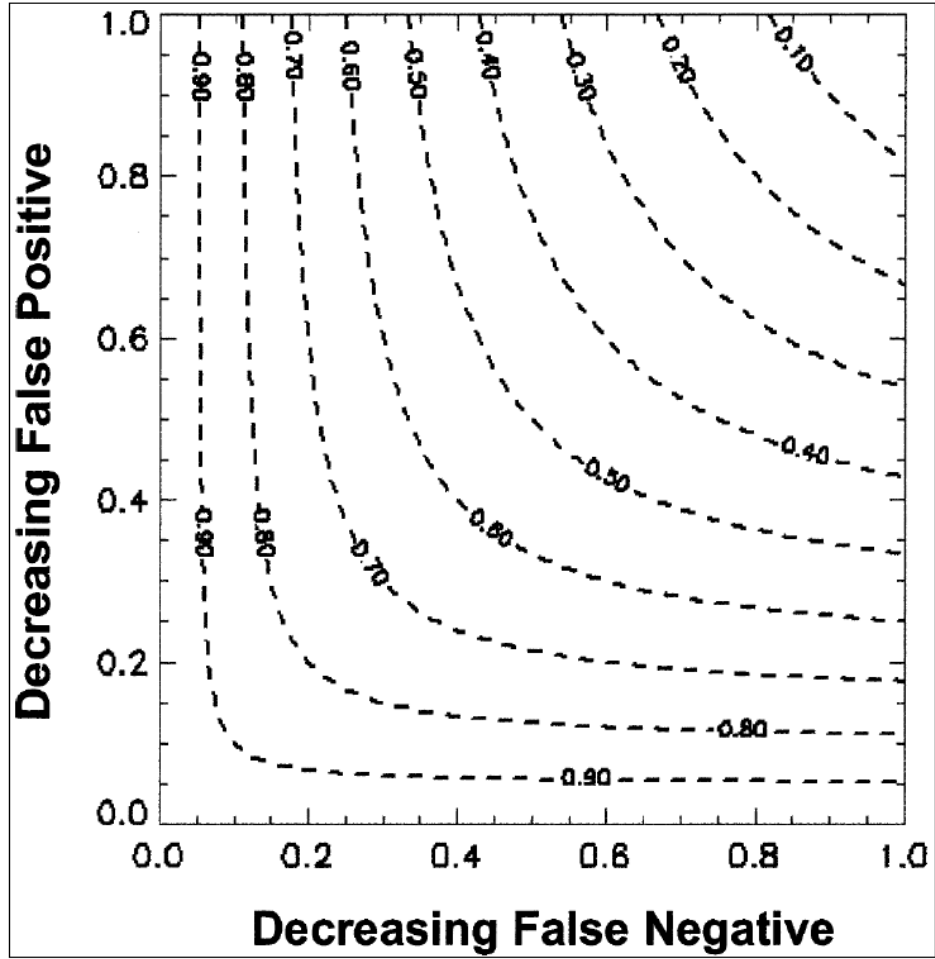


Figure 6. Isolines of Various NADs

### III. Methodology

This section provides a brief overview of the methodology used in this research.

Figure 7 shows the schematic diagram of this methodology.

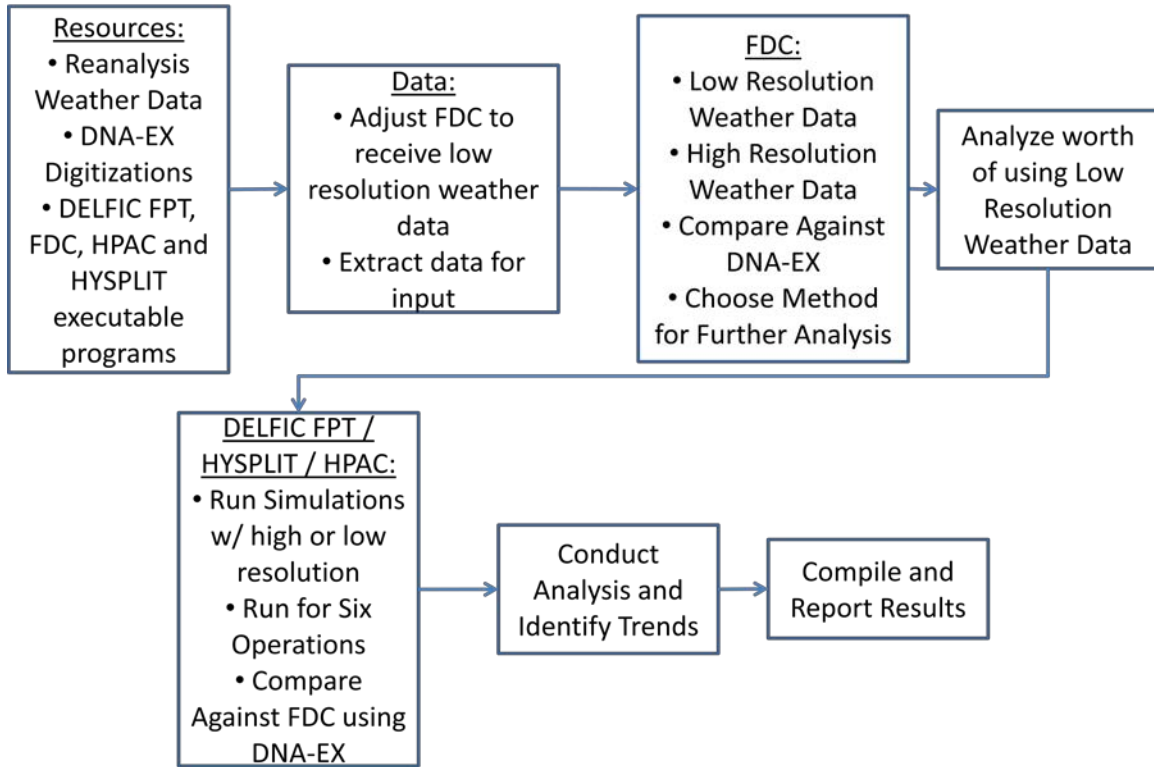


Figure 7. Problem Solving Methodology

The process starts with a comprehensive literature review in order to gain the knowledge and understanding of nuclear fallout, weather reanalysis data and the four nuclear modeling programs; HPAC, HYSPLIT, DELFIC FPT and FDC. Additionally, the required resources including the meteorological reanalysis data and the DNA-EX digitizations are acquired. The formats of the modeling programs' inputs and outputs are thoroughly analyzed and the necessary data is extracted and reformatted from the

acquired data to allow for input into the modeling programs. The process continues with adjustments made to the FDC to allow for low resolution weather reanalysis inputs.

Following the revisions of the FDC, the six nuclear tests shown in Table 1 are run using the FDC with low resolution reanalysis weather data as inputs. An additional six runs are completed utilizing the FDC and high resolution weather data. The twelve dose-rate contours are compared to the numerical dose-rates of the digitized contours developed by Chancellor [11] using the Warner and Platt's MOE [34] and the NAD. The objective for this part of the research is to potentially reduce computing time by using low resolution versus high resolution weather data. Additionally, using low resolution data allows for a more effective comparison due to the limitation of inputting high resolution weather data into HYSPLIT.

HPAC, HYSPLIT and the DELFIC FPT are run with the inputs from the same six historical nuclear tests. Appropriate calculations of the source term used for modeling fallout with HYSPLIT as well as the calculations for merging weather reanalysis data for use in the DELFIC FPT are conducted prior to running the programs. The contours are analyzed and again compared utilizing the Warner and Platt's MOE and NAD.

### **DNA-EX Extraction**

Chancellor extracted a digital format of the DNA-EX contour data using the Canvas software [5]. First a copy of the DNA-EX contours oriented with north at the top and east to the right is converted to a digital image. This is achievable due to each square mile in the DNA-EX plots representing a scaled area of the paper which is then represented by 9 pixels in the digital format (three pixels per linear mile). The digital image is created in grayscale, allowing for the assignment of a scalar value, representing

its darkness, ranging from zero to 255 to each pixel. The Canvas software exports the digital image as a table of values; a square matrix filled with values of the individual pixel's grayscale value. The lowest dose-rate contour is represented by a pixel value of 225 and the higher dose-rate contours by lower values (darker values) [6:70-71]. Each test has six to seven contours as seen in the DNA-EX. A FORTRAN95 program is developed in order to extract the DNA-EX files into a  $M \times M$  square matrix, where  $M$  is the number of kilometers from ground zero in each cardinal direction, with values containing the actual dose-rate in roentgen per hour at each point. All tests are compared against this extracted data.

### **FDC Adjustment and Data Extraction**

The FDC was developed specifically for the six nuclear tests listed in Table 1 and for the use of high resolution reanalysis weather data. A thorough analysis of the code is conducted line by line in order to revise the parameters to allow for low resolution reanalysis weather data. The major internal parameters requiring adjustment are the spatial limits and FORTRAN Do Loops. The input files required to run the FDC are the ground zero wind data (obtained from DNA-EX), the  $x$  and  $y$  grid points for each weather data location, the vertical heights that weather data is provided for and the  $u$  and  $v$  components calculated from the wind speed and direction. The data input files for the FDC are created through the development of a FORTRAN95 program to extract the appropriate data from the low resolution reanalysis weather file (.prf file).

### **Low and High Resolution Weather Inputs**

Using two versions of the FDC, one revised for low resolution and one for high resolution weather data, the dose-rates at one hour after detonation are calculated for the

six nuclear tests listed in Table 1. The results from the program are the dose-rates listed in a  $M \times M$  square matrix, the same size as the extracted DNA-EX data, where  $M$  is the number of kilometers in each cardinal direction from ground zero. This allows for a point-to-point comparison between the DNA-EX and the FDC matrices. A FORTRAN95 program is developed to calculate the NADs for each test with comparison to the DNA-EX contours.

The calculated NADs for each test using both low and high resolution weather data are compared. A lower NAD more accurately depicts the DNA-EX data. A visual analysis is also conducted to determine subjectively if low resolution weather data is sufficient to compare the remaining programs. It is believed that low resolution weather data will be sufficient and therefore reduce computing time.

### **HYSPLIT Source Term**

In order to model nuclear fallout with HYSPLIT a source term is calculated for the input parameters. The majority of the required inputs for HYSPLIT are weather data, the top and bottom vertical heights of the cloud (or particle group vertical range), the emission rate, the emission time and the fall velocity.

The weather data is retrieved through an internal process in HYSPLIT. The Meteorology section in HYSPLIT allows for meteorology data to be downloaded from the Air Resources Laboratory's website. The option of downloading reanalysis weather data is available by downloading a month of reanalysis data at a time. This reanalysis data is the same as the reanalysis weather data used from Pace and again in this research for low resolution reanalysis weather data. HYSPLIT has a limited capability of user



defined weather; however that option was not effective for this research. All HYSPLIT trials are run using low resolution reanalysis weather data.

HYSPLIT requires inputs for the top and bottom of the cloud but is not able to transport multiple sized particles in the same run. In order to accurately model nuclear fallout the stabilized cloud is divided into 20 equal activity particle groups and modeled in HYSPLIT using 20 different runs. The results are summed at the end of the 20 runs in order to represent one test case. This research uses O'Day's Particle Radius Module which is a modification of a program that Garcia developed to create 100 equal-activity particle size groups using the larger particle distribution and parameters from Baker's bimodal distribution [16:87]. The program assumes volumetrically distributed activity.

The particle radii are calculated by solving the cumulative distribution function of

$$F(x) = \int_0^x \frac{1}{\sqrt{2\pi}} e^{-\frac{1}{2}(x')^2} dx' \quad (19)$$

where

$$x' = \frac{\ln(r) - \alpha_3}{\beta}$$

$$\alpha_3 = \alpha_0 + 3\beta^2$$

$$\alpha_0 = \ln(0.2)$$

$$\beta = \ln(4.0)$$

To approximate the solution the following computational algorithm is used [1:932]:

$$F(x) = 1 - \frac{1}{2} \left[ 1 + 0.196854x + 0.115194x^2 + 0.000344x^3 + 0.019527x^4 \right]^{-4} \quad (20)$$

Each group's vertical center,  $Z_c^g$ , is calculated using Hopkins' empirical fit shown in Equation (3). Using Conners' standard deviation,  $\sigma_z$ , the particle group's top and bottom are calculated using Equations (6) and (7). Additional trials of one and two standard deviations are studied using test case George in order to determine that the three standard deviation model is the best approximation. The additional calculations are conducted using

$$\begin{aligned}
 Z_{top}^g &= Z_c^g + \sigma_z \\
 Z_{bottom}^g &= Z_c^g - \sigma_z \\
 Z_{top}^g &= Z_c^g + 2\sigma_z \\
 Z_{bottom}^g &= Z_c^g - 2\sigma_z.
 \end{aligned} \tag{21}$$

The emission time is calculated using the approximation that the cloud stabilizes in 6 to 8 min. This research uses the average time of 7 min. An additional trial is run using a 10s emission time, simulating that activity is released immediately following detonation, in order to compare results.

An approximated emission rate uses the estimation of the average total activity of  $5.30 \times 10^8$  gamma curies per kiloton of fission yield at one hour after burst [17:454]. Using the approximation of 20 equal activity groups the total activity is divided over 20 equal groups. HYSPLIT requires an input for emission rate in units per hour and an additional input of the total time of emission. In order to calculate the emission rate the total activity is divided by the emission time. This ensures that the total amount of activity at one hour is released in 7 min. An example calculation for test case George is

$$\left( \frac{5.3E8 \frac{\text{curies}}{KT} * 15KT}{20 \text{ groups}} \right) / \left( 7 \text{ min} * \frac{1hr}{60 \text{ min}} \right) = 3.40714E9 \frac{\text{curies}}{1hr}.$$

This value is used as the emission rate input for each of the 20 runs required to model one trial of George. When using this approximation the output in HYSPLIT is the ground concentration in units of curies per square meter. In order to convert these units to the gamma-ray exposure levels in roentgens per hour this research uses Hick's calculation of  $126 (\mu\text{Ci}/\text{m}^2)/(\text{mR}/\text{hr})$  at 24 hr post-shot, 1 m above unfractionated, unshielded fission products spread uniformly over a plane surface [18].

The final calculation is the fall velocity. This research uses Bridgman's particle settling routine [2:408-409] by first calculating  $Q$  from Equation (13), then  $R_y$  from Equation (14) or (15) and finally the velocity from Equation (12).

## **HYSPLIT**

Using the test data for George, multiple trials are run to compare results for future trials. The trials studied are listed in Table 2.

**Table 2. HYSPLIT Trials**

<b>George</b>
HYSPLIT 1 $\sigma$
HYSPLIT 2 $\sigma$
HYSPLIT 3 $\sigma$
100 Groups
3 Source Points
10s Emission Duration
Hybrid Gaussian Distribution
<b>Various Emission Rates (Ci/hr)</b>
1.00E+04
1.00E+06
1.00E+08
3.41E+09
1.00E+12

All trials were run using an emission rate derived from the average gamma activity of 5.3E8 curies/KT at one hour after the detonation except for the study of the varied emission rates. All trials' results were converted to roentgens per hour using Hick's approximation of  $126 (\mu\text{Ci}/\text{m}^2)/(\text{mR}/\text{hr})$  at 24 hr post-shot, 1 m above unfractionated, unshielded fission products spread uniformly over a plane surface [18].

The most effective vertical distribution model ( $1\sigma$ ,  $2\sigma$  or  $3\sigma$ ) is determined by comparing the NADs calculated when compared to the DNA-EX contours. The remaining trials are run using the best fit vertical distribution. Additional trials include one trial using 100 groups versus 20 groups. This trial requires the summation of 100 separate HYSPLIT runs to represent one test case. A trial using three point sources, the top of the cloud, the bottom of the cloud and the center of the cloud is run to understand how HYSPLIT is incorporating the top and bottom of the cloud. One trial is run varying

the emission time to simulate that the release of radioactivity occurs immediately after detonation using a 10 second emission time. HYSPLIT allows the option of using particles, puffs or a combination to determine emissions. Two options were studied, the 3-D particle mode in the horizontal and vertical and Gaussian in the horizontal and particle in the vertical. The final trials using George are run varying the emission rate to ensure that the same geographical area is covered for all emission rates and only the ground concentration changes.

Following the study of George, trials were run using the data for the remaining historical tests and the parameters producing the best results for George. A 10s emission rate is more realistic than a 7 min emission rate because radioactive particles begin to settle out of the cloud immediately following detonation, therefore five additional trials were run using a 10s emission rate with the data from the remaining five historical tests. Hicks' calculations were calculated using Beck's conversion factors which were calculated using the beta activity [3] and therefore two additional trials were run using the beta activity at one hour after detonation of  $4.3492E8$  curies per kiloton and a conversion factor of  $0.048 \text{ curies/m}^2$  per  $R/hr$  for George and Zucchini. These values were obtained from Dr. Vincent Jodoin using ORIGEN.

### **DELFC FPT Weather Input**

A Kriging method is used to incorporate the reanalysis weather data when running the DELFC FPT due to the limitations of the weather input in DELFC, and ultimately the DELFC FPT. DELFC limits the input of weather data to account for change in temporal domain only.

DELFIIC requires that the vertical heights do not vary for each time input. However, not all vertical heights are required for each input. To fulfill all the requirements of DELFIIC a FORTRAN95 program is written to average the reanalysis weather data at the various latitudes and longitudes for each vertical height during each of the six hour time periods using an inverse-distance weighted spatial Kriging routine similar to O'Day's Wind Module. The program reads in the weather data from the weather reanalysis file (.prf file) and immediately converts the wind direction and speed into its  $u$  and  $v$  components. The weighted average is calculated for each of the six hour time intervals. The program follows the path of the wind at each vertical height with an initial starting position at ground zero (0,0). The  $u$  and  $v$  components of each point surrounding the exact position of the path at each time is weighted,  $w_i^j$ , using

$$w_i^j = \frac{\frac{R_{\max}^j - R_i^j}{R_{\max}^j R_i^j}}{\sum_{i=1}^n \frac{R_{\max}^j - R_i^j}{R_{\max}^j R_i^j}} \quad (22)$$

where  $R_{\max}^j$  is the distance (radius) from the furthest point at time  $j$ ,  $R_i^j$  is the distance from point  $i$  at time  $j$ , and  $n$  is the total points. The final  $u$  and  $v$  components at each time interval for each vertical height is then calculated using

$$\begin{aligned} u_k^j &= \sum_{i=1}^n w_i^j u_i^j \\ v_k^j &= \sum_{i=1}^n w_i^j v_i^j. \end{aligned} \quad (23)$$

The new position for the next time step is calculated using the  $u$  and  $v$  components from the previous time step using

$$\begin{aligned}x_k^j &= x_k^{j-1} + u_k^{j-1} * 6hr \\y_k^j &= y_k^{j-1} + v_k^{j-1} * 6hr\end{aligned}\tag{24}$$

where  $x_k^j$  is the position's  $x$  coordinate at time  $j$  and vertical height  $k$ , and  $y_k^j$  is the position's  $y$  coordinate at time  $j$  and vertical height  $k$ .

### DELFIPT

In addition to using the weighted averaged in space reanalysis weather data, the weather data at ground zero recorded in the DNA-EX was used. Multiple trials were run for each test case varying the length of time the ground zero winds were used combined with the average reanalysis weather data in order to provide the best models. The average time the ground zero winds should be considered can be calculated by estimating that ground zero is located midway between spatial points and using the spatial resolution of 210 kilometers with wind speeds ranging from approximately 5 to 35 m/s. These calculations result in ground zero winds being considered between approximately 30 minutes to six hours, an example calculation of this approximation is shown below.

$$\left(\frac{210km}{2} * \frac{1000m}{km}\right) / \left(\frac{5m}{s} * \frac{3600s}{hr}\right) = 5.8hr\tag{25}$$

Table 3 outlines some of the trials studied. The DNA-EX document provides two data sets of ground zero winds for some of the test cases; the second data set is label as GW2 in Table 3. Two separate ground zero wind data sets were provided for Priscilla, Smoky and Johnie Boy at different times.

**Table 3. DELFIC FPT Trials**

<b>George</b>
Avg Reanalysis Weather Data (PRF)
Ground Winds (GW)
GW (2 hr) – PRF
<b>Ess</b>
Avg Reanalysis Weather Data (PRF)
Ground Winds (GW)
GW (.5 hr) – PRF
<b>Zucchini</b>
Avg Reanalysis Weather Data (PRF)
Ground Winds (GW)
GW (1.5hr) – PRF
GW (2hr) – PRF
<b>Priscilla</b>
Avg Reanalysis Weather Data (PRF)
Ground Winds (GW)
GW1(4hr) – GW2
GW (4hr) - GW2(.5hr) – PRF
GW (4hr) - GW(3.5hr) – PRF
<b>Smoky</b>
Avg Reanalysis Weather Data (PRF)
Ground Winds (GW)
GW1(3hr) – GW2
GW1(3hr) - GW2(1hr) – PRF
GW1(3hr) - GW2(.5hr) – PRF
<b>Johnie Boy</b>
Avg Reanalysis Weather Data (PRF)
Ground Winds (GW)
GW1(1hr) – GW2
GW1(1hr) - GW2(5hr) – PRF



## HPAC

HPAC has multiple settings that can be manipulated depending on the knowledge of the user. Aside from the location, time, event characterization, terrain and weather the remaining settings are set as the default settings. HPAC allows for different resolutions for the terrain data, this research runs two trials per test case varying the terrain resolution by 900 and 3500 which breaks up the geographical area in 900 and 3500 equal sized rectangles. A third trial is run using no terrain. Readers can refer to Pace for additional terrain resolution studies [31]. HPAC accepts Pace's and Jones' weather reanalysis data without any modifications.

## Comparison

Comparing HYSPLIT, HPAC, DELFIC FPT and FDC is a three step process which includes running the simulations using the various modeling programs and trials, converting the programs' outputs to the same format as the extracted DNA-EX data and numerically comparing the converted files using Warner and Platt's MOE and NAD.

HYSPLIT, HPAC and DELFIC FPT produce contours visually and numerically. In order to accurately compare all programs this research uses the numerical output and plots all programs' dose-rate contours using the same program developed in MATLAB.

A FORTRAN95 program is developed for each program containing one module to extract the numerical dose-rates and fill a  $M \times M$  array, where  $M$  is the number of kilometers from ground zero in each cardinal direction. This is the same size array as the DNA-EX array allowing for a point-to-point numerical comparison. All dose-rates are converted to roentgens per hour using the appropriate conversion factors and normalized to one hour after burst using Way-Wigner's  $t^{-1.2}$  approximation [35] except for HYSPLIT

dose-rates. The HYSPLIT source term was derived using the average gamma activity at one hour and therefore does not require normalization to one hour. The output of this module is then fed into the MOE Module which calculates the numerical comparisons.

The initial numerical comparisons are done by reading the dose-rates into the MOE Module and converting any value greater than the threshold (the lowest contour seen in the DNA-EX plots) to a value of one and the remaining to a value of zero. The same process is done for the data extracted from the modeling programs and the DNA-EX data. Following the data read-in, a point-to-point comparison is done. If both values have a value of one then that is considered an area of overlap. If the DNA-EX data has a value of one and the program file a value of zero then that is an area of false negative. If the program file has a value of one and the DNA-EX data a value of zero then that is an area of false positive.

A second comparison is done using the best model from each modeling program for each test case and comparing the individual contours. The data extracted from the modeling programs and the DNA-EX data is read-in and again numerically compared using a point-to-point comparison. This time each contour was compared starting with the lowest contour. All values less than the lowest contour are considered for the comparison of that contour. During these trials the *AFN* and *AFP* are not defined and only points where both the DNA-EX data and the program data have values less than or equal to the contour being studied are considered. Following the point-to-point comparison the NAD is calculated using Equation (18). This process continues for each contour using a similar process. For all contours greater than the lowest contour value

only those values (dose-rates) that fall between the one contour lower than the contour being studied and the contour value being studied are considered.

## IV. Results and Analysis

This chapter discusses the visual and numerical comparisons of the results from the trials discussed in the previous chapter. This chapter will first discuss the results of each of the six historical tests using the different programs and then the overall results of each test when comparing programs.

### FDC

The Fallout Deposition Code was successfully revised to accept low resolution weather reanalysis data. In order to accurately compare high versus low resolution the same limits are used. For each case the limits to the east, west, north and south are determined through the calculation of the limits of the DNA-EX contours, the limits of the overall area that weather was provided and  $M$  kilometers from O'Day's defined  $M \times M$  matrix. The parameter with the lowest limit in each cardinal direction becomes the limits for comparison. The area covered with low resolution data was larger than the area covered with high resolution data, therefore the high resolution limits were used in the overall calculation of the limits for comparison of the FDC only. The calculated NADs resulting from the use of both low resolution and high resolution weather data are shown in Table 4. Utilizing high resolution data provides better results in four of the six cases as expected. Low resolution data provides better results in the modeling of Smoky and Johnie Boy. This occurred due to the larger area between weather data points and a larger period of time elapsing prior to adjusting the wind speed and direction allowing for more dispersion which increased the area of overlap in these two specific cases. Analyzing the results, the maximum difference between NADs is seen in Ess and Priscilla with a difference of 0.12, the remaining tests' differences are shown in Table 5.

**Table 4. FDC Results for Low and High Resolution Reanalysis Weather**

	High Resolution			Low Resolution		
	MOEx	MOEy	NAD	MOEx	MOEy	NAD
<b>Ess</b>	0.26	0.86	0.60	0.17	0.70	0.72
<b>George</b>	0.90	0.95	0.08	0.88	0.93	0.09
<b>Zucchini</b>	0.90	0.86	0.12	0.90	0.79	0.16
<b>Priscilla</b>	0.49	0.72	0.42	0.41	0.51	0.54
<b>Smoky</b>	0.49	0.71	0.42	0.58	0.67	0.38
<b>Johnie Boy</b>	0.41	0.80	0.46	0.57	0.87	0.31

**Table 5. NAD Difference between Low and High Resolution Data**

Test	NAD Difference
<b>Ess</b>	0.12
<b>George</b>	0.02
<b>Zucchini</b>	0.04
<b>Priscilla</b>	0.12
<b>Smoky</b>	-0.04
<b>Johnie Boy</b>	-0.15

With better NADs in two of the six cases and low differences in two of the four cases further analysis is conducted using a visual comparison. The high and low resolution contours along with the DNA-EX contours are shown in the following figures with north oriented to the top of the page.

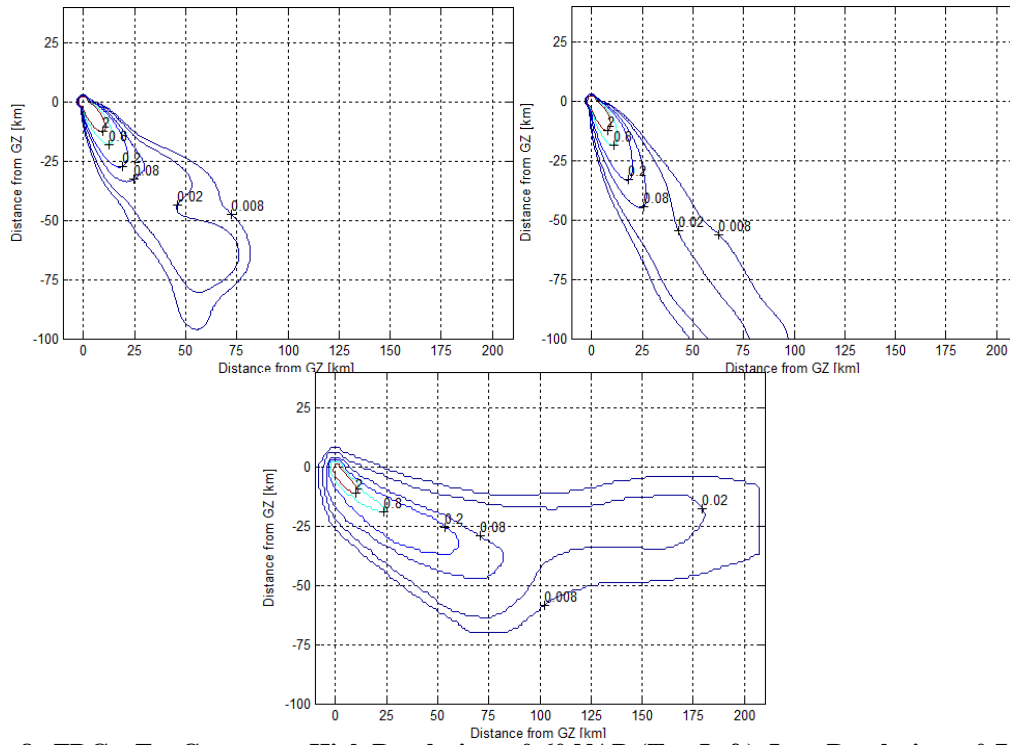


**Figure 8. FDC – Ess Contours: High Resolution – 0.60 NAD (Top Left), Low Resolution – 0.72 NAD (Top Right) and DNA-EX (Bottom)**

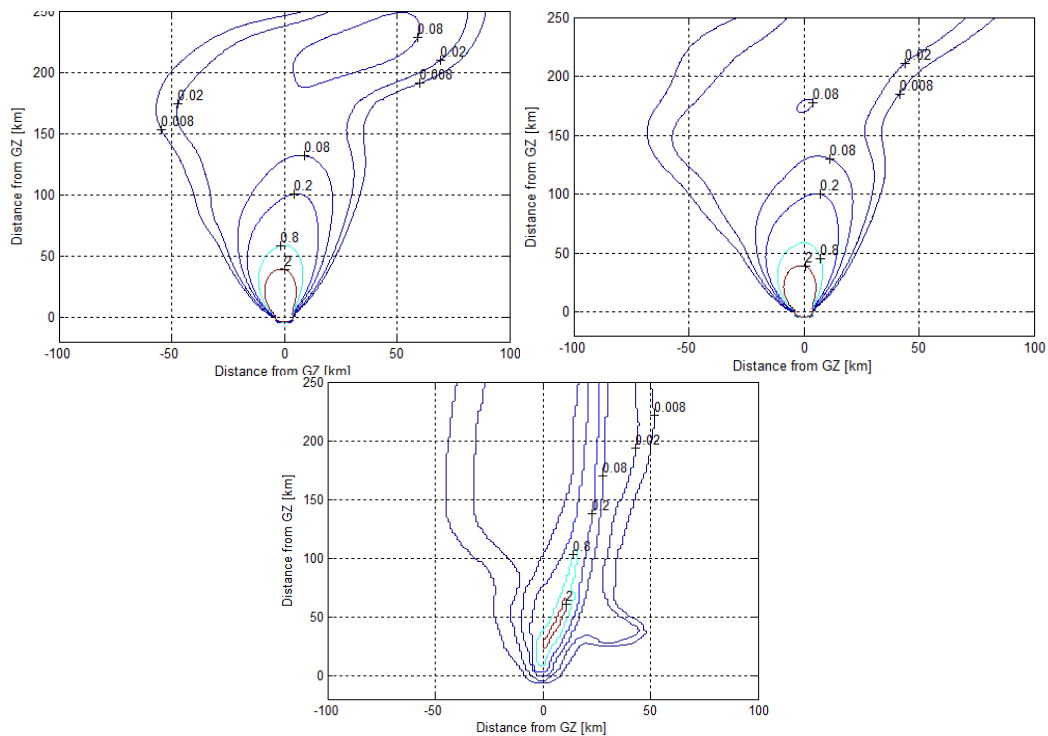


**Figure 9. FDC – George Contours: High Resolution – 0.08 NAD (Top Left), Low Resolution – 0.09 NAD (Top Right) and DNA-EX (Bottom)**

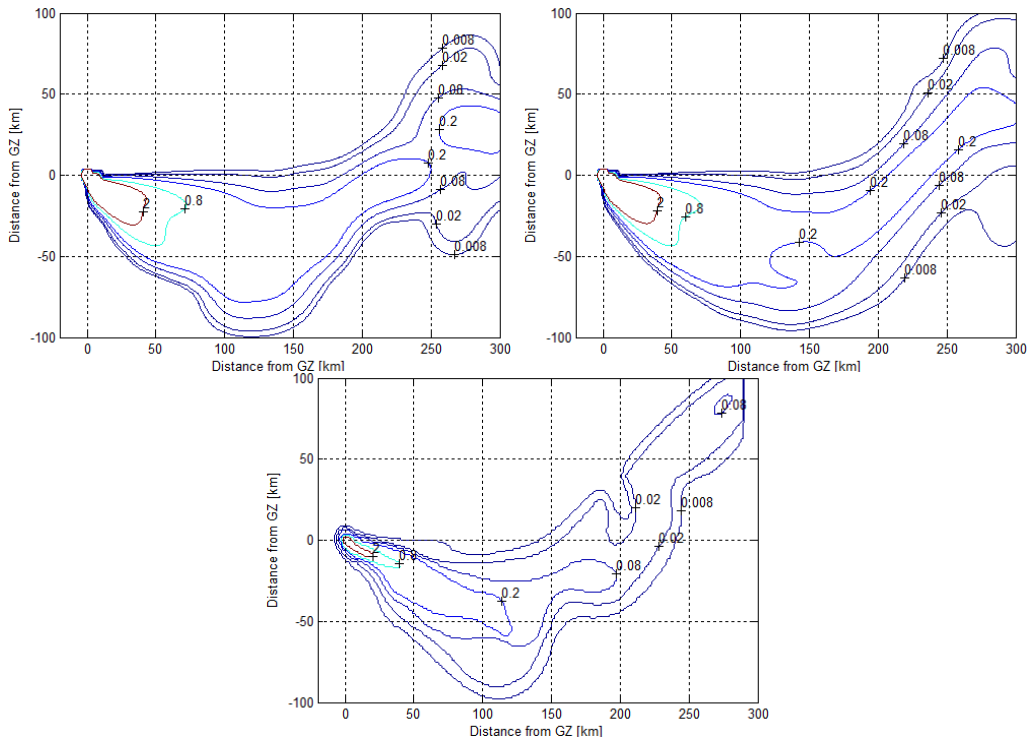


**Figure 10. FDC – Zucchini Contours: High Resolution – 0.12 NAD (Top Left), Low Resolution – 0.16 NAD (Top Right) and DNA-EX (Bottom)**

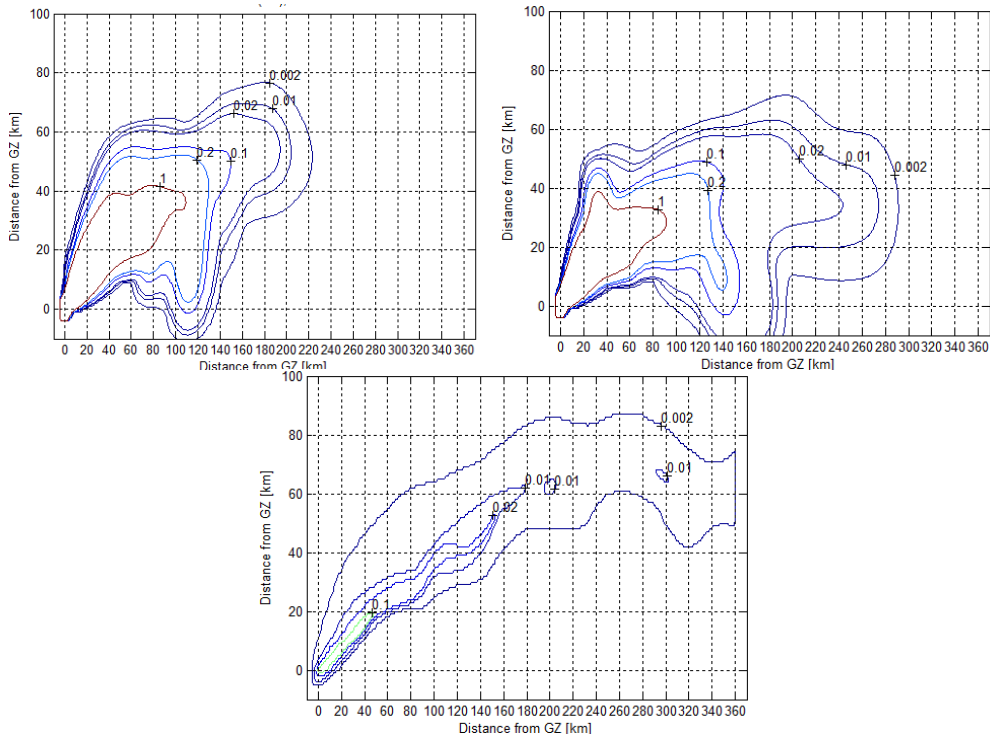


**Figure 11. FDC – Priscilla Contours: High Resolution – 0.42 NAD (Top Left), Low Resolution – 0.54 NAD (Top Right) and DNA-EX (Bottom)**

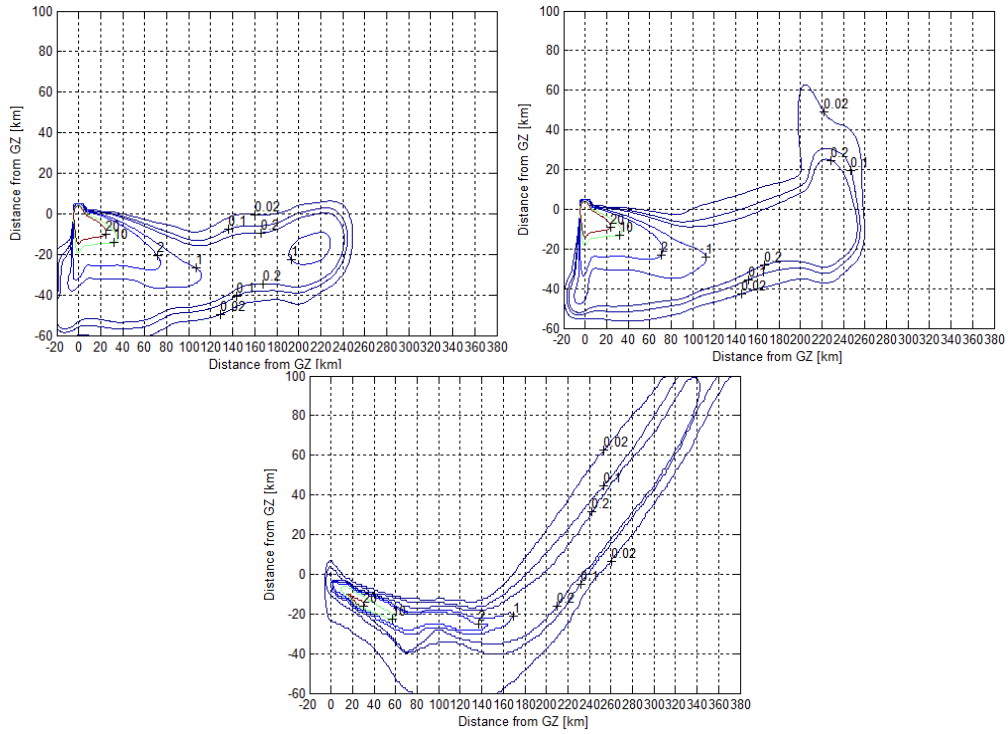


**Figure 12. FDC – Smoky Contours: High Resolution – 0.42 NAD (Top Left), Low Resolution – 0.38 NAD (Top Right) and DNA-EX (Bottom)**

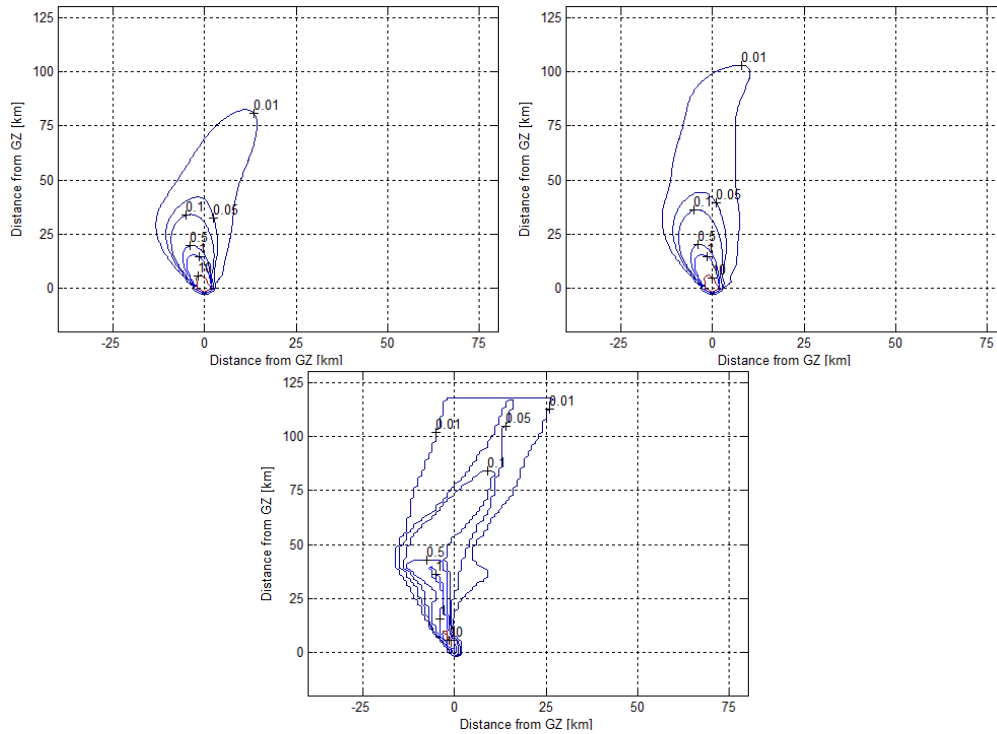


**Figure 13. FDC – Johnie Boy Contours: High Resolution – 0.46 NAD (Top Left), Low Resolution – 0.31 NAD (Top Right) and DNA-EX (Bottom)**



From a visual comparison of the six tests, Ess and Priscilla differ the most between low and high resolution. For Ess, both the low and high resolution contours do not show a curve towards the northeast approximately 100 km southeast of ground zero as shown in the DNA-EX contours. For a more thorough visual comparison all three of the lowest contours are combined on the same plot as shown in Figure 14, where green is the low resolution contour, red is the high resolution contour and black is the DNA-EX contour. This shows that both deviate significantly from the DNA-EX contours with high areas of false negatives. Due to the significant differences from the DNA-EX contours and the large area of false negatives, Ess is negated from the overall comparison of low and high resolution input for the FDC.

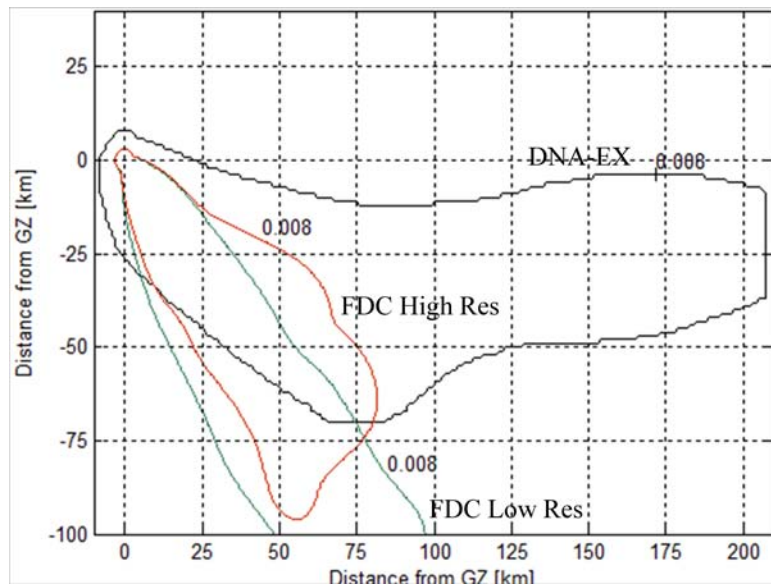
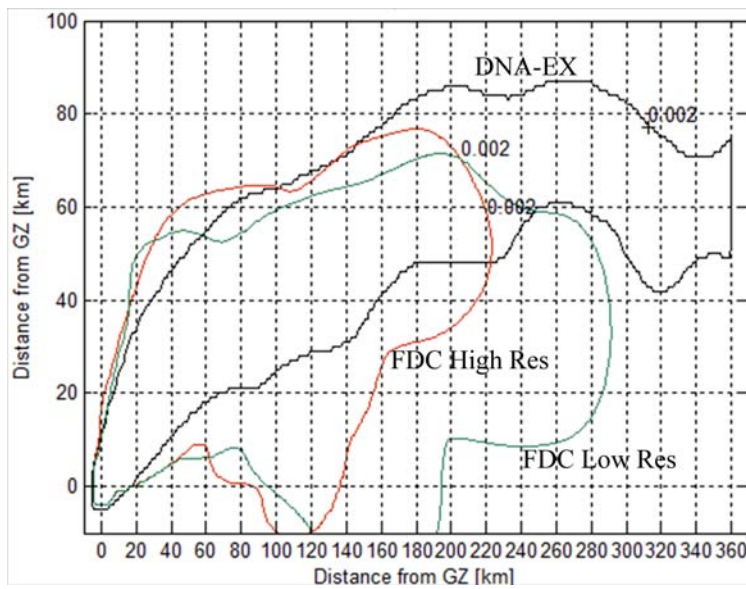


Figure 14. FDC – Combined Comparison for Ess using Lowest Contours

The individual DNA-EX contours for Priscilla follow a narrow path in the northeast direction while the FDC contours spread out immediately in the northwest and southeast directions, as seen in Figure 11. This results in large false positive areas for

both the low and high resolution contours. Neither the low nor the high resolution contours spread to the east as seen in the DNA-EX contours causing a large area of false negatives. Comparing the lowest contours of the three models, as seen in Figure 15, shows that the low resolution contour has a slightly lower overlap area with the DNA-EX contour and a larger area of false positives. This larger area of false positives is the cause of the high difference in NADs. False positives are less hazardous to CBRNE response personnel than a large area of false negatives. These results indicate that low resolution weather data is a viable input for the FDC when comparing Priscilla.



**Figure 15. FDC – Combined Comparison for Priscilla using Lowest Contours**

The remaining four cases have slight differences in NADs or the low resolution weather data produces more accurate models, therefore an overall comparison of the FDC contours using high and low resolution weather data show that low resolution weather data is a viable input for future comparisons. Additional arguments to strengthen the acceptance of using low resolution weather data are the easy access to low resolution

weather data and the limited user-defined weather inputs into HYSPLIT. The weather data available to the typical user for these fallout modeling programs is low resolution. It requires additional time and resources to convert the low resolution to high resolution weather data. This additional time required would delay the CBRNE responders. The final argument is the use of low resolution provides a better comparison to HYSPLIT due to the limited user-defined weather input capability.

## HYSPLIT

Test Case George was studied first using the trials outlined in Table 2. Additional trials were studied with similar results to the trials listed and not reported in this research. Example settings used for the trials studied are shown in Appendix A. The results are listed in Table 6.

**Table 6. HYSPLIT Results for George**

<b>George</b>			
<b>Trial</b>	<b>MOEx</b>	<b>MOEy</b>	<b>NAD</b>
<b>1<math>\sigma</math></b>	0.33	0.94	0.52
<b>2<math>\sigma</math></b>	0.43	0.93	0.41
<b>3<math>\sigma</math></b>	0.52	0.94	0.33
<b>100 Groups</b>	0.54	0.94	0.32
<b>3 Point Emission</b>	0.34	0.90	0.51
<b>10s Emission Time</b>	0.51	0.93	0.34
<b>Hybrid Gaussian</b>	0.64	0.92	0.25
<b>Various Emission Rates (Ci/hr)</b>			
<b>1.00E+04</b>	0.52	0.94	0.33
<b>1.00E+06</b>	0.52	0.94	0.33
<b>1.00E+08</b>	0.52	0.94	0.33
<b>1.00E+12</b>	0.52	0.94	0.33
<b>3.41E+09</b>	0.52	0.94	0.33

The first three trials conducted were varying the vertical distribution in order to determine which distribution was more effective for the remaining trials. The  $3\sigma$  distribution proved to be the dominant vertical distribution, as predicted, with a NAD of 0.33 and a visual comparison shown in Figure 16. The remaining trials conducted using HYSPLIT are run using a  $3\sigma$  vertical distribution and varying other parameters. A visual comparison shows that all plots do not represent the individual contours and only partially follow the overall area of contamination. The various curves and bulges of the 0.02 and 0.008 dose-rate contours shown in the DNA-EX plot are not seen in any of the HYSPLIT plots. The deviations of the contours are caused from the distinctive terrain features that are not replicated using either low or high resolution weather data.

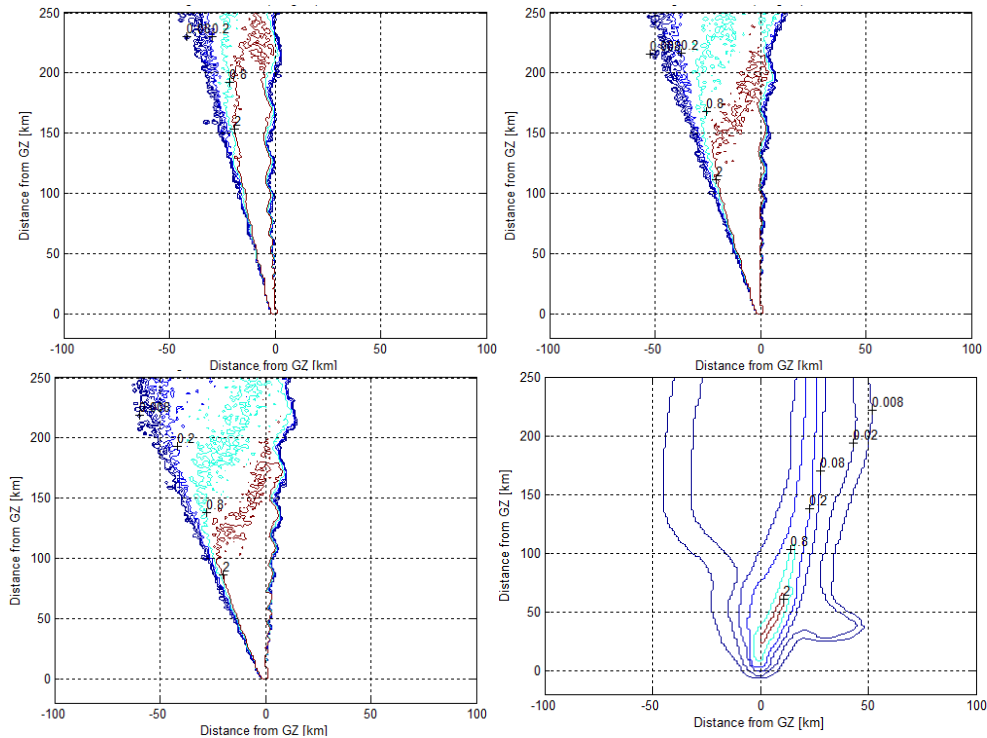


**Figure 16. HYSPLIT – Vertical Distribution Contours (George):  $1\sigma$  – 0.52 NAD (Top Left),  $2\sigma$  – 0.41 NAD (Top Right),  $3\sigma$  – 0.33 NAD (Bottom Left) and DNA-EX Contours (Bottom Right)**

The fourth trial was done using 100 equal activity particle groups which required the summation of 100 runs from HYSPLIT. This resulted in a NAD of 0.32 which is a better representative of the DNA-EX contours than the trial using 20 equal activity particle groups as shown in Figure 17.

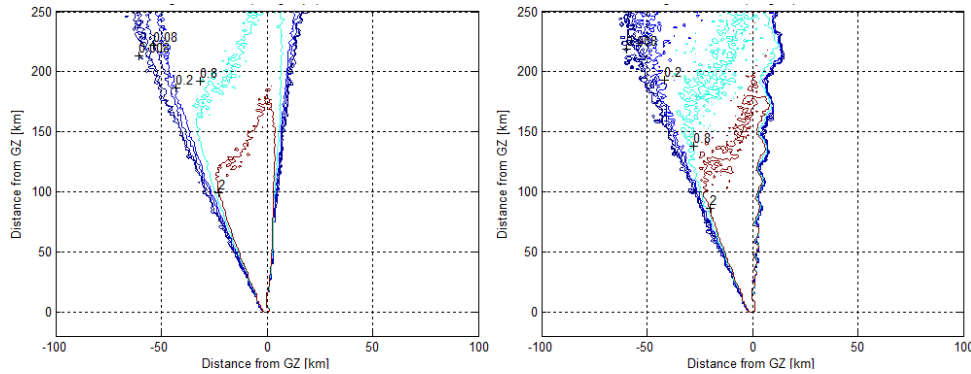


**Figure 17. HYSPLIT – 100 Particle Group (George): 100 particle groups – 0.32 NAD (Left) and 20 particle groups – 0.33 NAD (Right)**

From a visual comparison the 100 particle group produces a lower NAD due to smoother contours. The smoother contours in the 100 particle group allow for a larger area of overlap when compared to the DNA-EX contours and more defined individual contours. Running the 100 particle group trial was time consuming where the majority of the individual runs took 10 to 20 min each. Due to the time commitment and the minimal differences between the 20 and 100 particle group trials the remaining trials are run using 20 equal activity particle groups.

The fifth trial was done using three point sources. HYSPLIT inputs are the top and bottom of the cloud but are worded as two point sources. In order to ensure that using two point sources does not worsen the model a trial using three point sources was done. The third source point used was the vertical center of the cloud,  $Z_c^s$ . As shown in

Table 6 and Figure 18, a two point source for the top and bottom was a better representative than a three point source.

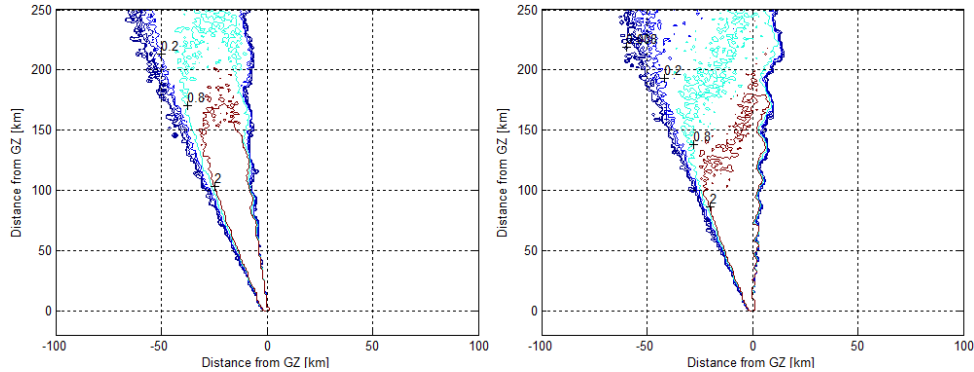


**Figure 18. HYSPLIT – Three Point Source (George): 3 point source – 0.51 NAD (Left) and 2 point source – 0.33 NAD (Right)**

The sixth trial was run in order to simulate the release of radioactivity immediately following detonation. A 10 second approximation was used for the emission time and the emission rate scaled to account for the release time using the following calculation:

$$\left( \frac{5.3E8 \frac{\text{curies}}{\text{KT}} * 15 \text{KT}}{20 \text{groups}} \right) / \left( 10s * \frac{1hr}{3600s} \right) = 1.431E11 \frac{\text{curies}}{1hr}. \quad (26)$$

As shown in Table 6 and Figure 19 the 10s emission rate closely resembles the 7 min emission rate with a difference in NAD of 0.01. With a slightly lower NAD the 7 min emission rate was used for the remaining trials.

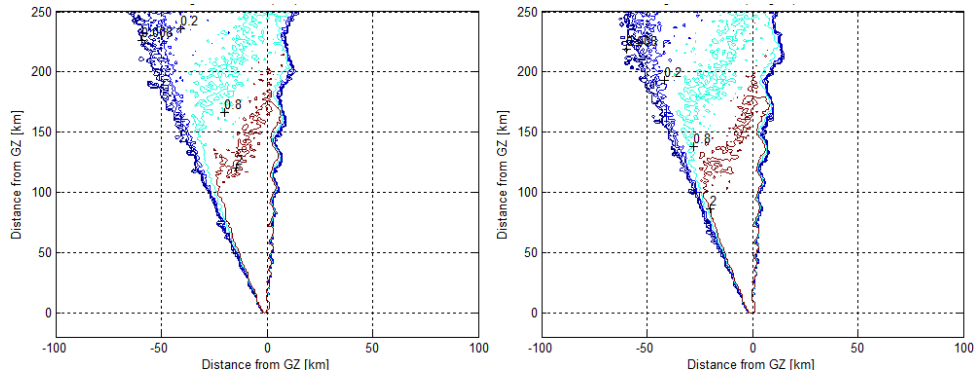


**Figure 19. HYSPLIT – 10s Emission Rate (George): 10s Emission Rate – 0.34 NAD (Left) and 7 min Emission Rate – 0.33 NAD (Right)**

The seventh trial studied an alternate particle-puff release distribution offered through HYSPLIT. Users have five particle-puff release mode combinations to choose from:

- 3D particle horizontal and vertical
- Gaussian-horizontal and Top-Hat-vertical puff
- Top-Hat-horizontal and vertical puff
- Gaussian-horizontal and particle-vertical
- Top-Hat-horizontal and particle-vertical

The puff mode is modeled using either a Top-Hat or Gaussian distribution where the Top-Hat uses a  $1.54\sigma$  standard deviation and the Gaussian puff uses a  $3\sigma$  standard deviation distribution. This research negates all Top-Hat distributions due to the limited standard deviations. This decision was determined from the results of the first three trials using HYSPLIT while varying the vertical distribution. The results from that study proved that a three standard deviation distribution improved the models. After eliminating the Top-Hat distribution two options are left, the three-dimensional particle

distribution and the hybrid model (puff in the horizontal and particle in the vertical). The resulting NAD of a 20 equal activity particle group using the hybrid model was 0.25, the lowest NAD of all the HYSPLIT George trials. A visual comparison, shown in Figure 20, shows smoother contours but more dispersion to the west producing a larger area of false positives. Using a hybrid distribution in HSYPLIT significantly increases the individual particle run times. Due to the time constraint and the objective to reduce computational time the remaining five historical tests are run using both methods, the hybrid and the three-dimensional particle distributions for comparison.

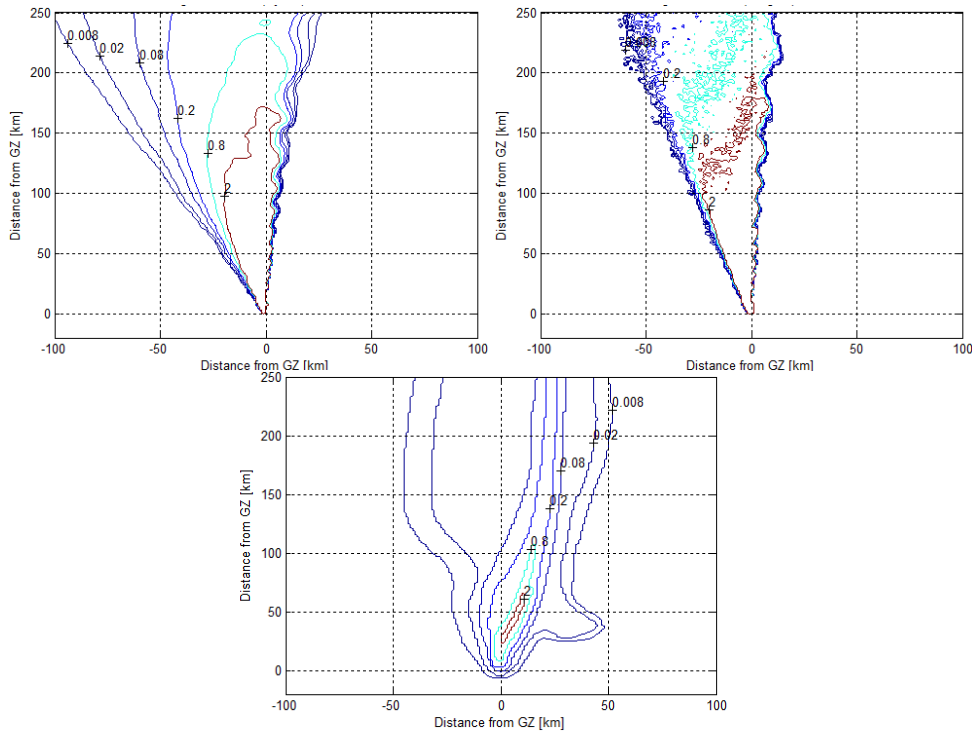


**Figure 20. HYSPLIT – Hybrid Gaussian Distribution (George): Hybrid Gaussian Distribution – 0.25 NAD (Top Left), 3D Particle Distribution – 0.33 NAD (Top Right) and DNA-EX Contours (Bottom)**

Six trials are conducted varying the emission rate to determine if HYSPLIT deposits particles in the same geographical area no matter how low the emission rate is or



if a smaller area is covered with lower emission rates. This research varied the emission rate from 1E4 to 1E12. In order to accurately compare all models the extracted HYSPLIT results were scaled to a  $3.4071E9$  curies/hr emission rate. These results are shown in Table 6. The trials resulted in a NAD of 0.33 with a slight deviation in the 1E4 emission rate. This shows that there is a reduction in the geographical area when the emission rates are dropped below 1E4.

Two additional trials were run using the test data for George and Zucchini and an emission rate derived from the beta activity of  $4.3492E8$  curies per kiloton at one hour after detonation, a conversion factor of  $0.048$  curies/m<sup>2</sup> per R/hr and an emission time of 10s. The results are shown in Table 7 with a visual comparison shown in Figure 21 and Figure 22. The trials ran using the beta activity had a slightly lower NAD and the visual comparison shows minor changes in the individual contours. The beta activity model extends the individual contours further to the north in George and further east in Zucchini than the gamma activity model.

**Table 7. HYSPLIT – NADs using an Emission Rate Derived from the Beta Activity**

	Gamma Activity - 7min			Beta Activity - 10s		
	MOEx	MOEy	NAD	MOEx	MOEy	NAD
<b>George</b>	0.52	0.94	0.33	0.52	0.94	0.33
<b>Zucchini</b>	0.49	0.65	0.44	0.51	0.65	0.43

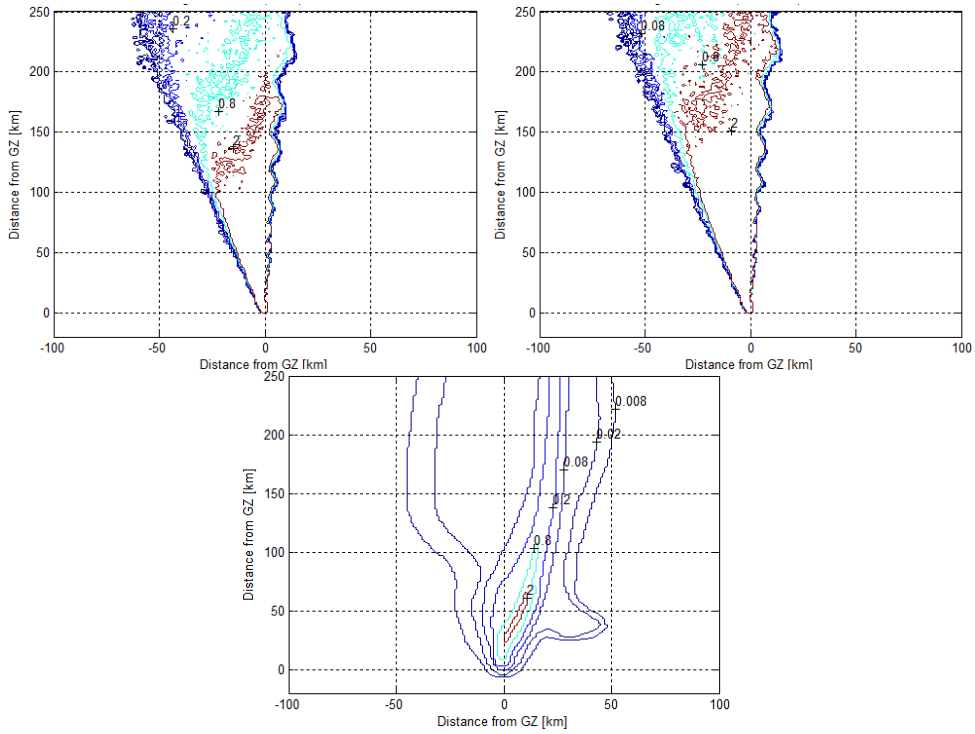


**Figure 21. HYSPLIT – Beta and Gamma Activity Comparison (George): Emission Rate derived from the Gamma Activity – 0.33 NAD (Top Left), Emission Rate derived from the Beta Activity – 0.33 NAD (Top Right) and DNA-EX Contours (Bottom)**

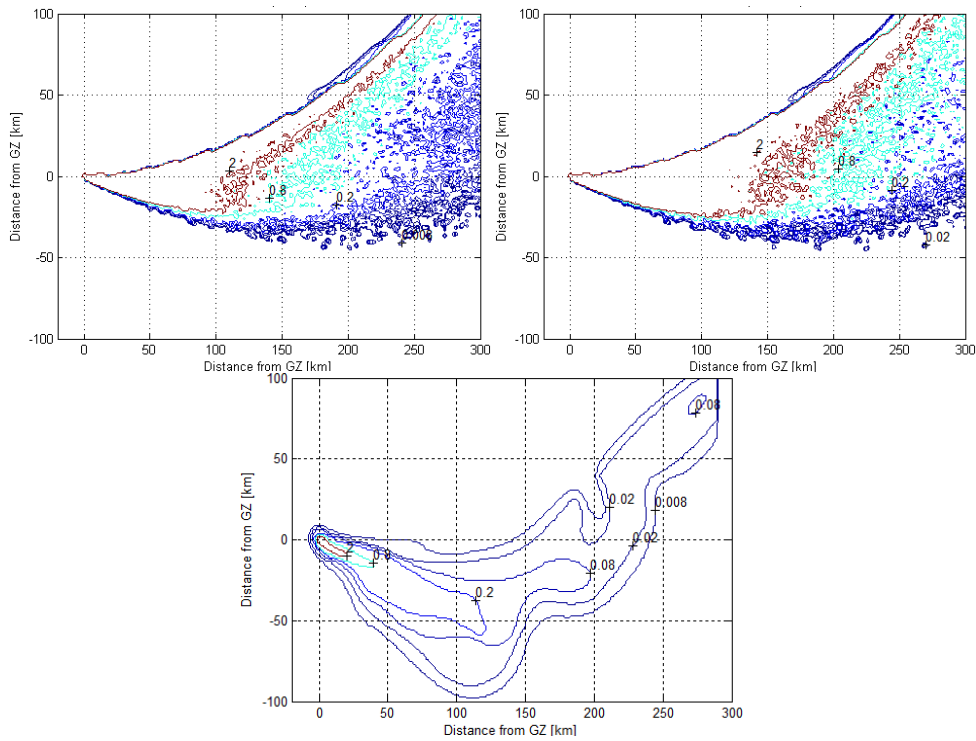


**Figure 22. HYSPLIT – Beta and Gamma Activity Comparison (Zucchini): Emission Rate derived from the Gamma Activity – 0.44 NAD (Top Left), Emission Rate derived from the Beta Activity – 0.43 NAD (Top Right) and DNA-EX Contours (Bottom)**

The following ten trials compares the results of the remaining five test cases using a 7 min emission time and a 10s emission time. All trials use 20 equal activity particle groups, three standard deviation vertical particle distributions, an emission rate derived from the gamma activity and Hick's conversion factor to convert to exposure rate. The resulting NADs are shown in Table 8 and the contours are shown in the following figures.

**Table 8. HYSPLIT – NADs for Remaining Five Test Cases comparing Emission Duration**

	HYSPLIT - 7min			HYSPLIT - 10s		
	MOEx	MOEy	NAD	MOEx	MOEy	NAD
<b>Ess</b>	0.18	0.76	0.71	0.18	0.77	0.71
<b>Zucchini</b>	0.49	0.65	0.44	0.50	0.65	0.44
<b>Priscilla</b>	0.60	0.40	0.52	0.59	0.40	0.53
<b>Smoky</b>	0.12	0.12	0.88	0.12	0.12	0.88
<b>Johnie Boy</b>	0.02	0.05	0.98	0.02	0.05	0.97

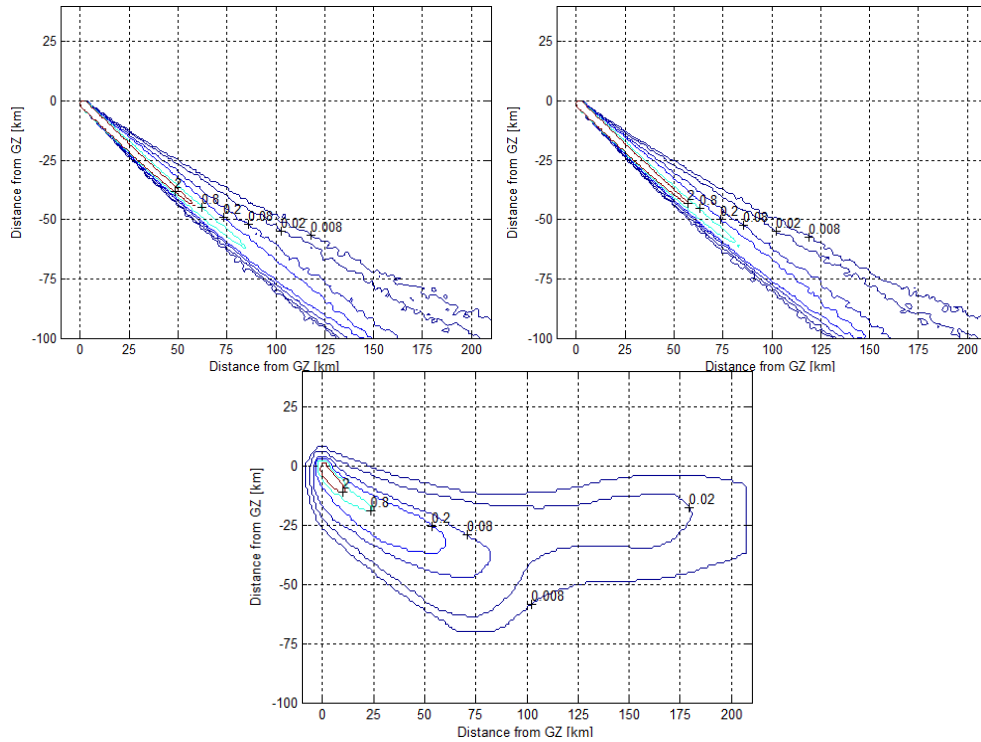


**Figure 23. HYSPLIT – Ess Contours: 7 min Emission Time – 0.71 NAD (Top Left), 10s Emission Time – 0.71 NAD (Top Right) and DNA-EX Contours (Bottom)**

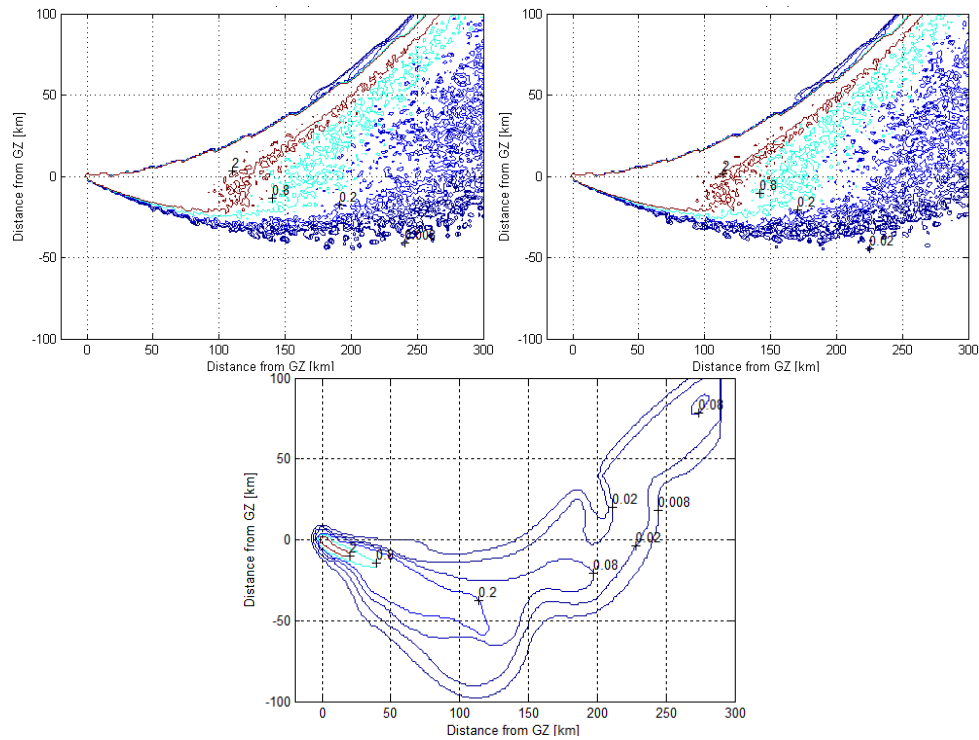


**Figure 24. HYSPLIT – Zucchini Contours: 7 min Emission Time – 0.44 NAD (Top Left), 10s Emission Time – 0.44 NAD (Top Right) and DNA-EX Contours (Bottom)**

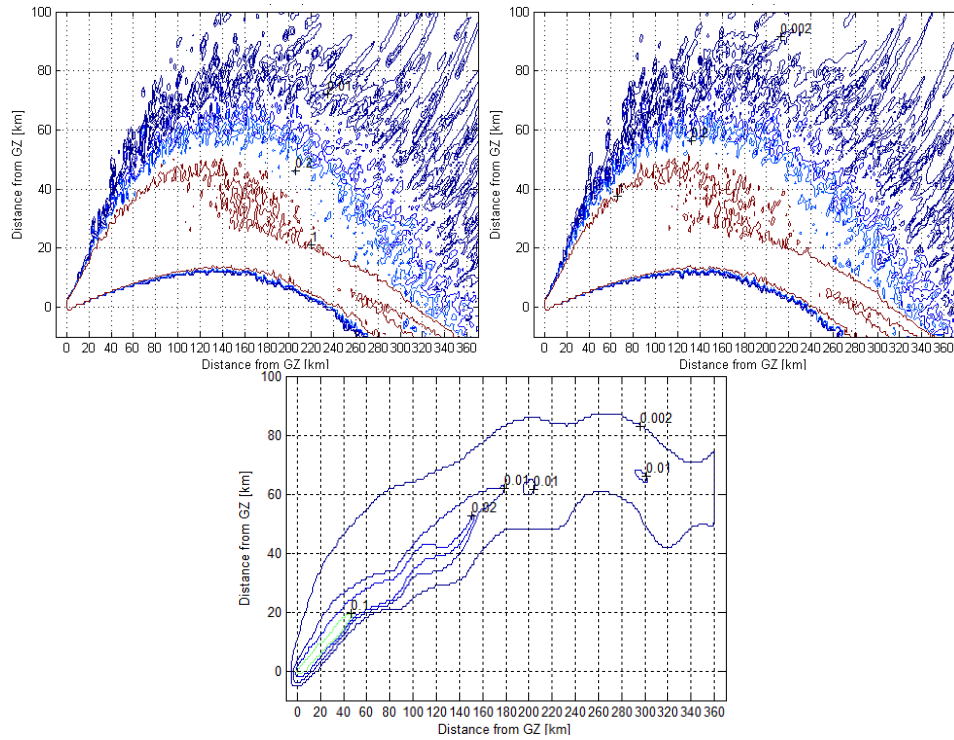


**Figure 25. HYSPLIT – Priscilla Contours: 7 min Emission Time – 0.52 NAD (Top Left), 10s Emission Time – 0.53 NAD (Top Right) and DNA-EX Contours (Bottom)**

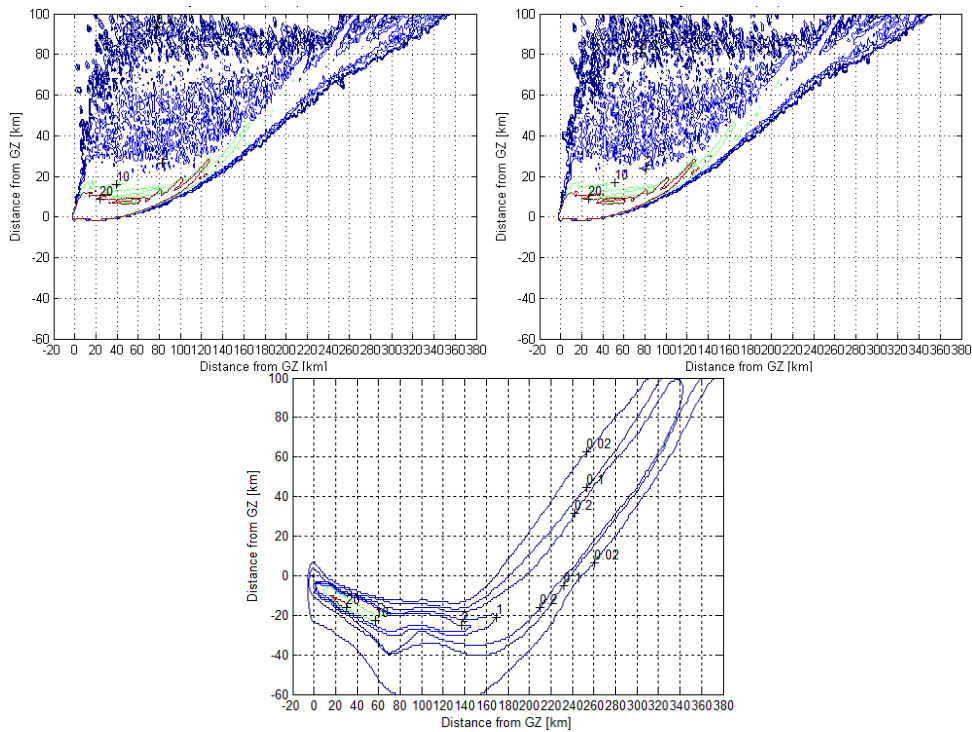


**Figure 26. HYSPLIT – Smoky Contours: 7 min Emission Time – 0.88 NAD (Top Left), 10s Emission Time – 0.88 NAD (Top Right) and DNA-EX Contours (Bottom)**

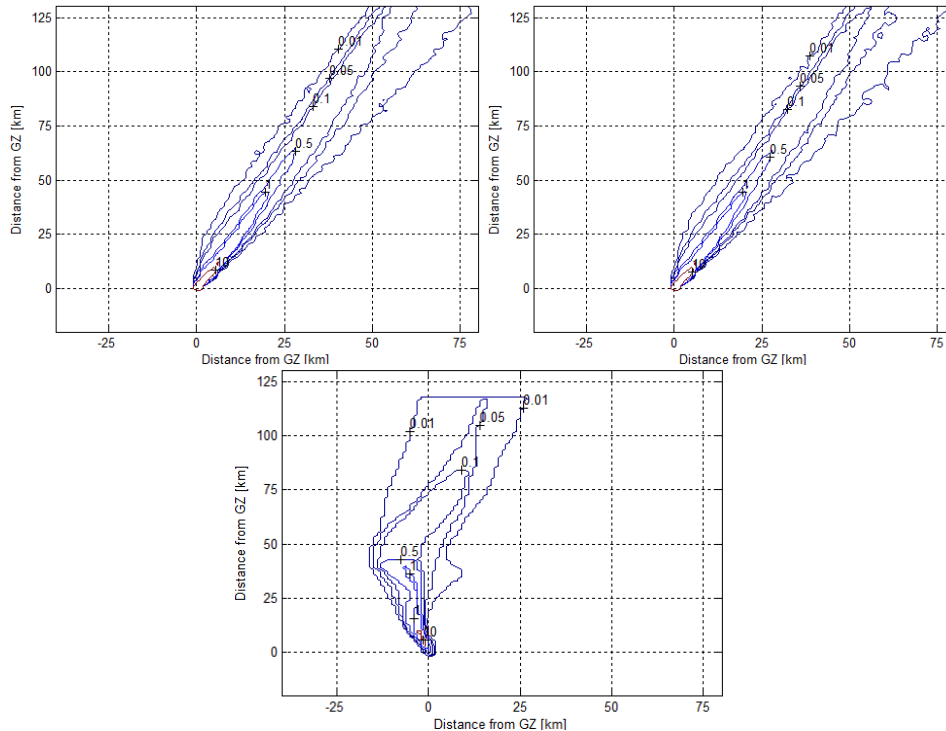


**Figure 27. HYSPLIT – Johnie Boy Contours: 7 min Emission Time – 0.98 NAD (Top Left), 10s Emission Time – 0.97 NAD (Top Right) and DNA-EX Contours (Bottom)**

There is no significant difference between the 7 min and 10s emission times as seen in the calculations of the NADs and a visual comparison. Therefore, future trials will use a 10s emission time because radioactive particles start to settle out of the cloud immediately following detonation.

Overall, from a visual comparison, high altitude winds cause a large area of isolated closed-in contours as seen in Zucchini, Priscilla and Smoky when using HYSPLIT. This may actually be a better representation than the DNA-EX contours. The data used to create the DNA-EX contours was collected using mobile detectors and taken at various points with large areas in between. There is significant error with the collection method due to detector error and the inability to cover the entire area. The DNA-EX dose-rate contours are determined by smoothing the data collected at the

various data points. HYSPLIT's three-dimensional particle distribution predicts the exact points where particles are deposited on the ground causing large areas of closed-in contours. In reality it is highly likely that deposition occurs in the same manner HYSPLIT is depicting. HYSPLIT follows the general patterns of the DNA-EX contours with a few issues. The main issue is the inability to incorporate the ground zero winds. Additionally, the large area of closed-in contours increases the area of false positives causing higher NADs. A third difference was none of the HYSPLIT plots show the unique bulges or curves in the outer (lower) dose-rate contours. For example, HYSPLIT does not model the right bulge shown to the east of the DNA-EX contours of George approximately 60 km northeast of ground zero, shown in Figure 21. This is a common issue amongst all modeling programs studied due to the distinctive terrain features.

A visual comparison of Ess shows a significant deviation from HYSPLIT and the DNA-EX contours. The HYSPLIT contours do not spread to the east due to the lack of winds from the west. Additionally, the DNA-EX contours show spreading in all directions near ground zero while HYSPLIT predicts narrow contours spreading to the southeast. This could be the result of two reasons. The first is the inability to incorporate ground zero winds. The ground zero winds have a slower wind speed allowing for more dispersion near ground zero. The other reason, the main reason, is the source term for the subsurface bursts. The method used to estimate the source term is done using a similar method to the source term development for the FDC which is not designed for subsurface bursts.

Zucchini, Priscilla, Smoky and Johnie Boy contours show a deviation from the DNA-EX contours due to the inability to incorporate ground zero winds. With the

incorporation of ground zero winds HSYPLIT is an extremely effective mapping tool. With the ground zero winds there would be minimal false negative areas which are the greatest hazard to CBRNE responders. However, incorporating the time commitment in calculating the source term and requirement to run multiple trials for one detonation makes HYSPLIT an ineffective mapping tool. Combining HYSPLIT with DELFIC or the FDC may provide a better model.

The remaining six models uses the test data from the six historical test cases, an emission rate derived from the beta activity, a 10s emission time and a hybrid distribution. The results are shown in Table 9 and the following figures.

**Table 9. HYSPLIT – Calculated NADs comparing 3D Particle Distribution and a Hybrid Distribution**

	3D Particle Distribution - Gamma Activity - 10s			Hybrid Distribution - Beta Activity - 10s		
	MOEx	MOEy	NAD	MOEx	MOEy	NAD
<b>Ess</b>	0.18	0.77	0.71	0.57	0.71	0.37
<b>George</b>	0.51	0.93	0.34	0.66	0.91	0.23
<b>Zucchini</b>	0.50	0.65	0.44	0.66	0.64	0.35
<b>Priscilla</b>	0.59	0.40	0.53	1.00	0.38	0.45
<b>Smoky</b>	0.12	0.12	0.88	0.28	0.15	0.80
<b>Johnie Boy</b>	0.02	0.05	0.97	0.59	0.44	0.49



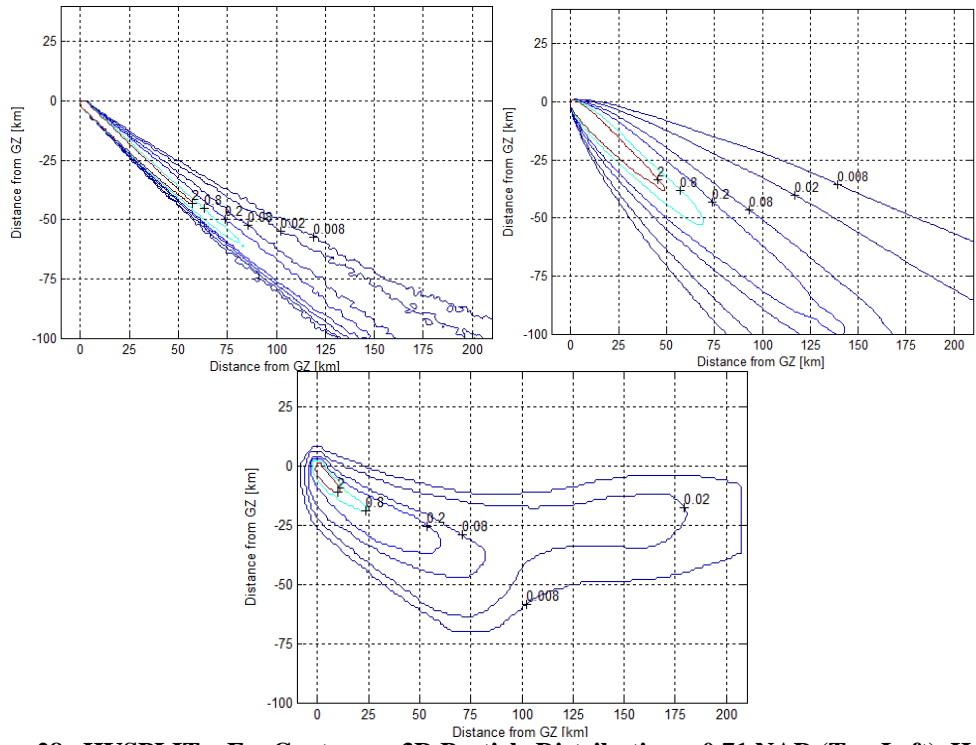


**Figure 28. HYSPLIT – Ess Contours: 3D Particle Distribution – 0.71 NAD (Top Left), Hybrid Distribution – 0.37 NAD (Top Right) and DNA-EX Contours (Bottom)**

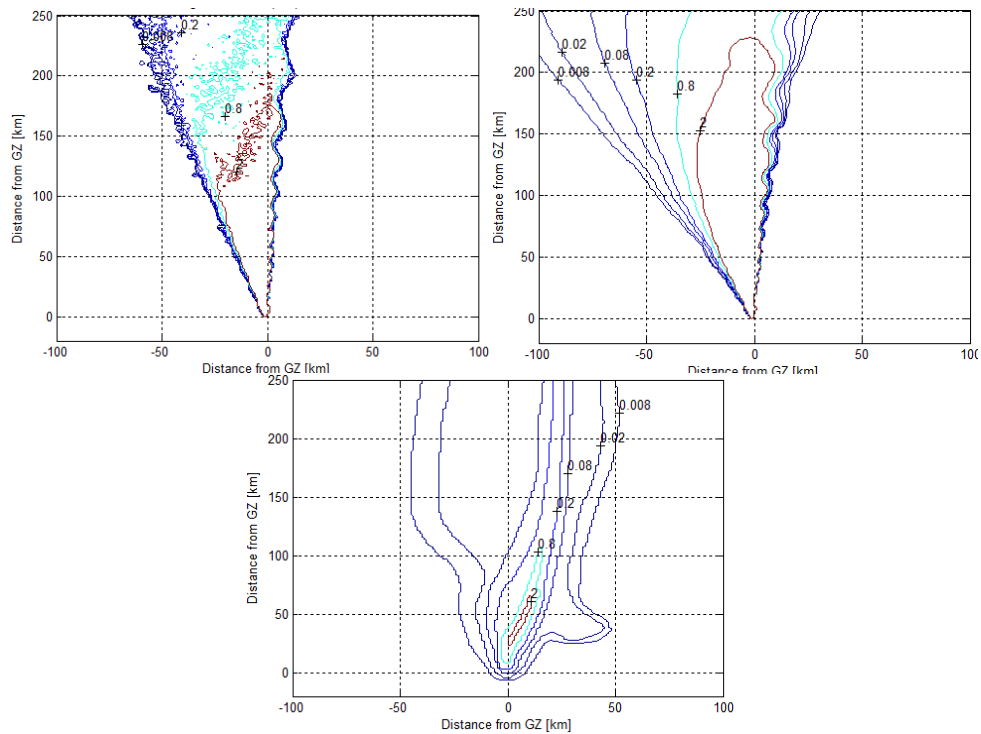


**Figure 29. George Contours: 3D Particle Distribution – 0.34 NAD (Top Left), Hybrid Distribution – 0.23 NAD (Top Right) and DNA-EX Contours (Bottom)**

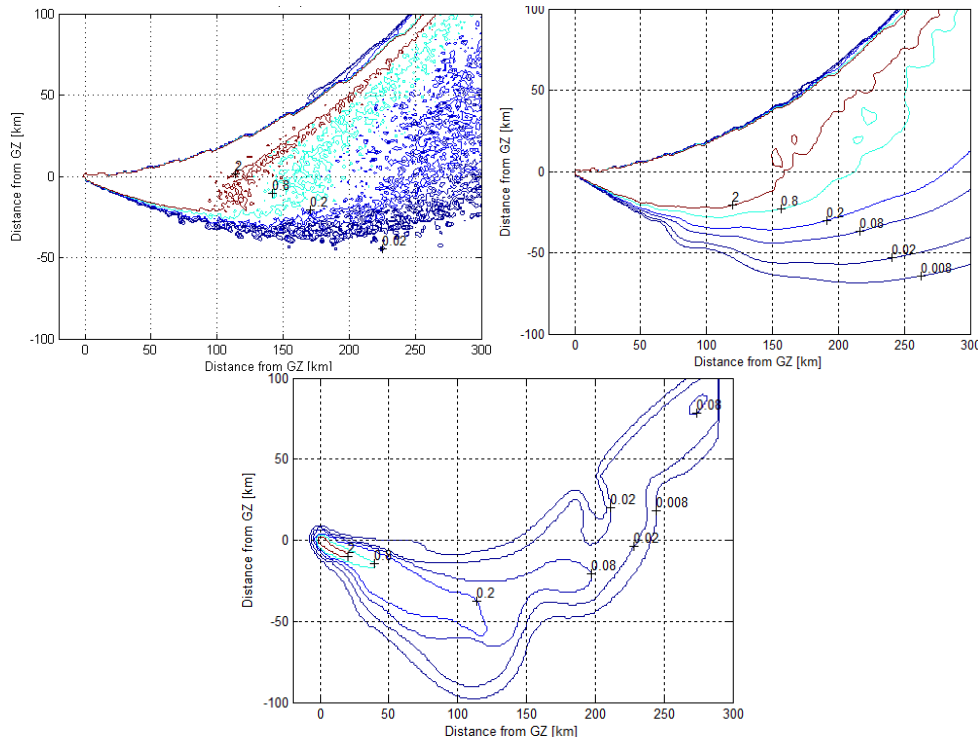


**Figure 30. Zucchini Contours: 3D Particle Distribution – 0.44 NAD (Top Left), Hybrid Distribution – 0.35 NAD (Top Right) and DNA-EX Contours (Bottom)**

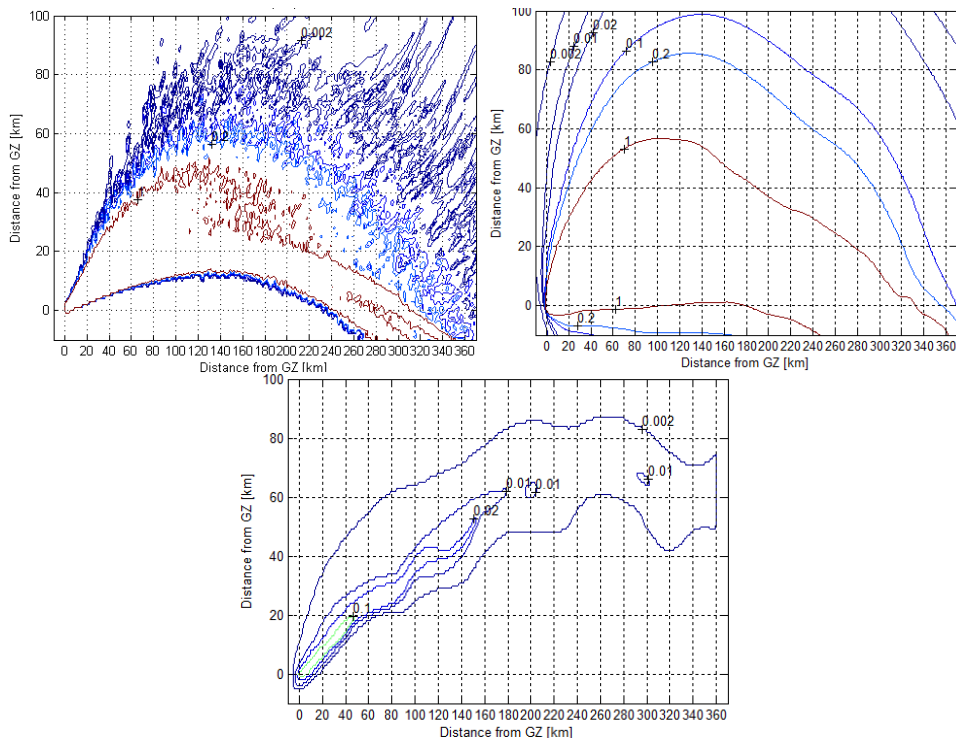


**Figure 31. Priscilla Contours: 3D Particle Distribution – 0.53 NAD (Top Left), Hybrid Distribution – 0.45 NAD (Top Right) and DNA-EX Contours (Bottom)**

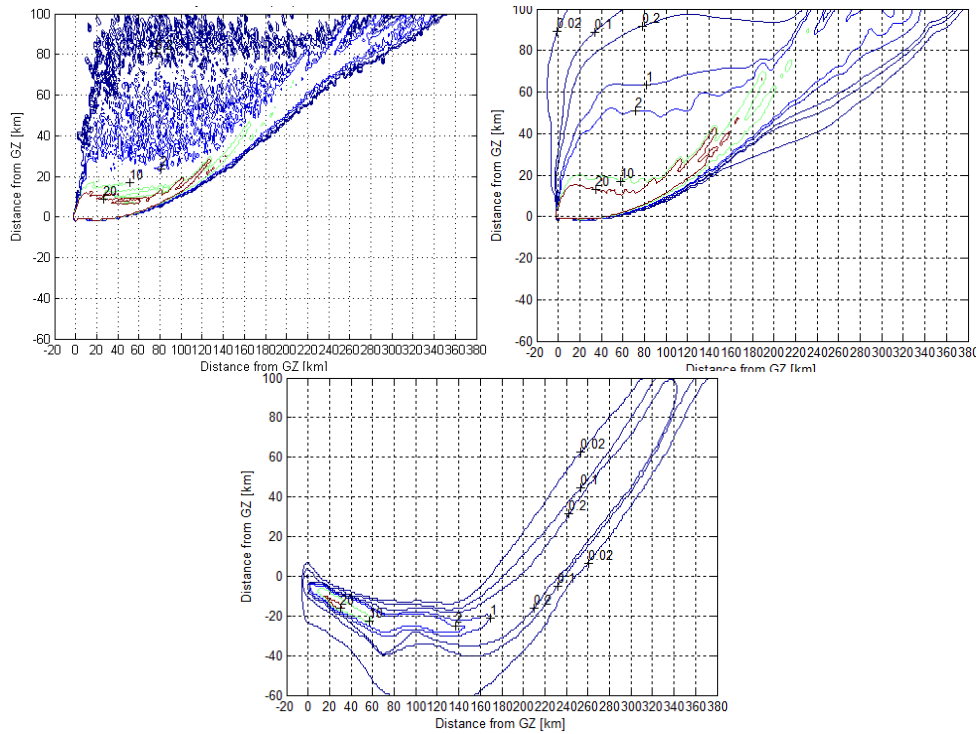


**Figure 32. Smoky Contours: 3D Particle Distribution – 0.88 NAD (Top Left), Hybrid Distribution – 0.80 NAD (Top Right) and DNA-EX Contours (Bottom)**

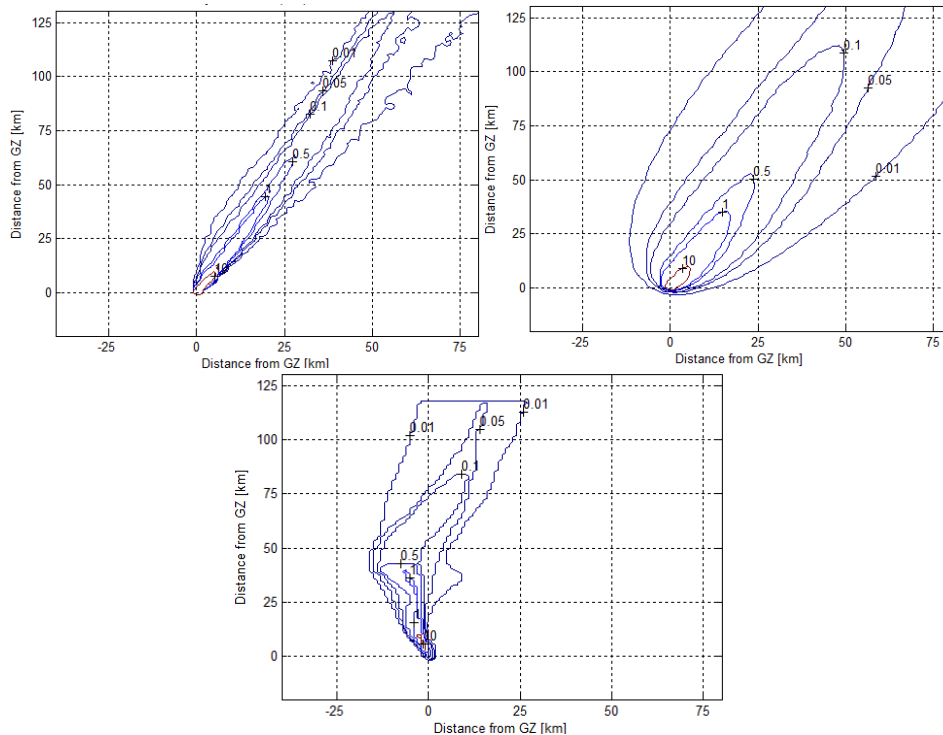


**Figure 33. Johnie Boy Contours: 3D Particle Distribution – 0.97 NAD (Top Left), Hybrid Distribution – 0.49 NAD (Top Right) and DNA-EX Contours (Bottom)**

The numerical comparison shows a significant improvement in NADs using the hybrid distribution combined with the beta activity and a 10s emission time compared with the three-dimensional particle distribution combined with the gamma activity and a 10s emission time.

A visual comparison of Ess shows a significant improvement in the overall and individual contours. The individual contours near ground zero more accurately follow the DNA-EX contours. However, HYSPLIT extends the high dose-rate contours further to the southeast than the DNA-EX and does not curve to the east as shown in the previous models of Ess.

A visual comparison of George, Zucchini and Smoky shows that the hybrid distribution produces models that more accurately follow the DNA-EX contours than the three-dimensional distribution because of the smoother contours. The hybrid distribution displays a smooth Gaussian representation resulting in smoother contours. The contours for George extend further to the west than the DNA-EX contours. For Zucchini the contours extend further to the south and do not initially extend to the southeast due to the inability of incorporating ground zero winds which is the same issue shown in the Smoky contours.

The hybrid distribution model for Priscilla extends too far to the north and south producing a significantly large area of false positives. The three-dimensional particle distribution is a more accurate model than the hybrid distribution when modeling Smoky.

A visual comparison of Johnie Boy shows that the hybrid distribution extends the contours further to the northwest and southeast and does not initially curve to the northwest due to the inability of incorporating the ground zero winds.

### **DELFIc FPT**

The DELFIc FPT is run using the averaged weather data and the ground zero winds listed in the DNA-EX document. Multiple trials are run in order to determine how long the ground zero winds should be incorporated. In order to input the calculated averaged weather data the DELFIc input file was adjusted for each case, an example file is shown in Appendix B. The study of each test case consist of trials using just the averaged weather file (averaged .prf file) (PRF) and just the ground zero winds (GW). The remaining trials are run with a combination of both and adjusting the time that the ground zero winds are incorporated. The results of using only the ground zero winds and only the average weather file are listed for all tests along with the top trials producing the lowest NADs. For Ess, Table 10 lists the trials producing the best results along with their NADs. Due to the limitations of DELFIc a height of burst of -5 meters was used when modeling Ess.

**Table 10. DELFIc FPT – NADs for Ess**

	<b>Ess</b>		
	<b>MOEx</b>	<b>MOEy</b>	<b>NAD</b>
<b>PRF</b>	0.16	0.61	0.75
<b>GW (.5 hr) - PRF</b>	0.14	0.72	0.76
<b>GW</b>	0.02	0.35	0.96

Using the averaged low resolution weather file (PRF) produced the lowest NAD of 0.75.

Using the ground zero winds for 30 minutes followed by the averaged weather file was the second lowest NAD of 0.76. Both plots are shown in Figure 34 along with the DNA-EX contours.

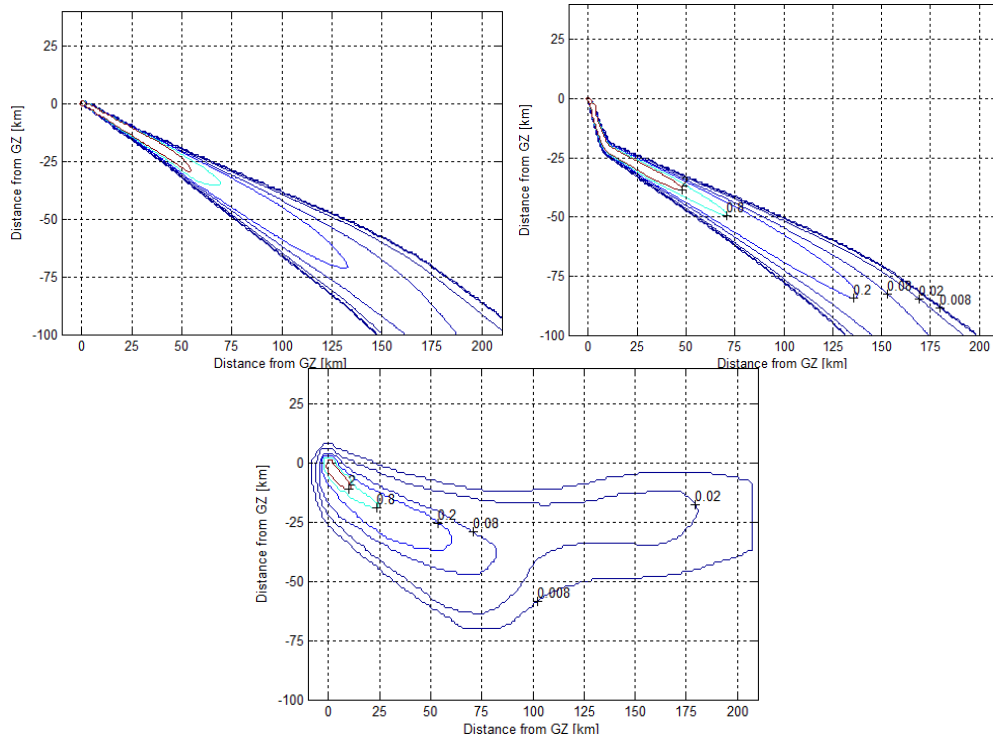


**Figure 34. DELFIC FPT – Ess Contours: Averaged weather file – 0.75 NAD (Top Left), GW for 30 min followed by the average weather file – 0.76 NAD (Top Right) and the DNA-EX Contours (Bottom)**

Through a visual comparison the DELFIC FPT does not accurately model Ess due to the lack of winds from the west (the same issue with the FDC and HYSPLIT). Additionally, the contours are extremely narrow near ground zero and gradually expand approximately 150 km southeast of ground zero. This deviates significantly from the DNA-EX contours. As predicted the DELFIC FPT is not an effective mapping tool for Ess due to the fact that it does not model detonations buried at the depth of Ess.

The trials ran for George that produced the best results are listed in Table 11.

**Table 11. DELFIC FPT – NADs for George**

	George		
	MOEx	MOEy	NAD
<b>GW</b>	0.59	0.98	0.26
<b>PRF</b>	0.33	0.97	0.50
<b>GW (2 hr) - PRF</b>	0.33	0.95	0.51

Using only the ground zero winds produced the lowest NAD of 0.26. This was followed by the averaged weather file with a NAD of 0.50. The plots are shown in Figure 35.

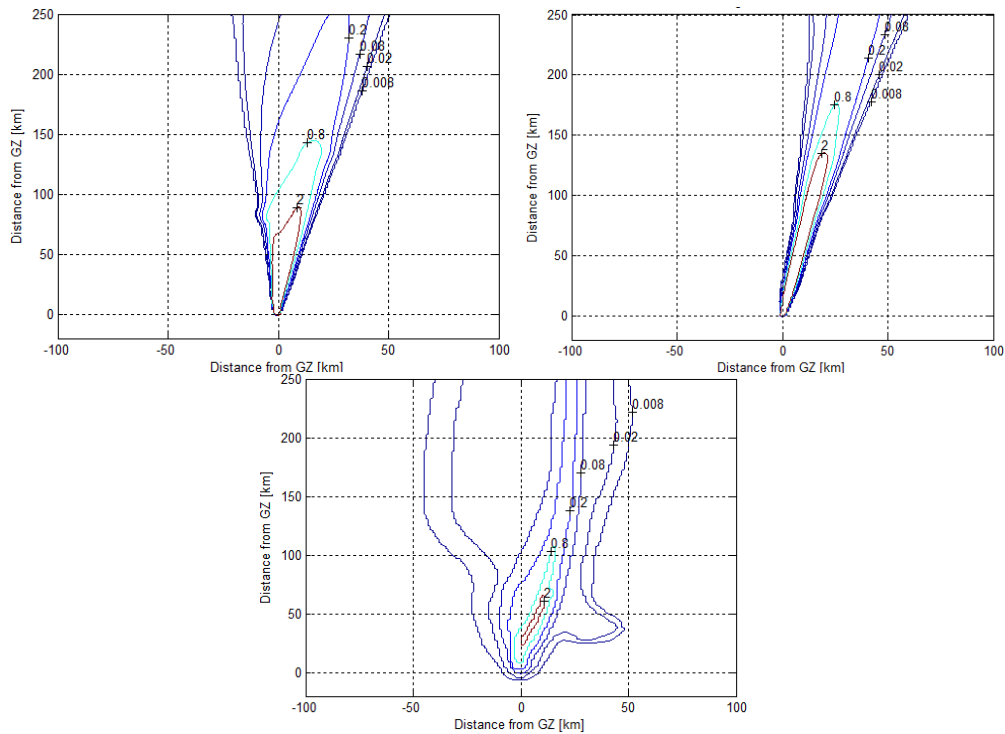


**Figure 35. DELFIC FPT – George Contours: Only GW – 0.26 NAD (Top Left), Averaged weather file – 0.50 NAD (Top Right) and DNA-EX Contours (Bottom)**

Conducting a visual comparison shows that although the ground zero winds produce the lowest NAD the contours spread in the east and west directions which varies from the DNA-EX contours. The high dose-rate contours shown using the averaged weather file more accurately follow the DNA-EX contours. Neither trial produces the bulge to the east or the curve to the northwest approximately 100 km downrange of ground zero.

The trials ran for Zucchini that produced the best results are listed in Table 12.

**Table 12. DELFIC FPT – NADs for Zucchini**

	<b>Zucchini</b>		
	<b>MOEx</b>	<b>MOEy</b>	<b>NAD</b>
<b>GW (1.5hr) - PRF</b>	0.39	1.00	0.44
<b>GW (2hr) - PRF</b>	0.38	0.88	0.47
<b>GW</b>	0.37	0.61	0.54
<b>PRF</b>	0.00	0.01	0.99

The two trials producing the best NADs are using the ground zero winds for an hour and a half followed by the averaged weather file and using the ground zero winds for two hours followed by the averaged weather file. The contours are shown in Figure 36.



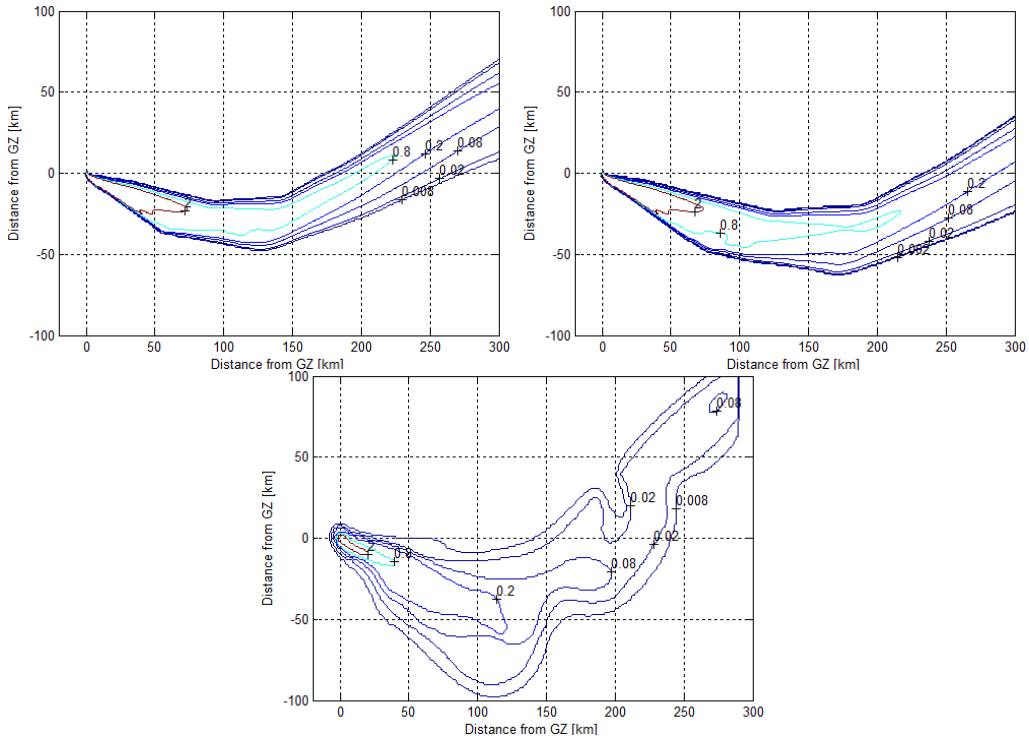


**Figure 36. DELFIC FPT – Zucchini Contours: GW for 1.5 hr and the averaged weather file – 0.44 NAD (Top Left), GW for 2 hr and the averaged weather file – 0.47 NAD (Top Right) and DNA-EX Contours (Bottom)**

Both Zucchini plots accurately follow the DNA-EX pattern but do not spread to the north and south as much as the DNA-EX contours causing a large area of false negatives. The individual contours follow closely to the DNA-EX contours but extend further to the northeast. Overall the plots are a good approximation of the DNA-EX as long as the CBRNE responders understand the possibility of large areas of false negatives.

The summary of the trials ran for Priscilla is listed in Table 13.

**Table 13. DELFIC FPT – NADs for Priscilla**

	<b>Priscilla</b>		
	<b>MOEx</b>	<b>MOEy</b>	<b>NAD</b>
<b>GW1</b>	0.77	0.70	0.26
<b>GW (4hr) - GW (3.5hr) - PRF</b>	0.82	0.64	0.28
<b>GW (4hr) - GW2(.5hr) - PRF</b>	0.92	0.55	0.31
<b>GW1(4hr) - GW2</b>	0.49	0.71	0.42
<b>PRF</b>	0.10	0.09	0.91

The DNA-EX document provided two sets of ground zero winds, one for one hour after detonation and one for four hours after detonation. The two trials producing the best comparison with the DNA-EX contours are using just the ground zero winds recorded one hour after detonation and the second using the one hour ground zero winds for four hours followed by the four hour ground zero winds for three and a half hours and the averaged weather file. The contours are shown in Figure 37.

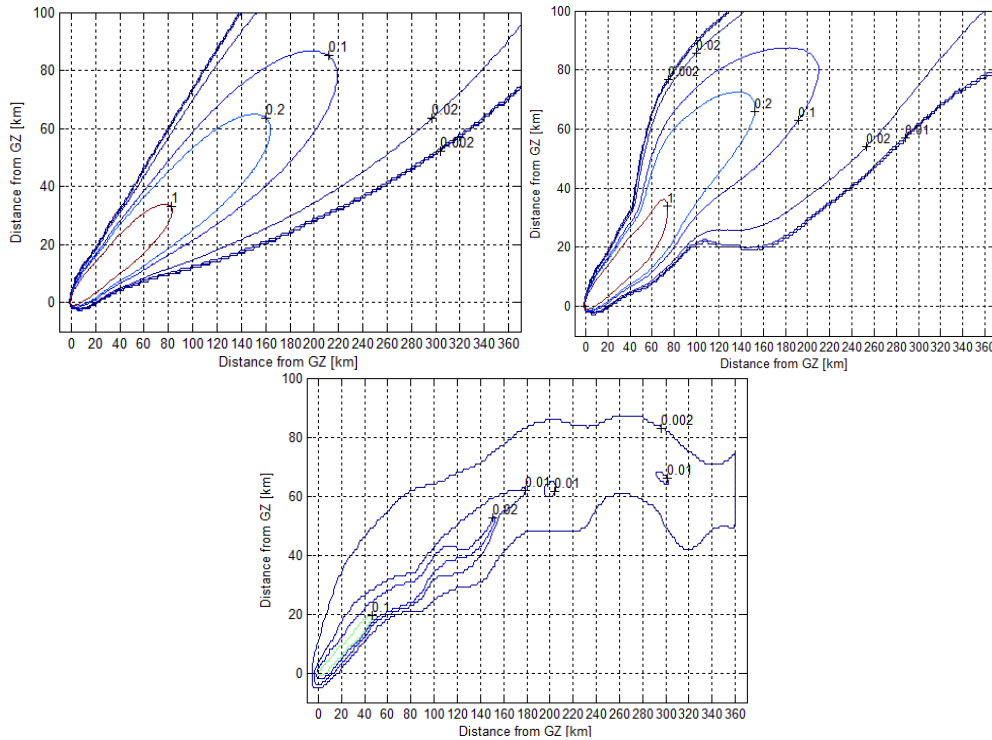


**Figure 37. DELFIC FPT – Priscilla Contours: Only GW – 0.26 NAD (Top Left), GW1 for 4 hr followed by GW2 for 3.5 hr and then the averaged weather file – 0.28 NAD (Top Right) and DNA-EX Contours (Bottom)**

The visual comparison shows that although the contours cover the area of fallout they do not accurately follow the overall contour pattern or the individual contours. The DELFIC FPT predicts the fallout along a northeast path from ground zero and does not curve to the east approximately 225 km northeast of ground zero. The advantage of these plots is there are minimal false negatives preventing responders from entering areas that were mapped as having no fallout when there was actually fallout. Visually, the contours’ using both ground zero winds and the averaged weather file more accurately follow the DNA-EX contours and is used for future comparisons. Overall, the predicted fallout area ensures the safety of CBRNE responders.

The summary of the trials ran for Smoky is listed in Table 14.

**Table 14. DELFIC FPT – NADs for Smoky**

	<b>Smoky</b>		
	<b>MOEx</b>	<b>MOEy</b>	<b>NAD</b>
<b>GW1(3hr) - GW2(.5hr) - PRF</b>	0.80	0.63	0.30
<b>GW1(3hr) - GW2(1hr) - PRF</b>	0.71	0.58	0.36
<b>GW1(3hr) - GW2</b>	0.27	0.62	0.63
<b>GW1</b>	0.25	0.66	0.64
<b>PRF</b>	0.00	0.00	1.00

The DNA-EX document provided two sets of ground zero winds, one at time of detonation and one for three hours after detonation. The trial producing the best comparison with the DNA-EX contours was using the ground zero winds recorded at detonation for three hours followed by the ground winds recorded at three hours for a half hour and then the averaged weather file. The second best model was using the detonation ground zero winds for three hours followed by the three hour ground zero winds for one hour and the averaged weather file. The contours are shown in Figure 38.

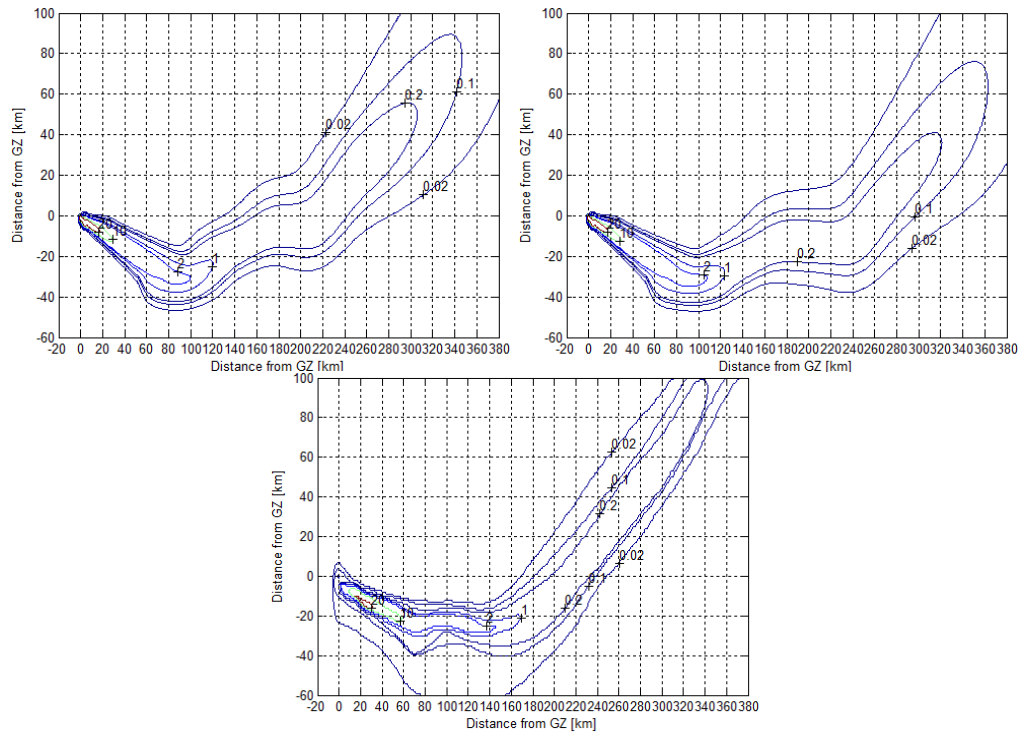


**Figure 38. DELFIC FPT – Smoky Contours: Only GW1 for 3hr followed by GW2 for .5 hr and then the average weather file – 0.30 NAD (Top Left), GW1 for 3 hr followed by GW2 for 1 hr and then the averaged weather file – 0.36 NAD (Top Right) and DNA-EX Contours (Bottom)**

The visual comparison shows that the overall contours cover the appropriate area of fallout and they do accurately follow the individual contour patterns. The only issues are the large area of false negatives to the south and underestimating the extent of the 2 and 1 R/hr dose-rate contours. The actual DNA-EX contours for the 2 and 1 R/hr dose-rates extend 20 km further east than the DELFIC FPT. Overall, the DELFIC FPT models Smoky effectively.

The summary of the trials ran for Johnie Boy is listed in Table 15.

**Table 15. DELFIC FPT – NADs for Johnie Boy**

	<b>Johnie Boy</b>		
	<b>MOEx</b>	<b>MOEy</b>	<b>NAD</b>
<b>GW1</b>	0.59	0.76	0.33
<b>GW1(1hr) - GW2(5hr) - PRF</b>	0.58	0.67	0.38
<b>GW1(1hr) - GW2</b>	0.58	0.67	0.38
<b>PRF</b>	0.00	0.01	1.00

The DNA-EX document also provided two sets of ground zero winds for Johnie Boy, one at time of detonation and one at one hour after detonation. The two trials producing the best comparison with the DNA-EX contours are using just the ground zero winds and the second using the ground zero winds at detonation for one hour followed by the one hour ground zero winds for five hours and then the averaged weather file. The contours are shown in Figure 39.

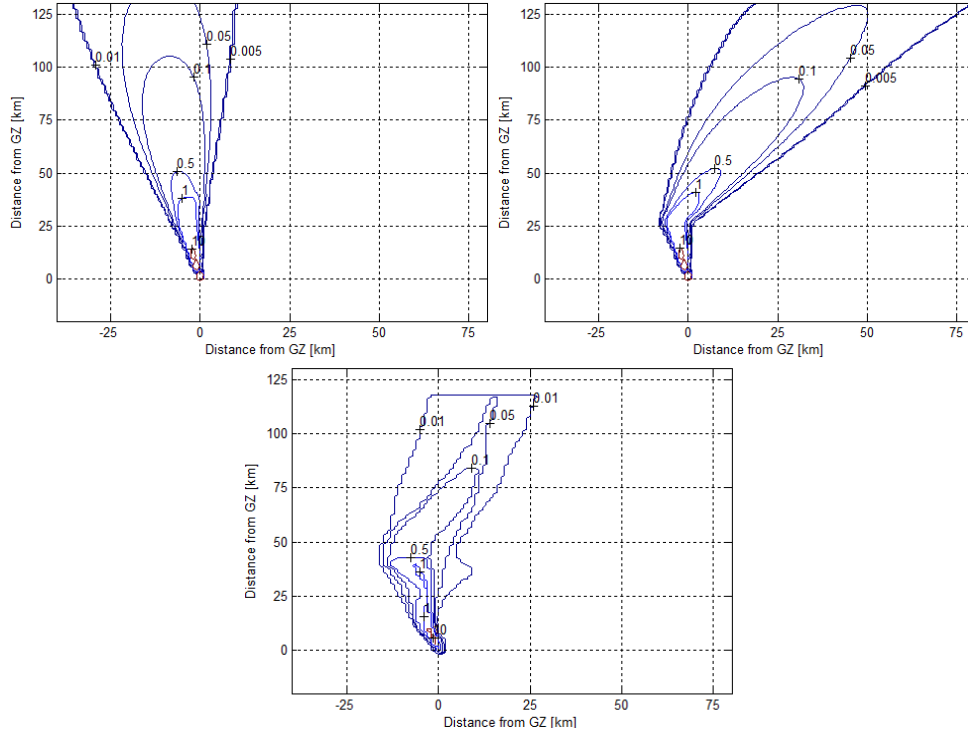


**Figure 39. DELFIC FPT – Johnie Boy Contours: Only GW1 – 0.33 NAD (Top Left), GW1 for 1 hr followed by GW2 for 5 hr and then the averaged weather file – 0.38 NAD (Top Right) and DNA-EX Contours (Bottom)**

The visual comparison shows that although the ground zero winds have a lower NAD it poorly represents the contours. The second model more accurately models the contours and the curve to the northeast than the ground zero winds model. The individual contours of the second model accurately follow the DNA-EX contours except for the excessive sharp curve to the northeast.

Overall, the DELFIC FPT is an effective modeling tool for planners. The issues with the DELFIC FPT are the limited weather input options and the inability for inputting various vertical heights. DELFIC only accepts weather input for the same vertical heights and does not allow inputs for altitudes lower than the inputted elevation.

DELFIC follows a flat earth model and therefore the inputted elevation is the elevation at

ground zero and cannot be changed in later time steps. Due to this limitation DELFIC does not accurately incorporate low altitude winds where the elevation drops below the elevation at ground zero.

## HPAC

Three trials were run for each test case using HPAC v5.0 SP1. One trial was run using no terrain and the other two varying the terrain resolution by 900 and 3500. This equates to the geographical area being divided into 900 or 3500 equal sized rectangles. The data was extracted using a 700x500 point matrix that was then converted to the DNA-EX  $M \times M$  matrix. The results are shown in Table 16.

**Table 16. HPAC – NADs for No Terrain and 900 and 3500 Resolution**

	900 Terrain Resolution			3500 Terrain Resolution			No Terrain		
	MOEx	MOEy	NAD	MOEx	MOEy	NAD	MOEx	MOEy	NAD
<b>Ess</b>	0.07	1.00	0.87	0.07	1.00	0.86	0.09	1.00	0.83
<b>George</b>	0.23	0.99	0.62	0.29	1.00	0.56	0.27	0.88	0.59
<b>Zucchini</b>	0.15	0.47	0.78	0.19	0.56	0.72	0.24	0.82	0.63
<b>Priscilla</b>	0.03	1.00	0.95	0.03	1.00	0.95	0.03	1.00	0.95
<b>Smoky</b>	0.00	0.09	0.99	0.00	0.09	0.99	0.01	0.11	0.99
<b>Johnie Boy</b>	0.00	0.03	0.99	0.00	0.03	0.99	0.01	0.04	0.98

The major differences between the use of no terrain and the two different terrain resolutions are shown in George and Zucchini. The visual comparisons show that there are slight differences between the use of no terrain and the varied terrain resolution.



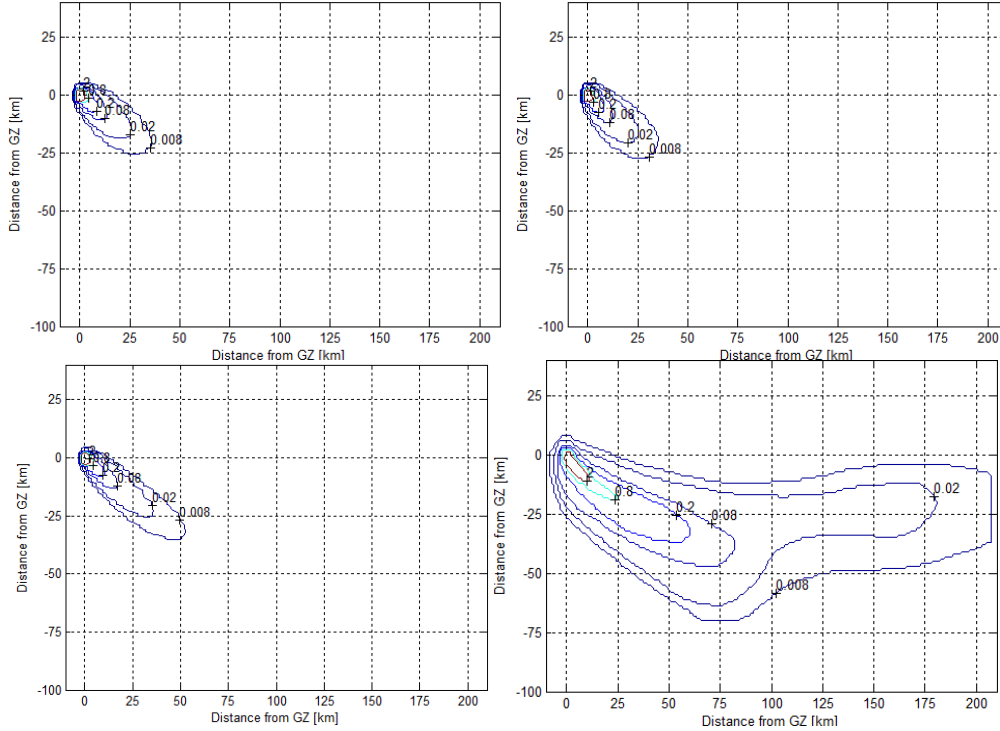


**Figure 40. HPAC – Ess Contours: Resolution of 900 – 0.87 NAD (Top Left), 3500 – 0.86 NAD (Top Right), No Terrain – 0.83 NAD (Bottom Left) and DNA-EX Contours (Bottom Right)**

For Ess, the use of no terrain extends further to the southeast than both the 900 and 3500 terrain resolution contours however does not extend nearly as far as the DNA-EX contours as shown in Figure 40. The contours follow the DNA-EX contours near ground zero but do not extend further than 60 km southeast of ground zero. This causes an extremely large area of false negatives. HPAC severely underestimates Ess’s fallout area.

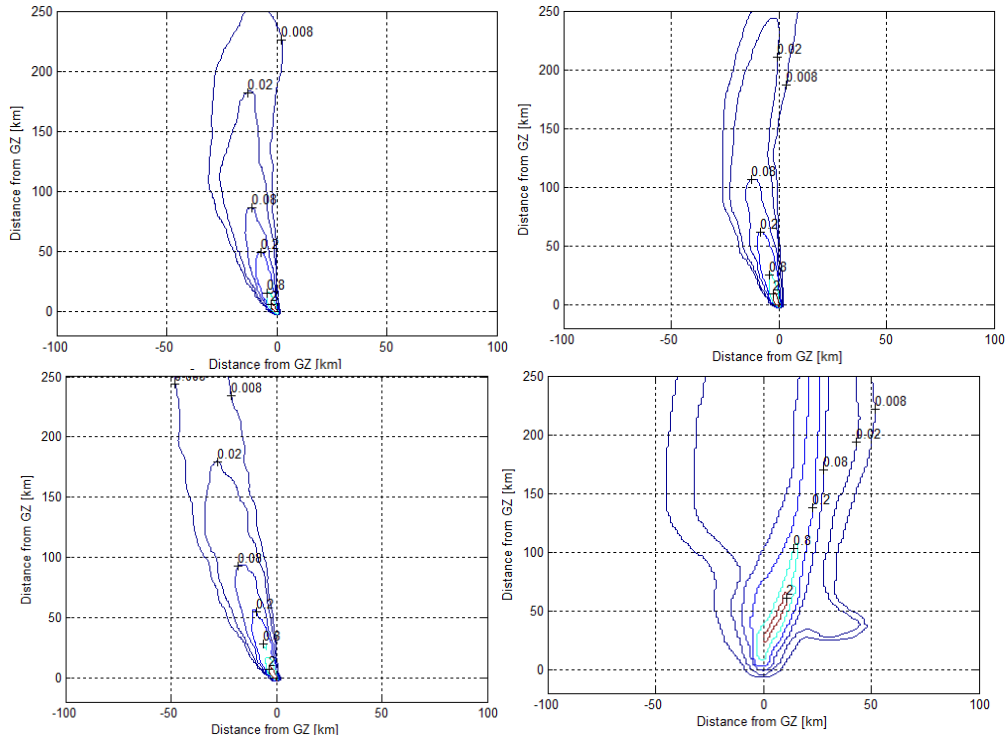


**Figure 41. HPAC – George Contours: Resolution of 900 – 0.62 NAD (Top Left), 3500 – 0.56 NAD (Top Right), No Terrain – 0.59 NAD (Bottom Left) and DNA-EX Contours (Bottom Right)**

For George, the individual contours shown in the 3500 resolution extend further to the north and more accurately follows the DNA-EX contours than the 900 resolution and the use of no terrain as shown in Figure 41. However, HPAC models the contours initially curving to the northwest and then to the northeast which is opposite of the DNA-EX contours. Additionally, the fallout does not spread to the east and west as shown in the DNA-EX contours. Again, HPAC underestimates the fallout area.

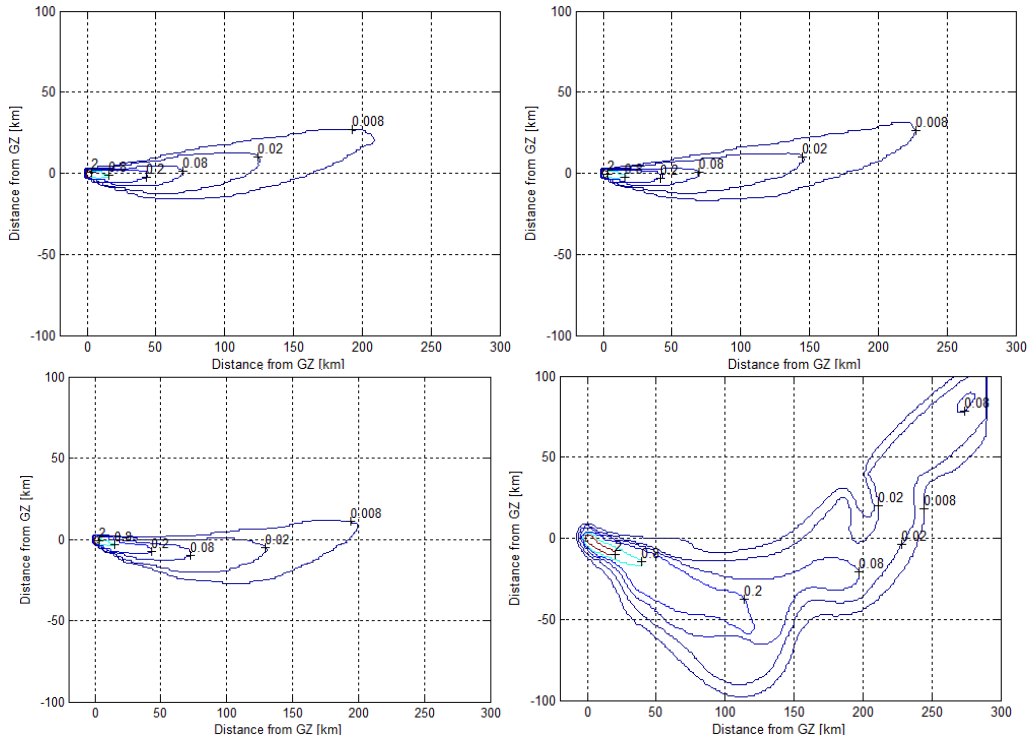


**Figure 42. HPAC – Zucchini Contours: Resolution of 900 – 0.78 NAD (Top Left), 3500 – 0.72 NAD (Top Right), No Terrain – 0.63 NAD (Bottom Left) and DNA-EX Contours (Bottom Right)**

For Zucchini, a visual comparison shows that the 3500 resolution contours extend further to the east but both the 900 and 3500 contours spread further to the north and does not curve to the southeast as seen in the DNA-EX contours, shown in Figure 42. The no terrain contours extend further to the south causing a larger area of overlap with the DNA-EX contours than the 900 and 3500 terrain resolutions, however, the no terrain contours do not extend to the southeast as shown in the DNA-EX. This is the result of the limitations of HPAC and not being able to incorporate the ground zero winds. Again, HPAC underestimates the fallout area and predicts a large area of false negatives.

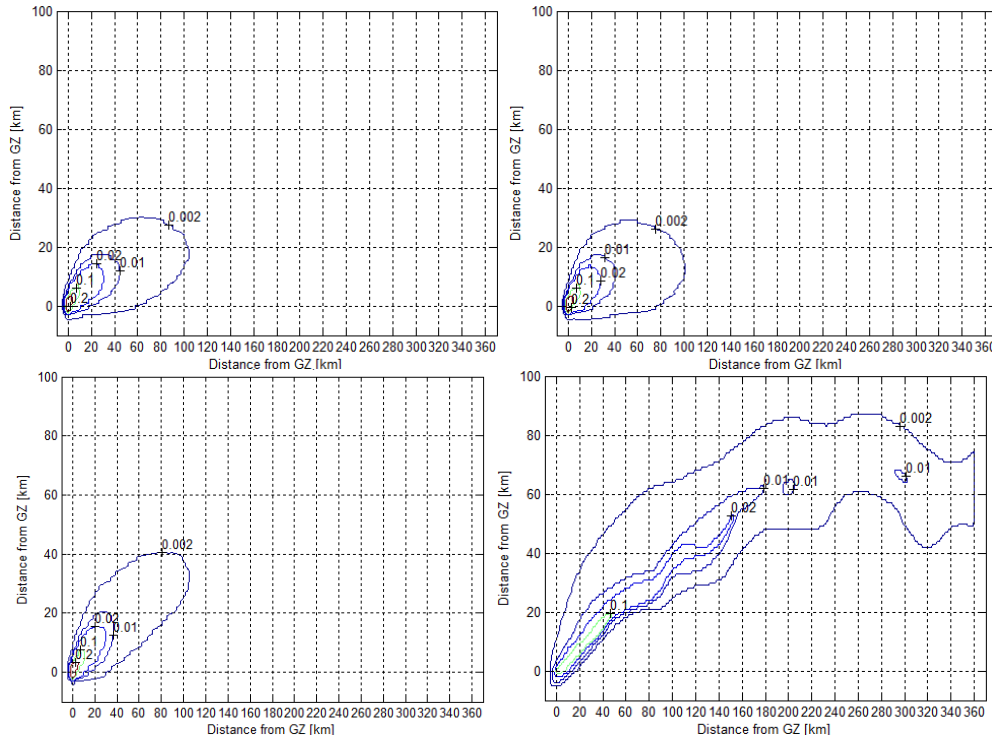


**Figure 43. HPAC – Priscilla Contours: Resolution of 900 – 0.95 NAD (Top Left), 3500 – 0.95 NAD (Top Right), No Terrain – 0.95 NAD (Bottom Left) and DNA-EX Contours (Bottom Right)**

For Priscilla, the 900 and 3500 terrain resolution extends further to the southeast causing a greater area of false positives than the no terrain contours as shown in Figure 43. This produces a slightly lower NAD for the no terrain contours. None of the trials extend the fallout area to the northeast with a slight curve to the east as shown in the DNA-EX contours. This causes a large area of false negatives. Overall HPAC completely underestimates the fallout patterns.

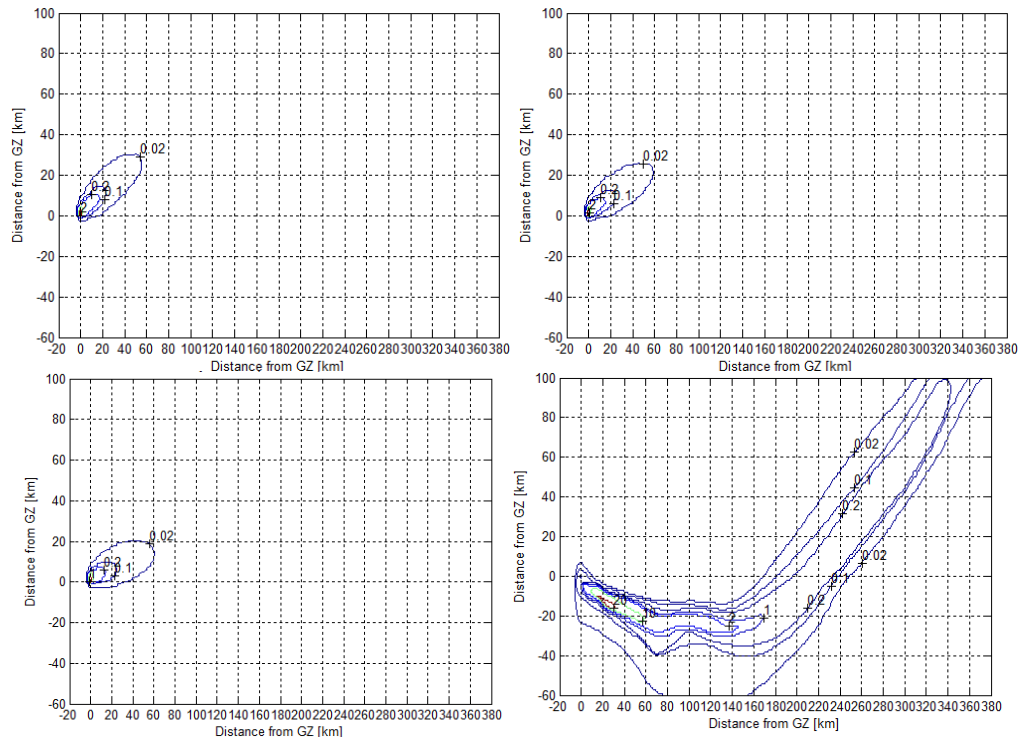


**Figure 44. HPAC – Smoky Contours: Resolution of 900 – 0.99 NAD (Top Left), 3500 – 0.99 NAD (Top Right), No Terrain – 0.99 NAD (Bottom Left) and DNA-EX Contours (Bottom Right)**

HPAC completely underestimates the fallout area for Smoky as shown in Figure 44. The major issue for the contours initially going in the northeast direction vice the southeast direction as shown in the DNA-EX contours is due to the inability of incorporating the ground zero winds in HPAC.

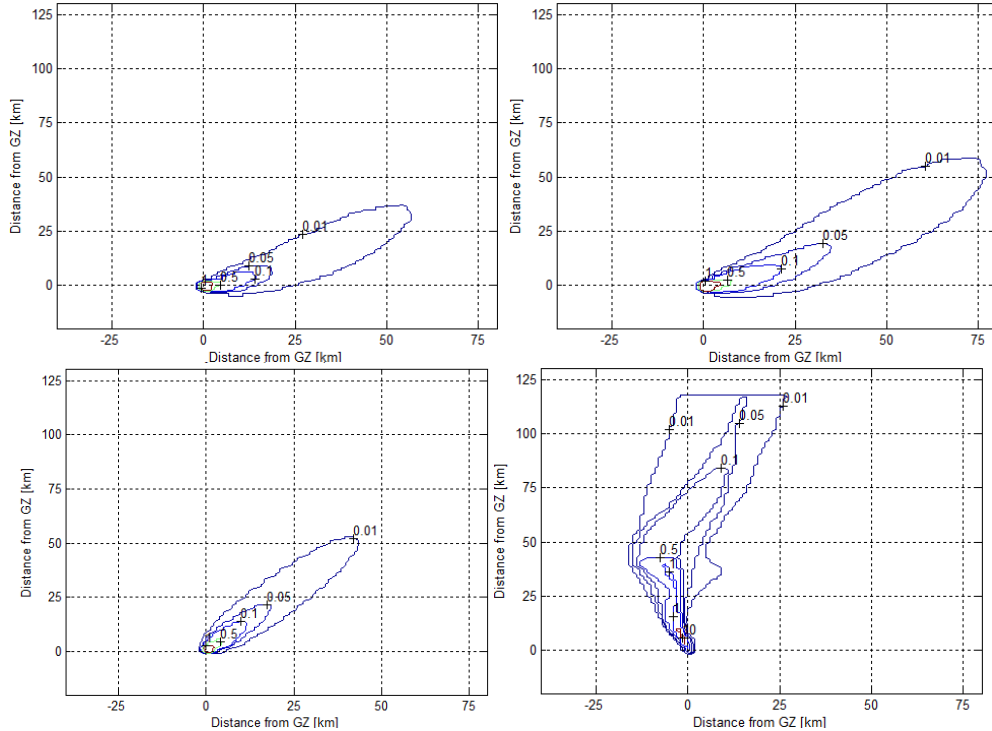


**Figure 45. HPAC – Johnie Boy Contours: Resolution of 900 – 0.99 NAD (Top Left), 3500 – 0.99 NAD (Top Right), No Terrain – 0.98 NAD (Bottom Left) and DNA-EX Contours (Bottom Right)**

For Johnie Boy, a height of burst of zero was used when running HPAC. The main difference between the HPAC contours and the DNA-EX contours for Johnie Boy are again due to the inability of incorporating the ground zero winds, a limitation to HPAC. Incorporating the ground winds would significantly improve the model.

Overall, HPAC significantly underestimates the fallout area in all the test cases. Jones concluded in his research that HPAC does not accurately disperse the particles on the ground because it neglects the weather dynamics at lower altitudes during cloud stabilization [23:90]. Incorporating the ground zero winds and advection during cloud stabilization will improve the models.

## Overall Comparison

An overall comparison was conducted using the best models for each test case from each modeling program. The following section will discuss the comparison for each test case.

The results of the overall comparison of Ess are shown in Table 17 in order of increasing NAD. HYSPLIT resulted in the lowest NAD, differing from the FDC by 0.35. Further comparisons were studied using a visual comparison and the individual contour comparison.

**Table 17. Overall Comparison of Ess Contours**

	Ess		
	MOEx	MOEy	NAD
<b>HYSPLIT</b>	0.18	0.76	0.37
<b>FDC</b>	0.17	0.70	0.72
<b>DELFIK FPT</b>	0.16	0.61	0.75
<b>HPAC</b>	0.09	1.00	0.83

The plots of the various programs are shown below in order of increasing NAD to allow for a visual comparison. The lowest NAD, numerically a better fit to the DNA-EX, is shown first.

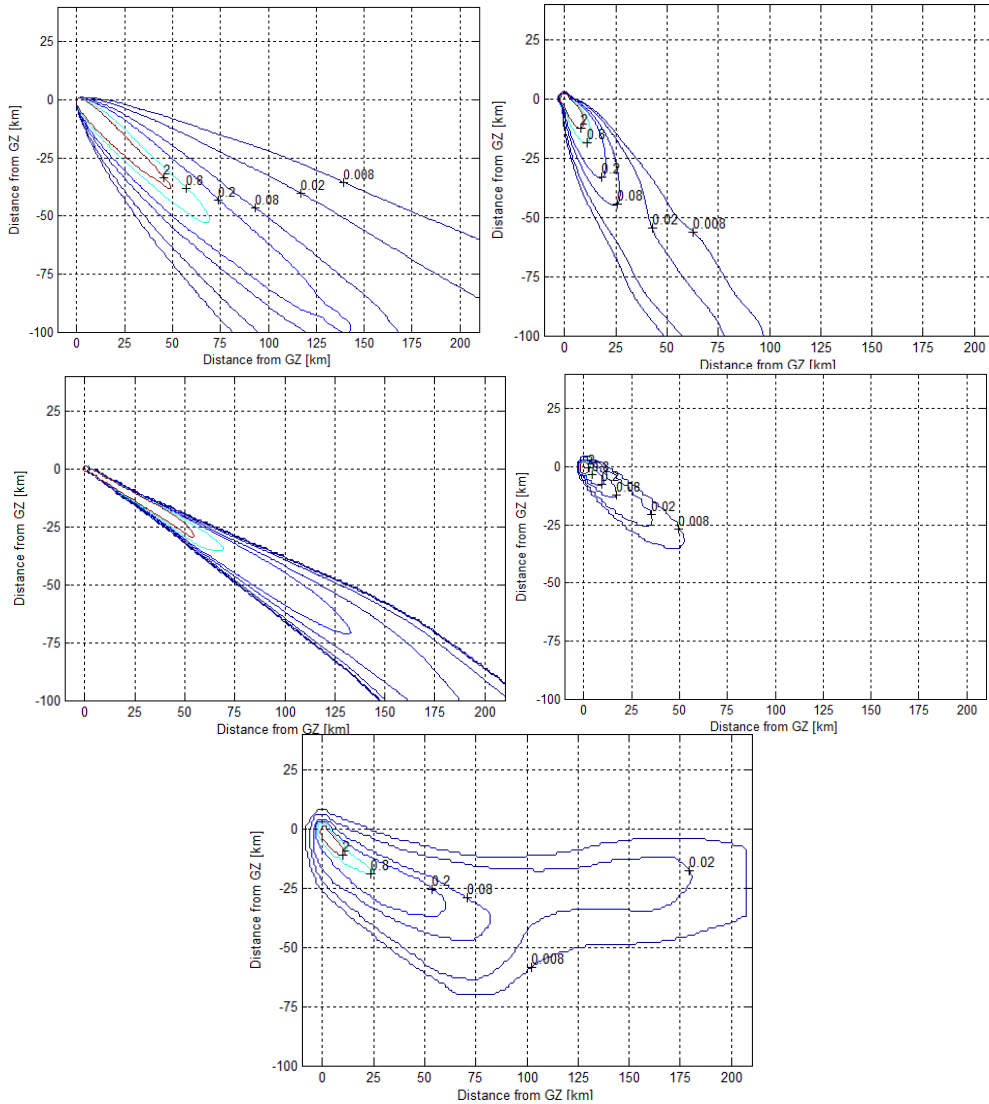


**Figure 46. Overall Comparison of Ess: HYSPLIT – 0.37 NAD (Top Left), FDC – 0.72 NAD (Top Right), DELFIPT – 0.75 NAD (Middle Left), HPAC – 0.83 NAD (Middle Right) and DNA-EX (Bottom)**

All contours differ from the DNA-EX contours due to the lack of winds from the west. This is caused from the resolution of the weather file. The weather data listed in the low resolution weather file has 2.5 degrees between points which is equivalent to approximately 210 km. The elevation provided in the weather file for each point remains constant until the parcels reach the limits of the next data point. This prevents lower altitude winds for terrain features that fall below the current elevation point. The low



altitude winds listed in the weather files are from the west and are the winds being neglected in all the modeling programs due to the actual changes in elevation that are not portrayed in the weather file. This prevents an accurate model of Ess, this occurred while using high resolution weather data as shown in Jones' research [23]. HYSPLIT more accurately models Ess of the four programs and spreads further to the east and west than the other three programs.

The third comparison done was studying the individual contours shown in Table 18.

**Table 18. NADs of Individual Contours for Ess**

Ess				
Contours (R/hr)	FDC	HYSPLIT	HPAC	DELFIC FPT
<b>2</b>	0.76	0.97	0.89	1.00
<b>0.8</b>	0.78	0.99	0.95	0.96
<b>0.2</b>	0.90	0.92	0.96	0.93
<b>0.08</b>	0.93	0.92	0.98	0.95
<b>0.02</b>	0.90	0.82	0.99	0.98
<b>0.008</b>	0.15	0.18	0.13	0.17

A better visual comparison of the individual contours is shown in Figure 47. This shows that the FDC more accurately models three of the six contours, HYSPLIT more accurately models two of the six contours and HPAC more accurately models one of the six contours (the lower the NAD the better the model). All models accurately model the lowest contour but are not very accurate in the remaining five contours due to the inability to incorporate low altitude winds. Modeling the higher dose-rates is more

pertinent than the low dose-rates due to the increased safety hazard to CBRNE personnel, none of the programs accurately model the high dose-rate contours.

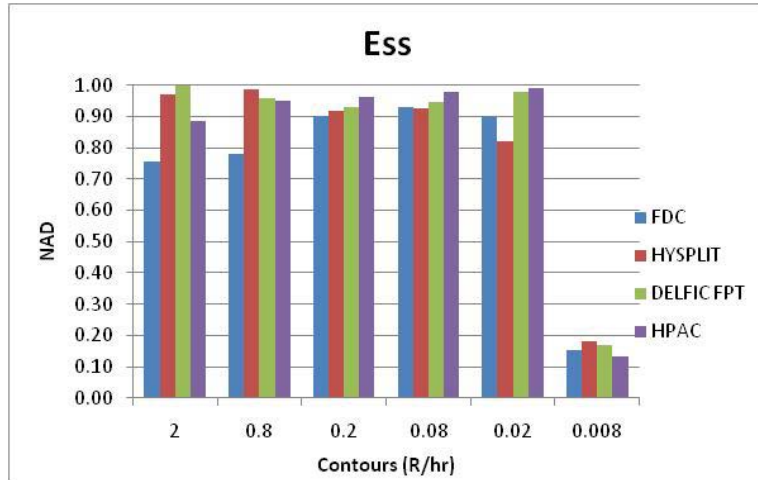


Figure 47. Overall Individual Contour Comparison for Ess

An overall assessment is conducted by summing the overall NAD, the average of the NADs for the individual contours and the percentage of the area of false negatives (number of points of false negatives divided by the number of points observed) shown in Table 19. A perfect model would have a sum of zero, the lower the sum the closer the model is to the DNA-EX contours. The overall assessment shows that HYSPLIT is the preferred modeling program for modeling Ess.

**Table 19. Overall Assessment of Ess**

	Ess			
	HYSPLIT	FDC	DELFIPT	HPAC
<b>Overall NAD</b>	0.37	0.72	0.75	0.83
<b>Individual Comparison</b>	0.80	0.74	0.83	0.82
<b>Total False Negatives</b>	4241	8177	8304	8973
<b>AFN Rating</b>	0.43	0.83	0.84	0.91
<b>Total</b>	1.60	2.29	2.42	2.56

The overall comparison results for George are shown in Table 20 in order of increasing NAD. The FDC resulted in the lowest NAD, differing from HYSPLIT by 0.09. Further comparisons were studied using a visual comparison and comparing the individual contours.

**Table 20. Overall Comparison of George Contours**

	George		
	MOEx	MOEy	NAD
<b>FDC</b>	0.80	0.94	0.14
<b>HYSPLIT</b>	0.52	0.94	0.23
<b>DELFIPT</b>	0.59	0.98	0.26
<b>HPAC</b>	0.29	1.00	0.56

The plots of the various programs are shown below in order of increasing NAD for the visual comparison. All programs except for HPAC provide approximately the right area of fallout with the FDC predicting a smaller false negative area. None of the programs accurately follow the individual contours as shown in Table 21 and Figure 49. However, of the four programs, the DELFIPT contours are directed in the right direction as shown in Figure 48. None of the four programs accurately portray the bulge to the east

due to the inability to accurately map the elevations of the terrain. This would occur whether using low or high resolution weather data.

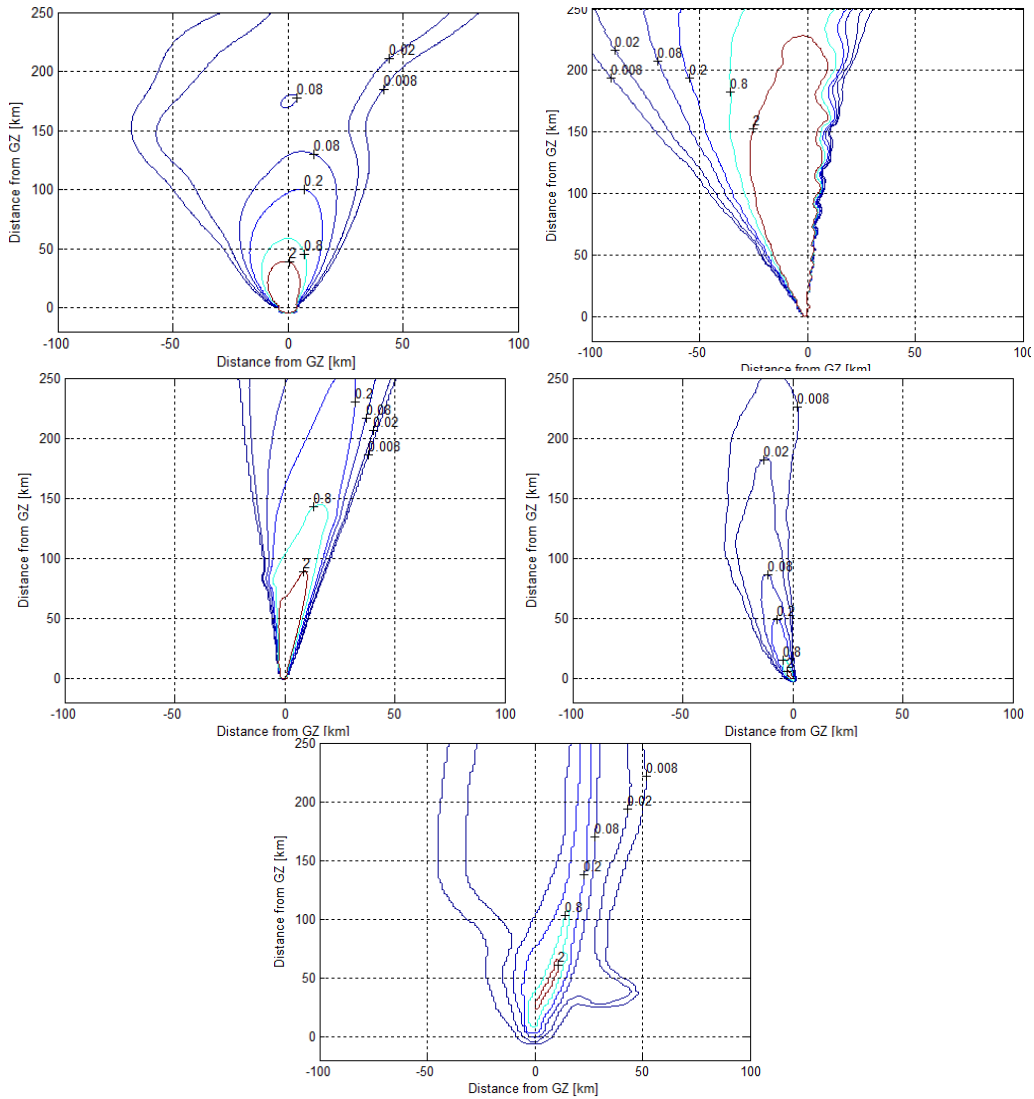


**Figure 48. Overall Comparison of George: FDC – 0.14 NAD (Top Left), HYSPLIT – 0.23 NAD (Top Right), DELFC FPT – 0.26 NAD (Middle Left), HPAC – 0.56 NAD (Middle Right) and DNA-EX (Bottom)**

The DELFC FPT and FDC both more accurately model two each of the six individual contours and both model the 0.2 R/hr contour approximately the same. HPAC more accurately models the 0.02 R/hr contour.

**Table 21. NADs of Individual Contours for George**

George				
Contours (R/hr)	FDC	DELFIK FPT	HPAC	HYSPLIT
2	0.78	0.85	0.97	1.00
0.8	0.69	0.65	0.93	1.00
0.2	0.78	0.78	0.94	0.96
0.08	0.37	0.66	0.85	0.88
0.02	0.74	0.89	0.72	0.96
0.008	0.32	0.20	0.37	0.46

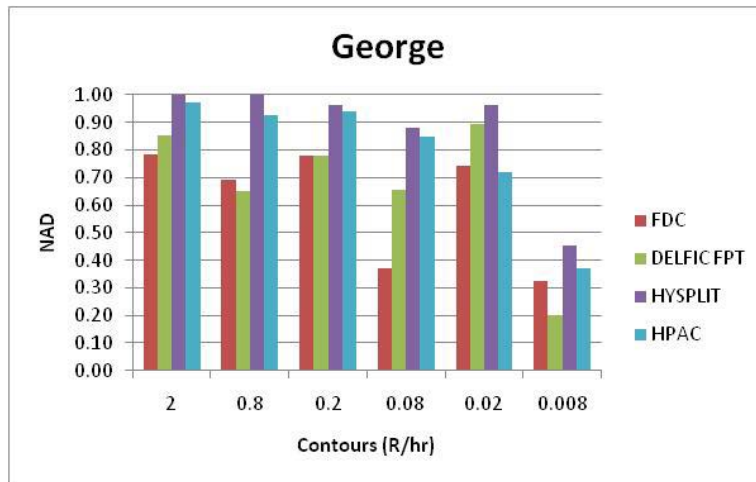


**Figure 49. Overall Individual Contour Comparison for George**

The overall assessment using the total sum of the overall NAD, the average of the NADs for the individual contours and the percentage of the area of false negatives is shown in Table 22. The overall assessment shows that the FDC is the preferred modeling program for modeling George. This is due to the smaller area of false negatives resulting from the use of the FDC. A visual comparison shows that the DELFIK FPT more accurately models George and its contours but has a larger area of false negatives preventing it from being the preferred model.

**Table 22. Overall Assessment of George**

<b>George</b>				
	<b>FDC</b>	<b>DELFC FPT</b>	<b>HYSPLIT</b>	<b>HPAC</b>
<b>Overall NAD</b>	0.14	0.26	0.23	0.56
<b>Individual Comparison</b>	0.61	0.67	0.88	0.80
<b>Total False Negatives</b>	4923	10187	8385	17649
<b>AFN Rating</b>	0.20	0.41	0.34	0.71
<b>Total</b>	0.95	1.35	1.45	2.07

The overall comparison results for Zucchini are shown in Table 23 in order of increasing NAD. The FDC resulted in the lowest NAD, differing from HYSPLIT by 0.19.

**Table 23. Overall Comparison of Zucchini Contours**

	<b>Zucchini</b>		
	<b>MOEx</b>	<b>MOEy</b>	<b>NAD</b>
<b>FDC</b>	0.90	0.79	0.16
<b>HYSPLIT</b>	0.49	0.65	0.35
<b>DELFC FPT</b>	0.39	1.00	0.44
<b>HPAC</b>	0.24	0.82	0.63

The plots of the various programs are shown below in order of increasing NAD for the visual comparison.

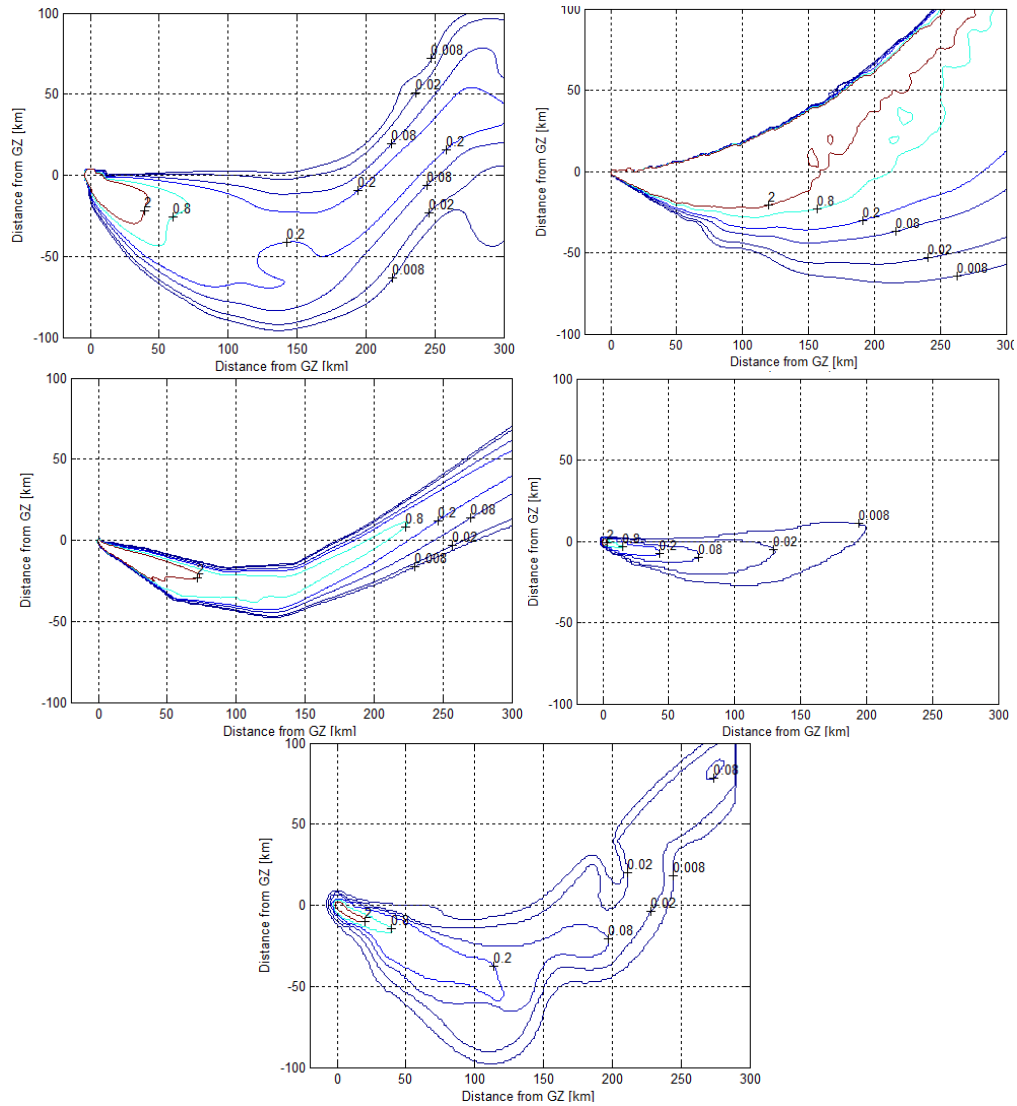


**Figure 50. Overall Comparison of Zucchini: FDC – 0.16 NAD (Top Left), HYSPLIT – 0.35 NAD (Top Right), DELFIC FPT – 0.44 NAD (Middle Left), HPAC – 0.63 NAD (Middle Right) and DNA-EX (Bottom)**

The visual comparison shows that the FDC has the smallest area of false negatives followed by HYSPLIT. The DELFIC FPT accurately follows the path of the particles but does not completely cover the entire fallout area causing a high area of false negatives. HPAC does not accurately follow the fallout area. HYSPLIT accurately follows the overall contours but does not initially go to the southeast due to the inability to incorporate ground zero winds. None of the four programs accurately portray the nub to

the north of the fallout area approximately 200 kilometers east of ground zero due to the inability to accurately model the changes in terrain elevations. Comparing individual contours using Table 24 and Figure 51 shows that the FDC and HPAC more accurately model two of the six contours.

**Table 24. NADs of Individual Contours for Zucchini**

<b>Zucchini</b>				
<b>Contours (R/hr)</b>	<b>FDC</b>	<b>HPAC</b>	<b>DELFC FPT</b>	<b>HYSPLIT</b>
<b>2</b>	0.99	0.85	0.99	1.00
<b>0.8</b>	0.71	0.89	0.86	0.98
<b>0.2</b>	0.87	0.95	0.90	0.88
<b>0.08</b>	0.85	0.93	0.87	0.83
<b>0.02</b>	0.89	0.72	0.96	0.97
<b>0.008</b>	0.11	0.14	0.08	0.19

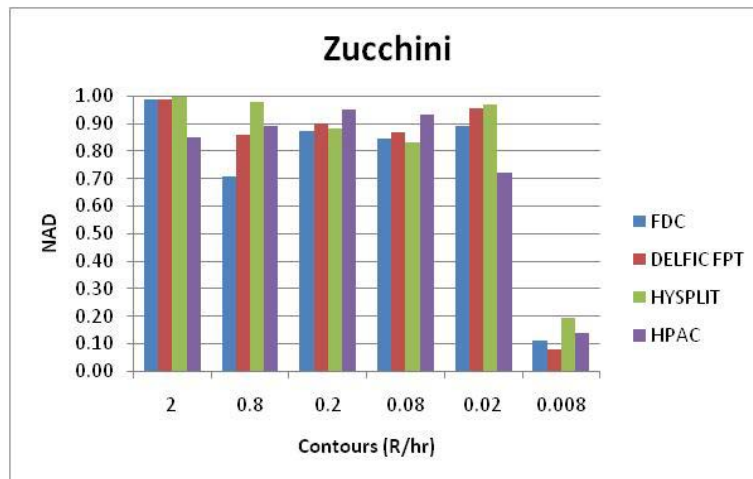


**Figure 51. Overall Individual Contour Comparison for Zucchini**

The overall assessment using the total sum of the overall NAD, the average of the NADs for the individual contours and the percentage of the area of false negatives is shown in



Table 25. The overall assessment shows that the FDC is the preferred modeling program for modeling Zucchini.

**Table 25. Overall Assessment of Zucchini**

<b>Zucchini</b>				
	<b>FDC</b>	<b>HYSPLIT</b>	<b>DELFIPT</b>	<b>HPAC</b>
<b>Overall NAD</b>	0.16	0.35	0.44	0.63
<b>Individual Comparison</b>	0.74	0.81	0.78	0.75
<b>Total False Negatives</b>	1601	5417	9682	12174
<b>AFN Rating</b>	0.10	0.34	0.61	0.76
<b>Total</b>	1.00	1.50	1.82	2.14

The overall comparison results for Priscilla are shown in Table 26 in order of increasing NAD. The DELFIPT resulted in the lowest NAD, differing from HYSPLIT by 0.24.

**Table 26. Overall Comparison of Priscilla Contours**

	<b>Priscilla</b>		
	<b>MOEx</b>	<b>MOEy</b>	<b>NAD</b>
<b>DELFIPT</b>	0.82	0.64	0.28
<b>HYSPLIT</b>	0.60	0.40	0.52
<b>FDC</b>	0.41	0.51	0.54
<b>HPAC</b>	0.03	1.00	0.95

The plots of the various programs used for visual comparison are shown below in order of increasing NAD.

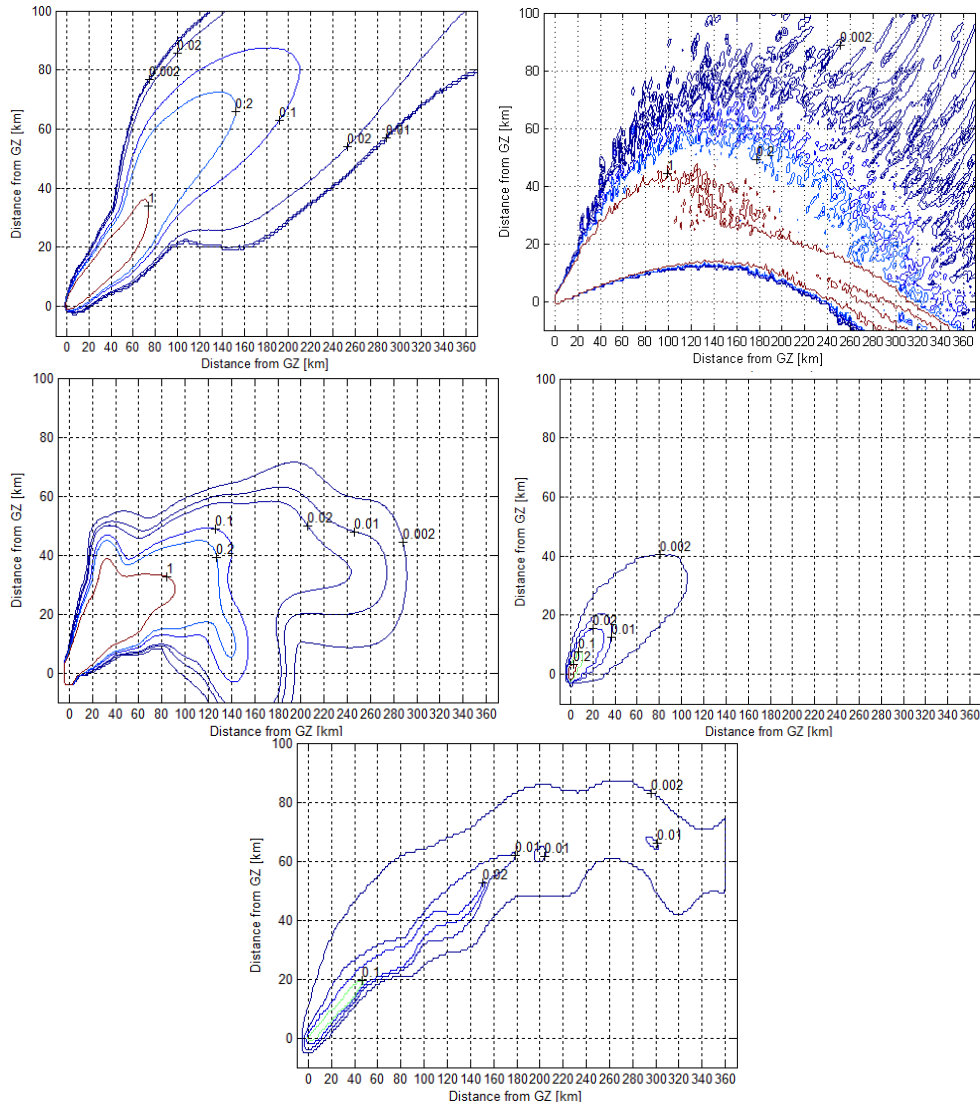


**Figure 52. Overall Comparison of Priscilla: DELFC FPT – 0.28 NAD (Top Left), HYSPLIT – 0.52 NAD (Top Right), FDC – 0.54 NAD (Middle Left), HPAC – 0.95 (Middle Right) and DNA-EX (Bottom)**

Of the four plots HYSPLIT more accurately models Priscilla as seen in Figure 52.

HYSPLIT follows the right curvature but expands too much in the north and south causing a high area of false positives. The DELFC FPT covers the appropriate area but does not following the contours properly and has an increased value of false positives.

The FDC also has a large area of false positives from the dispersion to the southeast along with an area of false negatives to the east. HPAC has a significantly large area of

false negatives. Comparing contours shows that HPAC more accurately models five of the six contours, shown in Table 27 and Figure 53. However, due to HPAC's significantly large area of false negatives HPAC fails to properly map the fallout area of Priscilla. Overall, the DELFIC FPT and HYSPLIT provide the best fallout patterns for planning purposes because an area of false positives is less hazardous to CBRNE planners than an area of false negatives.

**Table 27. Comparison of Individual Contours for Priscilla**

Priscilla				
Contours (R/hr)	HPAC	FDC	DELFCFPT	HYSPLIT
<b>1</b>	0.91	1.00	1.00	1.00
<b>0.2</b>	0.88	1.00	1.00	1.00
<b>0.1</b>	0.74	0.98	1.00	1.00
<b>0.02</b>	0.93	0.95	0.98	1.00
<b>0.01</b>	0.92	0.85	1.00	0.99
<b>0.002</b>	0.05	0.28	0.28	0.51

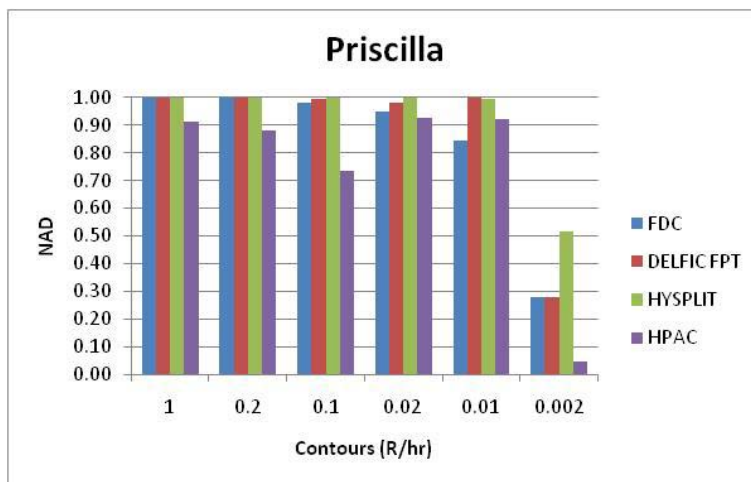


**Figure 53. Overall Individual Contour Comparison for Priscilla**

The overall assessment using the total sum of the overall NAD, the average of the NADs for the individual contours and the percentage of the area of false negatives is shown in Table 28. The overall assessment of Priscilla shows that the DELFIC FPT is the preferred modeling program due to the smaller area of false negatives when compared to HYSPLIT.

**Table 28. Overall Assessment of Priscilla**

<b>Priscilla</b>				
	<b>DELFIC FPT</b>	<b>HYSPLIT</b>	<b>FDC</b>	<b>HPAC</b>
<b>Overall NAD</b>	0.28	0.52	0.54	0.95
<b>Individual Comparison</b>	0.88	0.92	0.84	0.74
<b>Total False Negatives</b>	2226	4986	7406	12201
<b>AFN Rating</b>	0.18	0.40	0.59	0.97
<b>Total</b>	1.33	1.83	1.98	2.66

The overall comparison results for Smoky are shown in Table 29 in order of increasing NAD. The DELFIC FPT resulted in the lowest NAD, differing from the FDC by 0.14.

**Table 29. Overall Comparison of Smoky Contours**

	<b>Smoky</b>		
	<b>MOEx</b>	<b>MOEy</b>	<b>NAD</b>
<b>DELFIC FPT</b>	0.80	0.63	0.30
<b>FDC</b>	0.48	0.67	0.44
<b>HYSPLIT</b>	0.12	0.12	0.80
<b>HPAC</b>	0.01	0.11	0.99

The plots of the various programs used for visual comparison are shown below in order of increasing NAD.

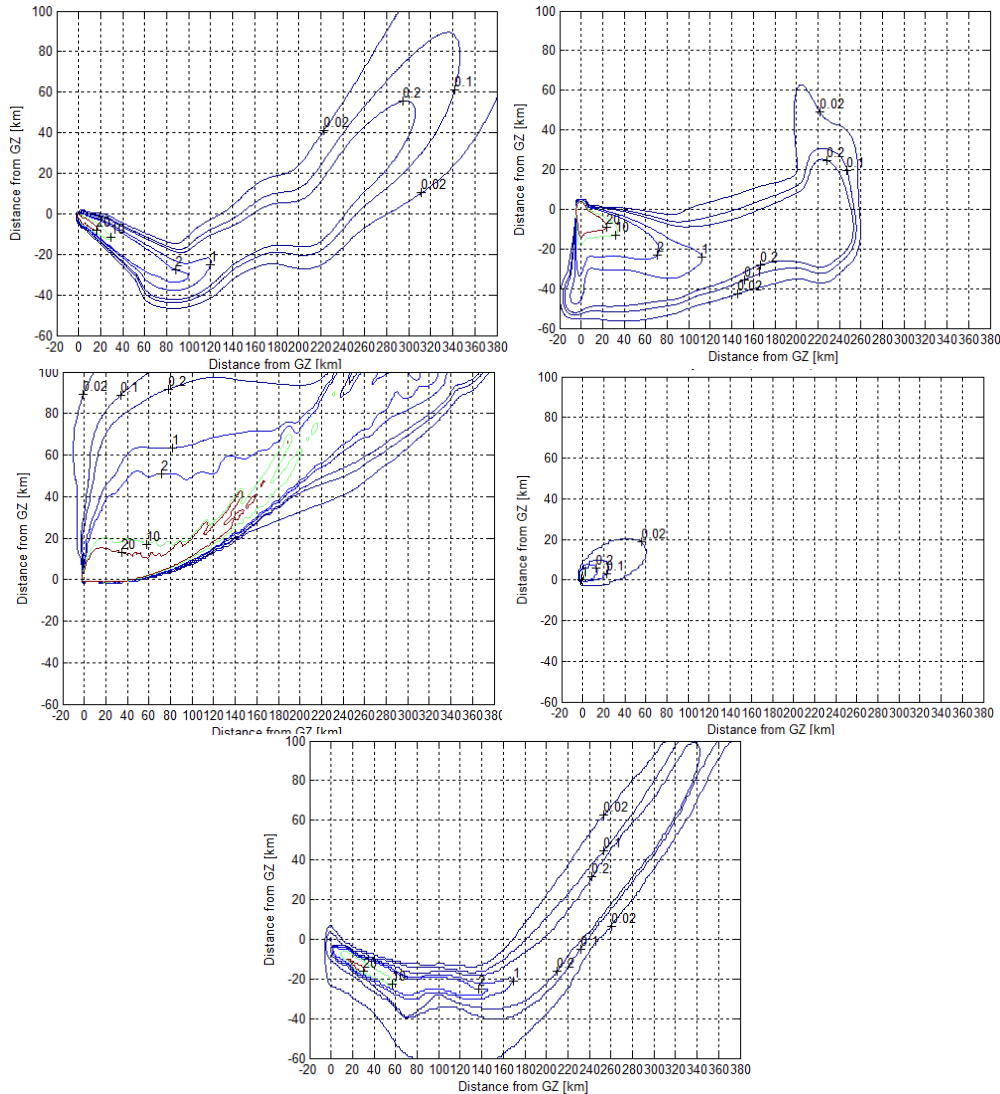


**Figure 54. Overall Comparison of Smoky: DELFIPT – 0.30 NAD (Top Left), FDC – 0.44 NAD (Top Right), HYSPLIT – 0.80 NAD (Middle Left), HPAC – 0.99 NAD (Middle Right) and DNA-EX (Bottom)**

From the plots, it is clear that the DELFIPT provides the best modeling program when modeling Smoky. From Table 30 and Figure 55, the DELFIPT more accurately models four of the seven contours for Smoky. It does not accurately model the 20 and 2

R/hr contours but does an effective job with the remaining five contours. HYSPLIT follows the right pattern but does not initially disperse to the southeast due to the inability of incorporating ground zero winds.

**Table 30. NADs of Individual Contours for Smoky**

Smoky				
Contours (R/hr)	DELFIPT	FDC	HPAC	HYSPLIT
20	0.75	0.28	1.00	1.00
10	0.50	0.65	1.00	1.00
2	0.75	0.67	1.00	1.00
1	0.44	0.61	1.00	0.97
0.2	0.70	0.91	1.00	0.96
0.1	0.56	0.85	0.99	0.93
0.02	0.10	0.07	0.06	0.27

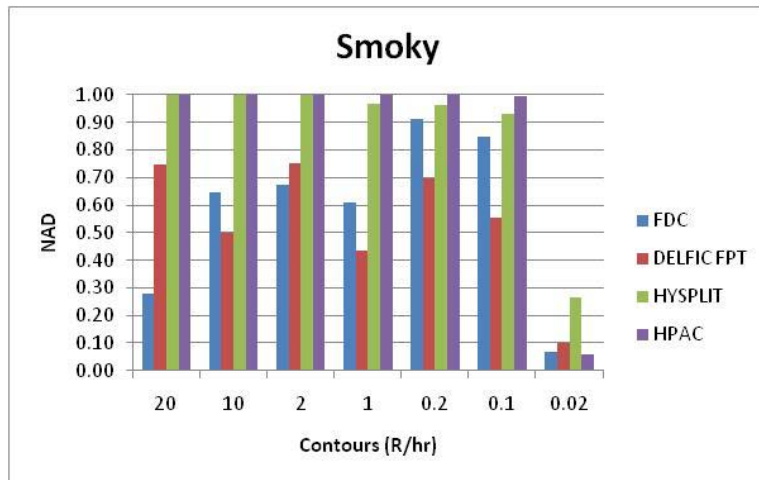


**Figure 55. Overall Individual Contour Comparison for Smoky**

The overall assessment using the total sum of the overall NAD, the average of the NADs for the individual contours and the percentage of the area of false negatives is shown in

Table 31. The overall assessment shows that the DELFIC FPT is the most accurate modeling program for modeling Smoky.

**Table 31. Overall Assessment of Smoky**

<b>Smoky</b>				
	<b>DELFIC FPT</b>	<b>FDC</b>	<b>HYSPLIT</b>	<b>HPAC</b>
<b>Overall NAD</b>	0.30	0.44	0.80	0.99
<b>Individual Comparison</b>	0.54	0.58	0.88	0.86
<b>Total False Negatives</b>	4313	11410	15855	21792
<b>AFN Rating</b>	0.20	0.52	0.72	0.99
<b>Total</b>	1.03	1.54	2.40	2.85

The overall comparison results for Johnie Boy are shown in Table 32 in order of increasing NAD. The FDC resulted in the lowest NAD, differing from the DELFIC FPT by 0.02.

**Table 32. Overall Comparison of Johnie Boy Contours**

	<b>Johnie Boy</b>		
	<b>MOEx</b>	<b>MOEy</b>	<b>NAD</b>
<b>FDC</b>	0.57	0.87	0.31
<b>DELFIC FPT</b>	0.59	0.76	0.33
<b>HYSPLIT</b>	0.02	0.05	0.49
<b>HPAC</b>	0.01	0.04	0.98

The plots of the various programs used for visual comparison are shown below in order of increasing NAD.

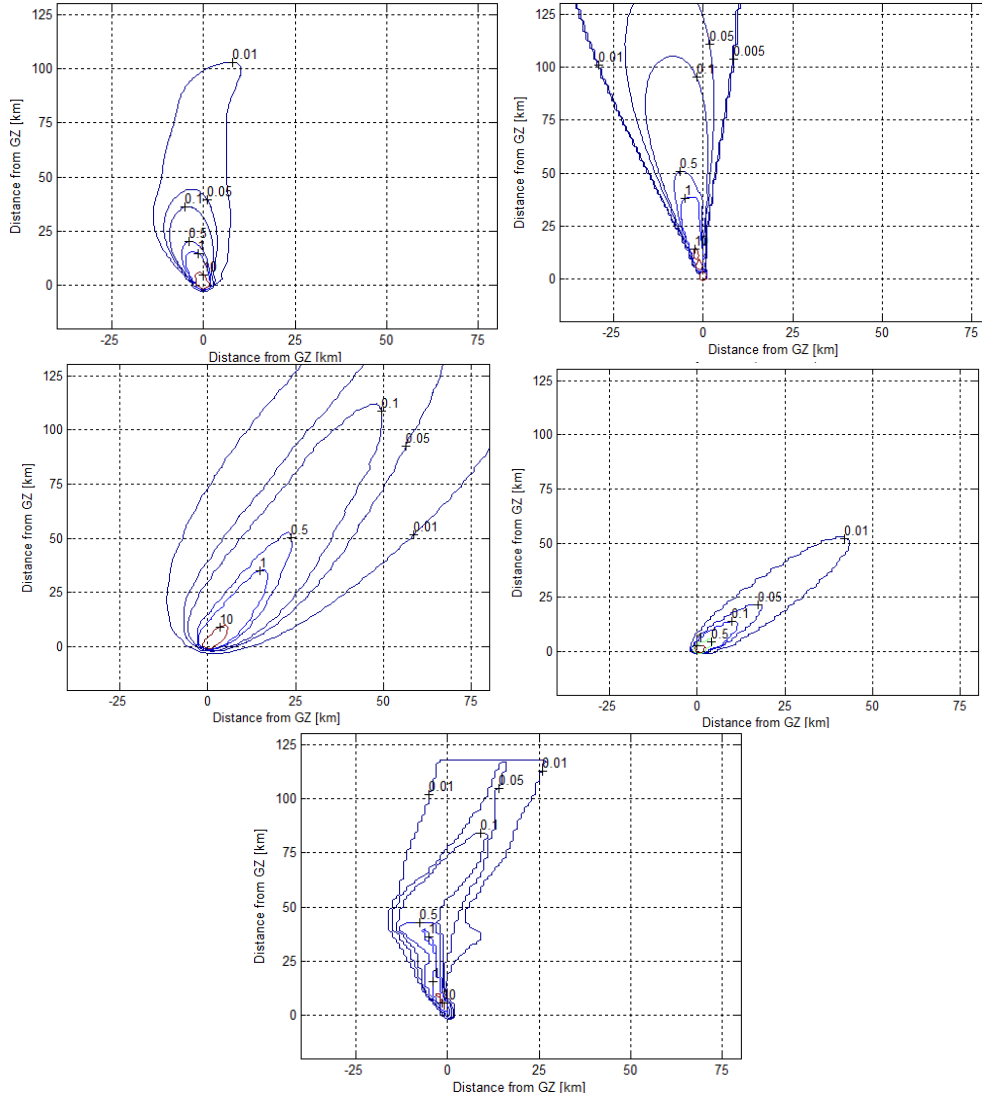


**Figure 56. Overall Comparison of Johnie Boy: FDC – 0.31 NAD (Top Left), DELFC FPT – 0.33 NAD (Top Right), HYSPLIT – 0.49 NAD (Middle Left), HPAC – 0.98 NAD (Middle Right) and DNA-EX (Bottom)**

A visual comparison shows that the FDC and the DELFC FPT equally model Johnie Boy. The DELFC FPT has a larger area of overall lap and a smaller area of false negatives; however it has a larger area of false positives than the FDC resulting in a slightly higher NAD. The DELFC FPT’s fallout area is less hazardous to CBRNE responders than the FDC’s fallout area. A comparison of the individual contours, as



shown in Table 33 and Figure 57, show that the DELFIC FPT more accurately models three of the six contours and the FDC more accurately models the remaining three.

**Table 33. NADs of the Individual Contours for Johnie Boy**

<b>Johnie Boy</b>				
<b>Contours (R/hr)</b>	<b>FDC</b>	<b>DELFC FPT</b>	<b>HYSPLIT</b>	<b>HPAC</b>
<b>10</b>	0.60	0.57	0.96	0.93
<b>1</b>	0.82	0.76	0.98	1.00
<b>0.5</b>	0.79	0.67	0.92	0.99
<b>0.1</b>	0.90	0.91	0.93	1.00
<b>0.05</b>	0.58	0.77	0.47	1.00
<b>0.01</b>	0.13	0.22	0.46	0.21

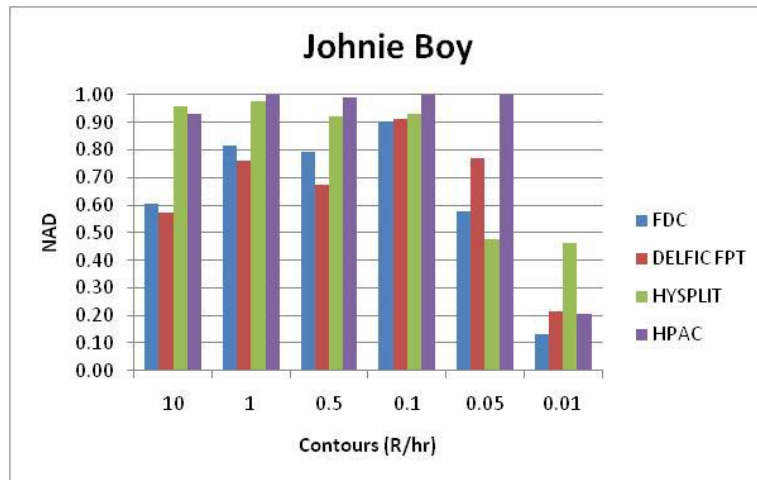


**Figure 57. Overall Individual Contour Comparison for Johnie Boy**

The overall assessment using the total sum of the overall NAD, the average of the NADs for the individual contours and the percentage of the area of false negatives is shown in Table 34. The overall assessment shows that the FDC and DELFC FPT are equally effective in modeling Johnie Boy. However, due to the fact that the DELFC FPT

provides less of a hazardous fallout area for CBRNE planners the DELFIC FPT is the preferred model in modeling Johnie Boy.

**Table 34. Overall Assessment of Johnie Boy**

<b>Johnie Boy</b>				
	<b>FDC</b>	<b>DELFC FPT</b>	<b>HYSPLIT</b>	<b>HPAC</b>
<b>Overall NAD</b>	0.31	0.33	0.49	0.98
<b>Individual Comparison</b>	0.64	0.65	0.85	0.85
<b>Total False Negatives</b>	1072	1014	1022	2475
<b>AFN Rating</b>	0.43	0.41	0.41	0.99
<b>Total</b>	1.38	1.39	1.76	2.83

## V. Conclusions and Recommendations

Since September 11<sup>th</sup>, 2001 thousands of hours have been devoted to the study of nuclear fallout modeling. Multiple modeling programs were created and improved upon to assist CBRNE planners and responders at all levels. The most recent program developed was the Fallout Deposition Code, developed by O'Day and proved to more effectively recreate DNA-EX dose-rate contours than HPAC using high resolution reanalysis weather data. Unfortunately, high resolution weather data requires additional time to produce and is less accessible than low resolution weather data. This research proved that the FDC effectively recreates DNA-EX dose-rate contours while using the more easily obtainable low resolution weather data. This accomplishment was critical to allow for effective comparisons of the FDC, DELFIC FPT, HPAC and HYSPLIT due to the limitations of HYSPLIT weather inputs and reducing computation time.

**Table 35. Overall NADs for all Historical Test Cases**

	NAD					
	Ess	George	Zucchini	Priscilla	Smoky	Johnie Boy
<b>DELFIK FPT</b>	0.75	0.26	0.44	0.28	0.30	0.33
<b>FDC</b>	0.72	0.14	0.16	0.54	0.44	0.31
<b>HYSPLIT</b>	0.37	0.23	0.35	0.52	0.80	0.49
<b>HPAC</b>	0.83	0.56	0.63	0.95	0.99	0.98

The FDC and the DELFIC FPT proved to more accurately recreate DNA-EX dose-rate contours than HPAC and HYSPLIT as shown in Table 35. HPAC, a program designed and revised to assist Military CBRNE responders and planners, continuously underestimated the fallout area. This results in extensive false negative areas causing a

significant safety hazard to CBRNE responders. HYSPLIT, developed for the atmospheric community for atmospheric transport modeling, moderately recreates DNA-EX dose-rate contours. HYSPLIT required the summation of multiple runs to represent one nuclear detonation causing a large time commitment to produce one fallout pattern. This time commitment combined with the inability to incorporate ground zero winds prevents HYSPLIT from being an effective nuclear fallout modeling program for CBRNE planners at this time. The DELFIC FPT which uses DELFIC to create the source term would be the preferred modeling program if it were combined with a more effective transport program. The weather input capabilities for DELFIC are limited resulting in deviations from the DNA-EX dose-rate contours. The DELFIC FPT and FDC both more accurately modeled three of the six cases each. The FDC slightly deviated from the individual DNA-EX dose-rate contours due to the limitation of incorporating winds during cloud rise. Another issue with the FDC is that it was created for six specific nuclear tests and requires additional improvements to create a user friendly interface to allow for user defined inputs.

Overall, the Fallout Planning Tool which already has a user friendly interface and a well known and effective program, DELFIC, to define the source term is potentially the preferred nuclear fallout modeling program. The DELFIC FPT requires low computation time and resources. The additional advantage of the DELFIC FPT is the CBRNE planner tool that allows planners to map routes through the contaminated area, allowing for sampling points, and calculates the overall estimated dose received per person executing the sampling mission. With the appropriate improvements in its weather transport

module or combining it with the FDC or HYSPLIT, the DELFIC FPT could be the preferred fallout modeling program for CBRNE planners and responders.

### **Recommendations for Future Work**

A few potential follow up research projects are revising the FDC, conduct a thorough study of HYSPLIT's source term and investigate future options for the DELFIC FPT's weather transport module.

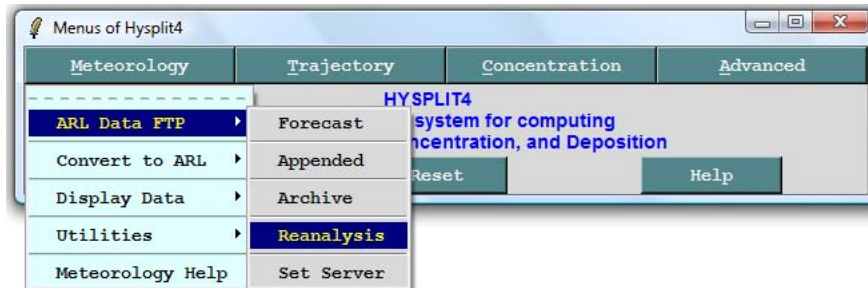
The FDC requires additional improvement to the source term in order to effectively model subsurface and underground bursts and incorporate winds during the cloud rise. Additionally, a user friendly interface is required to allow for user defined inputs. These improvements will allow for future studies to determine additional improvements.

This research used an oversimplified source term as an input for HYSPLIT. A future project is to determine a more accurate ground concentration to exposure rate conversion factor using ORIGEN to identify all the fission products and Beck's conversion factors [3].

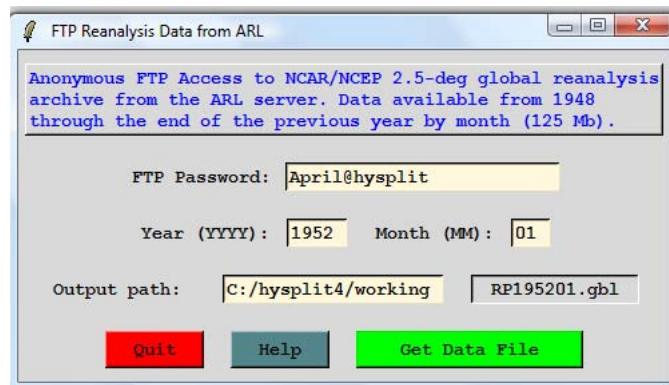
The final area of research is to investigate improvements for the DELFIC FPT's weather transport method. This may require a program to extract information from DELFIC and feed the extracted data into a newly developed weather transport module/program.

## Appendix A. HYSPLIT Settings

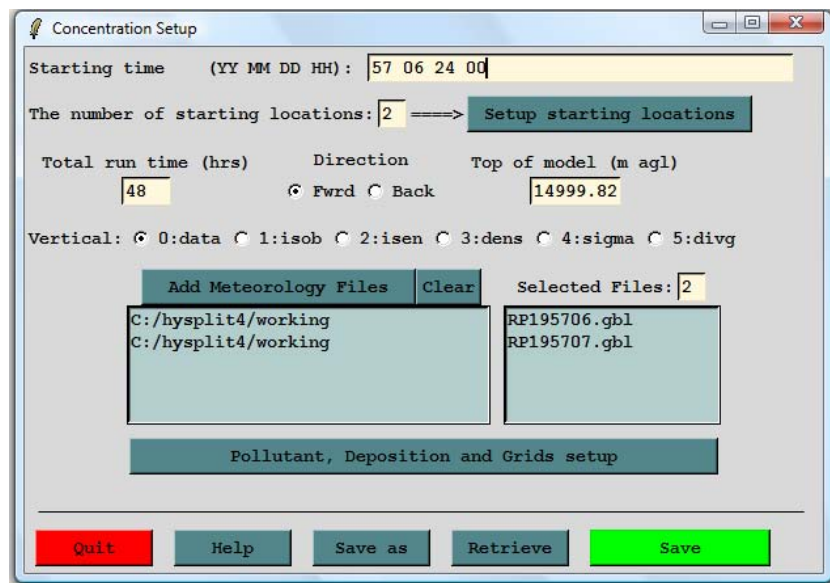
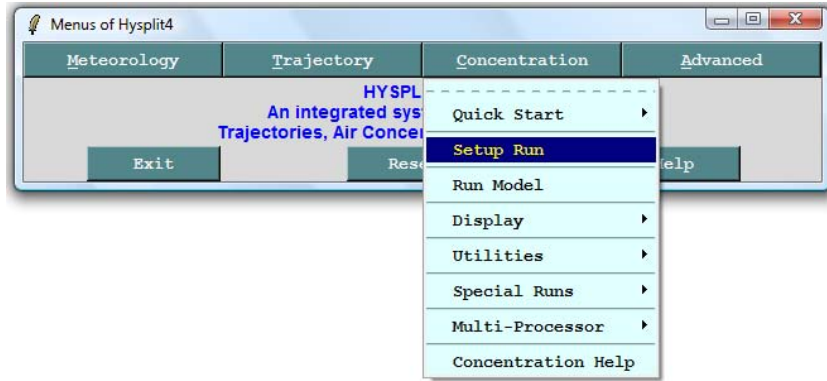
This Appendix outlines the settings used for HYSPLIT and describes the parameters that vary per trial. The low resolution meteorology data is obtained through the Reanalysis section of the HYSPLIT's Meteorology tab.



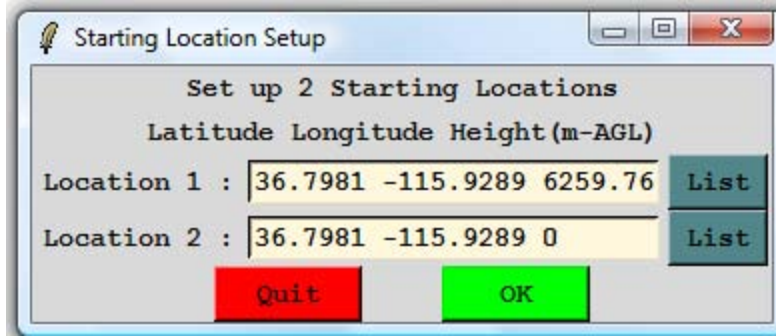
Inputting the year and month enables the download of one month's worth of low resolution weather data.



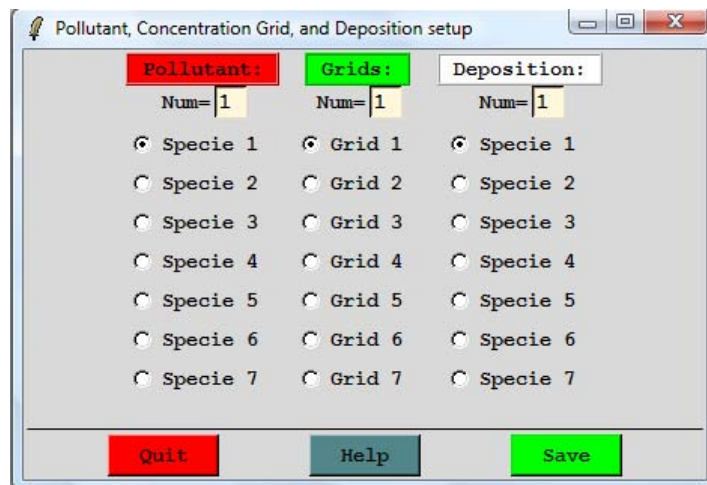
The source term is inputted using the Settings tab under Concentration.



The Starting Time is the time to start the meteorology data. Two is inputted for the number of starting locations which is the top and bottom boundaries of the particle group.

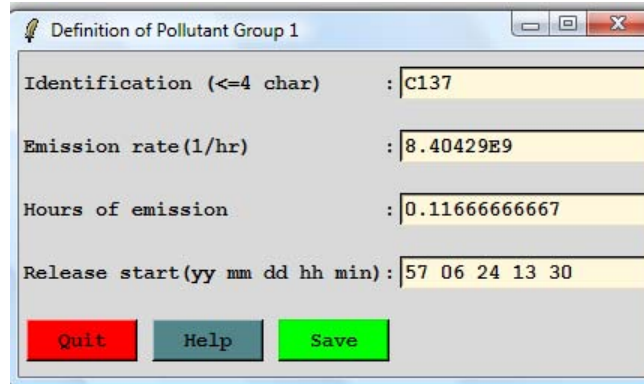


The latitude and longitude of detonation are inputted for each location along with the top and bottom boundary heights. The total run time is set to 48 hours. The direction is forward. The top of the model is the height of the troposphere included in the DNA-EX data. The Vertical motion option is set for the default of 0 which will use the meteorological model's vertical velocity fields. To add the downloaded weather files click the Add Meteorology Files and select the appropriate files. The Selected Files box will update on its own depending on how many weather files are imported. The Pollutant, Deposition and Grids setup opens three additional options.





All boxes remain as one. The Species tab allows for the inputs of emission time and rate.



Identification (<=4 char)	: C137
Emission rate (1/hr)	: 8.40429E9
Hours of emission	: 0.11666666667
Release start (yy mm dd hh min)	: 57 06 24 13 30

Buttons: Quit, Help, Save

The Release Start is the time of detonation. The Grid Section allows for the inputs of the limits. The center of mass of the DNA-EX contours were calculated and inputted as the center of latitude and longitude. Kilometer spacing was used to be consistent with the  $MxM$  matrix. A span of 7 degrees in each direction was used to ensure the extracted data covered an area larger than the DNA-EX data. The Height of Levels is the vertical location at which the samples were recorded; a value of 0 is required for deposition. The Sampling Start and Stop were varied depending on the test. Some inputs resulted in no contours, adjusting the time to the left or right was required in order to produce contours. The final input was the total time to take samples. The average was taken over a 24 hours period.

Definition of Concentration Grid 1

Center of Lat and Lon : 37.1761 -113.3524

Spacing(deg) Lat, Lon : 0.00898 0.00898

Span (deg) Lat, Lon : 7 7

Output grid directory : ./

Output grid file name : cdump

Num of vertical levels : 1

Height of levels(M Agl) : 0

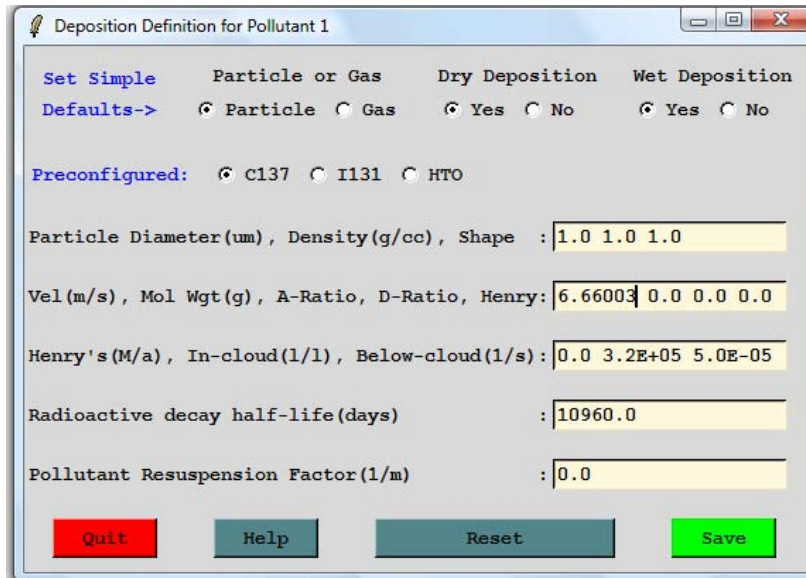
Sampling start(yy mm dd hh min) : 57 06 24 13 00

Sampling stop(yy mm dd hh min) : 57 06 25 14 00

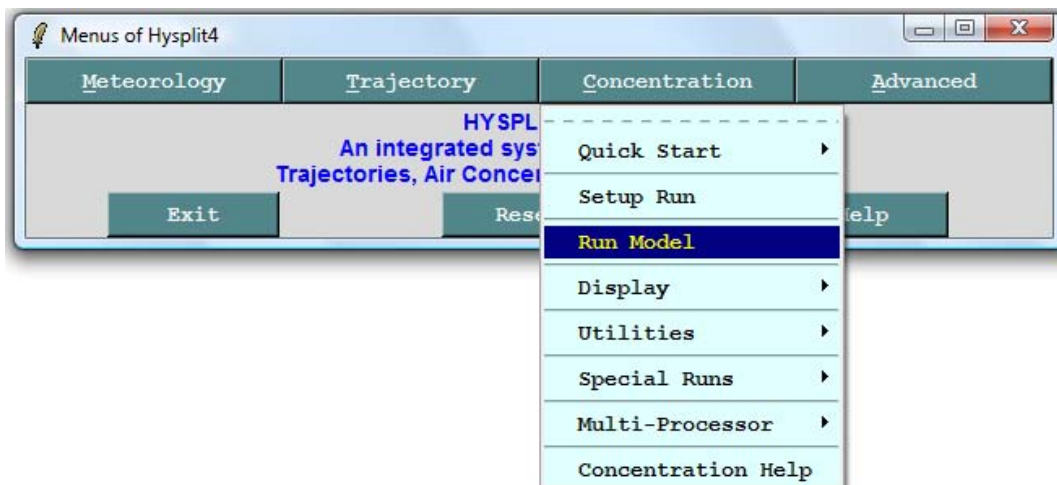
(Avg:0 Now:1 Max:2) (hrs) (min) : 0 24 0

Quit Help Save

The Pollutant Section allowed for the input of the particle settling velocity. This research uses the preconfigured settings for C137 and updates the Velocity as appropriate for each trial. The three values that are updated for each run for each test case are the heights of the top and bottom boundaries for the particle group and the fall velocity.



After updating all fields and pressing Save the Run Model option is selected.



## Appendix B. DELFIC Input File

This Appendix shows an example of the DELFIC Input File. In order to run the DELFIC FPT while updating the weather at various time intervals the DELIFC Input File was updated and then imported into the DELFIC FPT.

```

George
0 0 0 0 0 0 0
15.0      15.0      91.44      1227.60  2200.0  1.0

0.0      0.0      0.0
2.6      0.407    4.0
Alt(m)   Temp(C)   Press(mb) RHum(%)   Dens      U.S. Standard Atmosphere
(6f10.0)
1.0      1.0      100.0      1.0      1.0      1.0      0.0      273.15
1  2  3  4  5  6
1481.8   18.2   850.0     37.3
3118.2   6.9    700.0     39.9
4364.4   -2.0   600.0     42.1
5786.4   -11.2  500.0     37.4
7456.4   -23.3  400.0     44.5
9494.4   -38.9  300.0     22.2
10721.2  -46.6  250.0     -9999
12177.3  -52.5  200.0     -9999
14012.2  -57.7  150.0     -9999
16550.1  -61.9  100.0     -9999
18752.3  -62.8  70.0      -9999
20851.6  -58.3  50.0      -9999
24115.7  -52.2  30.0      -9999
26767.9  -47.4  20.0      -9999
31376.3  -46.3  10.0      -9999
999999.
wind meteorological Effective wind: dir=0, speed=NaN
(3f10.0)
1.0      1.0      1.0      0.0      0.0
1  2  3
1432.3   170.0   0.4
3072.2   160.0   7.6
4314.2   180.0   13.4
5724.3   190.0   15.6
7373.3   200.0   21.5
9383.4   190.0   18.3
999999.
DTM George
0 0 0 1 0 0
1 1 1
1.0E+10 -5.0E+09 -5.0E+09 48.0      4.0
wind meteorological      1 0.0      Alt(m) Dir(deg) speed(m/s)
(3f10.0)
1.0      1.0      1.0      0.0      0.0
1  2  3
1432.3   170.0   0.4
3072.2   160.0   7.6
4314.2   180.0   13.4
5724.3   190.0   15.6
7373.3   200.0   21.5
9383.4   190.0   18.3
999999.
turb wilkins method      1 0.0
    
```

wind meteorological (3f10.0)			2 0.2	Alt(m)	Dir(deg)	Speed(m/s)
1.0	1.0	1.0	0.0	0.0		
1	2	3				
1432.3	196.8	8.5				
3072.2	190.2	9.8				
4314.2	184.9	10.6				
5724.3	187.0	12.9				
7373.3	188.3	15.6				
9383.4	189.7	16.2				
10595.9	192.7	15.3				
12037.3	211.4	12.9				
13882.6	233.8	11.8				
16461.7	244.4	8.7				
18700.2	278.3	3.7				
20820.3	34.8	2.2				
24108.2	78.8	4.2				
26778.9	59.8	5.0				
31390.1	111.6	7.3				
999999.						
turb wilkins method			2 0.2			
wind meteorological (3f10.0)			3 6.0	Alt(m)	Dir(deg)	Speed(m/s)
1.0	1.0	1.0	0.0	0.0		
1	2	3				
1432.3	190.9	4.6				
3072.2	186.6	10.4				
4314.2	178.8	12.4				
5724.3	176.8	14.9				
7373.3	182.3	19.2				
9383.4	185.7	17.8				
10595.9	188.5	15.1				
12037.3	216.7	10.2				
13882.6	239.6	11.2				
16461.7	236.3	8.2				
18700.2	232.2	0.7				
20820.3	75.6	3.9				
24108.2	86.8	5.4				
26778.9	67.7	6.8				
31390.1	90.7	10.8				
999999.						
turb wilkins method			3 6.0			

## Bibliography

1. Abramowitz, M. and I. Stegun. *Handbook of Mathematical Functions with Formulas, Graphs, and Mathematical Tables*. Washington, D.C.: U.S. Government Printing Office, March 1964.
2. Baker III, George H. *Implications of Atmospheric Test Fallout Data for Nuclear Winter*. Wright-Patterson AFB: Air Force Institute of Technology, February 1987.
3. Beck, H. L. *Exposure Rate Conversion Factors for Radionuclides Deposited on the Ground*. Environmental Measurements Laboratory, Department of Energy, July 1980.
4. Bridgman, Charles J. *Introduction to the Physics of Nuclear Weapons Effects*. Fort Belvoir: Defense Threat Reduction Agency, 2001.
5. *Canvas*. Version 9.0.4, CD, Computer Software. ACD Systems Inc., 2004.
6. Chancellor, Richard W. *A Comparison of Hazard Prediction and Assessment Capability (HPAC) Software Dose-Rate Contour Plots to a sample of Local Fallout Data from Test Detonations in the Continental United States, 1945-1962*. Wright Patterson AFB: Air Force Institute of Technology, March 2005.
7. Conners, Stephen P. *Aircrew Dose and Engine Dust Ingestion from Nuclear Cloud Penetration*. Wright Patterson AFB: Air Force Institute of Technology, September 1985.
8. Davies, C. N. "Definitive Equations for the Fluid Resistance of Spheres," *The Proceedings of the Physical Society*, 57: 259-270 (July 1945).
9. Department of Defense. *United States Quadrennial Defense Review Report*. February 2010.
10. Department of Energy. *United States Nuclear Tests: July 1945 through September 1992*. December 2000.
11. Defense Nuclear Agency 1251-1-EX. *Compilation of Local Fallout Data from Test Detonations 1945-1962 Extracted from DASA 1251. Volume I – Continental U.S. Tests*. Defense Nuclear Agency, Washington D.C., 1979.
12. Defense Threat Reduction Agency. *Hazard Prediction and Assessment Capability (HPAC), HPAC 4.04 On-Line Help*. Alexandria VA, April 2005.
13. Draxler, Roland R. and G.D. Hess. *Description of the HYSPLIT\_4 Modeling System*. NOAA Technical Memorandum ERL ARL-224. Silver Spring, MD, January 2004.

14. Draxler, Roland R. and G.D. Hess. "An Overview of the HYSPLIT\_4 Modeling System for Trajectories, Dispersion and Deposition," *Australia Meteorology Magazine*, 47: 295-308 (1998).
15. Draxler, Roland, Barbara Stunder, Glen Rolph, and Albion Taylor. *HYSPLIT4 User's Guide*. NOAA, November 2005.
16. Garcia, Fred E. *Aircrew Ionizing Doses from Nuclear Weapon Bursts*. Wright Patterson AFB: Air Force Institute of Technology, March 2001.
17. Glasstone, Samuel and Philip J. Dolan. *The Effects of Nuclear Weapons*. Alexandria, VA: The United States Department of Defense and the United States Department of Energy, 1977.
18. Hicks, Harry G. "Calculation of the Concentration of any Radionuclide Deposited on the Ground by Offsite Fallout from a Nuclear Detonation," *Health Physics*, 42: 585-600 (May 1982).
19. Hopkins, A. T. *Development and Validation of a new Fallout Transport Method using Variable Spectral Winds*. Wright Patterson AFB: Air Force Institute of Technology, September 1984.
20. Hultquist, Thomas R., Michael R. Dutter, and David J. Schwab. "Reexamination of the 9-10 November 1975 "Edmund Fitzgerald" Storm using today's Technology," *Bulletin of the American Meteorological Society*, 87: 607-622 (16 December 2006).
21. Izrael, YU. A. *Radioactive Fallout after Nuclear Explosions and Accidents*. Amsterdam: Elsevier, 2002.
22. Jodoin, V. J. *Nuclear Cloud Rise and Growth*. Wright Patterson AFB: Air Force Institute of Technology, June 1994.
23. Jones, Christopher P. *High Resolution Mesoscale Weather Data Improvement to Spatial Effects for Dose-Rate Contour Plot Predictions*. Wright Patterson AFB: Air Force Institute of Technology, March 2007.
24. Kalnay, Eugenia and others. "The NCEP/NCAR 40-Year Reanalysis Project," *Bulletin of the American Meteorological Society*, 77: 437-431 (3 March 1996).
25. Moroz, Brian E., Harold L. Beck, Andre Bouville, and Steven L. Simon. "Predictions of Dispersion and Deposition of Fallout from Nuclear Testing using the NOAA-HYSPLIT Meteorological Model," *Health Physics*, 99: 252-269 (August 2010).
26. Norment, Hillyer G. *DELFI: Department of Defense Fallout Prediction System. Volume I - Fundamentals*. Atmospheric Science Associates, Bedford, MA, 31 December 1979 (ADA 088 367).

27. Norment, Hillyer G. *DELFIIC: Department of Defense Fallout Prediction System. Volume II - User's Guide*. Atmospheric Science Associates, Bedford, MA, 31 December 1979 (ADA 088 512).
28. National Oceanic and Atmospheric Administration. "NOAA Operational Model Archive Distribution System." <http://nomad3.ncep.noaa.gov/>. October 2005.
29. Norment, Hillyer G. *Validation and Refinement of the DELFIIC Cloud Rise Module*. Washington D.C.: Defense Nuclear Agency, 1977.
30. O'Day, Buckley E. *Estimation of Weapon Yield from Inversion of Dose-rate Contours*. Wright Patterson AFB: Air Force Institute of Technology, March 2009.
31. Pace, Kevin D. *Terrain and Spatial Effects on a Hazard Prediction and Assessment Capability (HPAC) Software Dose-rate Contour Plot Predictions as Compared to a Sample of Local Fallout Data from Test Detonations in the Continental United States, 1945-1962*. Wright Patterson AFB: Air Force Institute of Technology, March 2006.
32. St. Ledger, John W. *Incorporation of Hopkins' Variable Wind Model into a Population-Dose Fallout Code*. Wright Patterson AFB: Air Force Institute of Technology, March 1985.
33. US Government. *National Strategy for Combating Terrorism*. Washington, D.C.: United States Government, 2006.
34. Warner, Steve and others. "User-Oriented Two-Dimensional Measure of Effectiveness for the Evaluation of Transport and Dispersion Models," *Journal of Applied Meteorology*, 43: 58-73 (January 2004).
35. Way, Kathrine and E. P. Wigner. "The Rate of Decay of Fission Products," *Physical Review*, 76: 375 (1948).
36. Westinghouse Savannah River Company. *Use of the Hazard Prediction and Assessment Capability (HPAC) at the Savannah River Site (U)*. Aiken, SC, September 2004.
37. Willis, Jay C. *The History of Fallout Prediction*. Report prepared for Nuclear Effects 6.99 (Fallout Modeling), Air Force Institute of Technology, 1 June 1977 (ADA 079 560).



**REPORT DOCUMENTATION PAGE**

Form Approved  
OMB No. 0704-0188

The public reporting burden for this collection of information is estimated to average 1 hour per response, including the time for reviewing instructions, searching existing data sources, gathering and maintaining the data needed, and completing and reviewing the collection of information. Send comments regarding this burden estimate or any other aspect of this collection of information, including suggestions for reducing the burden, to Department of Defense, Washington Headquarters Services, Directorate for Information Operations and Reports (0704-0188), 1215 Jefferson Davis Highway, Suite 1204, Arlington, VA 22202-4302. Respondents should be aware that notwithstanding any other provision of law, no person shall be subject to any penalty for failing to comply with a collection of information if it does not display a currently valid OMB control number.

**PLEASE DO NOT RETURN YOUR FORM TO THE ABOVE ADDRESS.**

1. REPORT DATE (DD-MM-YYYY) 24-03-2011	2. REPORT TYPE Master's Thesis	3. DATES COVERED (From - To) Sept 2009 - Mar 2011
---	-----------------------------------	--

4. TITLE AND SUBTITLE A Comparison in the Accuracy of Mapping Nuclear Fallout Patterns using HPAC, HYSPLIT, DELFIC FPT and an AFIT FORTRAN95 Fallout Deposition Code	5a. CONTRACT NUMBER
	5b. GRANT NUMBER
	5c. PROGRAM ELEMENT NUMBER

6. AUTHOR(S) Miller, April D., Major, USA	5d. PROJECT NUMBER
	5e. TASK NUMBER
	5f. WORK UNIT NUMBER

7. PERFORMING ORGANIZATION NAME(S) AND ADDRESS(ES) Air Force Institute of Technology Graduate School of Engineering and Management (AFIT/EN) 2950 Hobson Way WPAFB OH 45433-7765	8. PERFORMING ORGANIZATION REPORT NUMBER AFIT/GNE/ENP/11-M16
--	---

9. SPONSORING/MONITORING AGENCY NAME(S) AND ADDRESS(ES) Intentionally Left Blank	10. SPONSOR/MONITOR'S ACRONYM(S)
	11. SPONSOR/MONITOR'S REPORT NUMBER(S)

12. DISTRIBUTION/AVAILABILITY STATEMENT  
APPROVED FOR PUBLIC RELEASE; DISTRIBUTION UNLIMITED

13. SUPPLEMENTARY NOTES

14. ABSTRACT  
Four nuclear fallout mapping tools are studied to determine which tool predicts the most accurate fallout dose-rate contours with low computation time and resources. The four programs consist of the FORTRAN95 based Fallout Deposition Code (FDC), the Hazard Prediction and Assessment Capability's (HPAC) Nuclear Weapon (NWP), the Defense Land Fallout Interpretative Code (DELFI) Fallout Planning Tool (FPT) and the Hybrid Single-Particle Lagrangian Integrated Trajectory (HYSPLIT) Model. The models were compared to the Defense Nuclear Agency's (DNA) DNA 1251-1-EX, Compilation of Local Fallout Data from Test Detonations 1945-1962 Extracted from DASA 1251, using Warner and Platt's Measure of Effectiveness (MOE) method. In order to accurately compare models the use of the FDC and low resolution weather data was validated. HYSPLIT trials were studied varying the vertical distribution, horizontal distribution, emission rate, emission time and number of equal activity particle groups. HPAC trials were run varying the use of terrain and the terrain resolution and the DELFI FPT trials were ran varying the length of time the ground zero winds were incorporated. The best results of each of the four nuclear mapping tools were compared with the

15. SUBJECT TERMS  
Dose-Rate Contours, Fallout, Radioactive Fallout, Measure of Effectiveness, Normalized Absolute Difference, Areal Comparison, Modeling Atomic Tests, Modeling Nuclear Tests, Modeling Fallout

16. SECURITY CLASSIFICATION OF:			17. LIMITATION OF ABSTRACT UU	18. NUMBER OF PAGES 136	19a. NAME OF RESPONSIBLE PERSON Dr. Steven T. Fiorino, AFIT/ENP
a. REPORT U	b. ABSTRACT U	c. THIS PAGE U			19b. TELEPHONE NUMBER (Include area code) sfiorino@afit.edu / (937) 255-3636, ext 4506

Reset

Standard Form 298 (Rev. 8/98)  
Prescribed by ANSI Std. Z39.18

